Advances in Chemical Physics, Volume 125
Edited by I. Prigogine and Stuart A. Rice

ISBN: 0-471-21452-3

FINITE-SIZE SCALING FOR ATOMIC AND MOLECULAR SYSTEMS

SABRE KAIS

Department of Chemistry, Purdue University, West Lafayette, Indiana, U.S.A.

PABLO SERRA

Facultad de Matemática, Astronomía y Física, Universidad Nacional de Córdoba, Ciudad Universitaria, Córdoba, Argentina

CONTENTS

I. INTRODUCTION

Phase transitions and critical phenomena continue to be a subject of great interest in many fields [1]. A wide variety of physical systems exhibit phase transitions and critical phenomena, such as liquid–gas, ferromagnetic–paramagnetic, fluid–superfluid, and conductor–superconductor [2]. Over the last few decades, a large body of research has been done on this subject, mainly using classical statistical mechanics. Classical phase transitions are driven by thermal energy fluctuations, like the melting of an ice cube. Heating the ice above the freezing point causes molecules in the solid phase to break to become liquid water. If you heat them even more, they vaporize into steam. However, in the last decade, considerable attention has concentrated on a qualitatively different class of phase transitions, transitions that occur at the absolute zero of temperature. These are quantum phase transitions that are driven by quantum fluctuations as a consequence of Heisenberg's uncertainty principle [3,4]. These new transitions are tuned by parameters in the Hamiltonian. An example of this kind of transition is the melting of a Wigner crystal, orderly arrangement of electrons. As one makes the crystal more dense, the electrons become more confined, the uncertainty principle takes over, and the fluctuations in the momentum grow. Squeezing more on the crystal, the system transforms from insulator to conductor [5]. Other examples from condensed matter physics include the magnetic transitions of cuprates, superconductor–insulator transitions in alloys, metal–insulator transitions, and the Quantum–Hall transitions [4,6].

In the field of atomic and molecular physics, the analogy between symmetry breaking of electronic structure configurations and quantum phase transitions has been established at the large-dimensional limit [7]. The mapping between symmetry breaking and mean-field theory of phase transitions was shown by allowing the nuclear charge Z, the parameter that tunes the phase transition, to play a role analogous to temperature in classical statistical mechanics. For

two-electron atoms, as the nuclear charge reaches a critical value $Z_c \simeq 0.911$, which is the minimum charge necessary to bind two electrons, one of the electrons jump, in a first-order phase transition, to infinity with zero kinetic energy [8]. The fact that this charge is below $Z = 1$ explains why H^- is a stable negative ion. For three-electron atoms, the transition occurs at $Z_c \simeq 2.0$ and resembles a second-order phase transition [9]; this tells us that He^- is an unstable ion. The estimated values of the critical nuclear charges for N-electron atoms show that, at most, only one electron can be added to a free atom, which means that no doubly charged atomic negative ions exist in the gas phase [10]. For simple one-electron molecular systems $Z_c \simeq 1.228$, and it follows that only the H_2^+ molecular ion is stable. The dissociation of this system occurs in a first-order phase transition [11]. The study of quantum phase transitions and critical phenomena continues to be of increasing interest in the field of atomic and molecular physics. This is motivated by the recent experimental searches for the smallest stable multiply charged anions [12,13], experimental and theoretical work on the stability of atoms and molecules in external electric and magnetic fields [14,15], design and control electronic properties of materials using quantum dots [16], the study of selectively breaking chemical bonds in polyatomic molecules [14], threshold behavior in ultracold atomic collision [17], quantum anomalies in molecular systems [18], stability of exotic atoms [19], and phase transitions of finite clusters [20,21].

Phase transitions in statistical mechanical calculations arise only in the thermodynamic limit, in which the volume of the system and the number of particles go to infinity with fixed density. Only in this limit the free energy, or any thermodynamic quantity, is a singular function of the temperature or external fields. However, real experimental systems are finite and certainly exhibit phase transitions marked by apparently singular thermodynamic quantities. Finite-size scaling (FSS), which was formulated by Fisher [22] in 1971 and further developed by a number of authors (see Refs. 23–25 and references therein), has been used in order to extrapolate the information available from a finite system to the thermodynamic limit. Finite-size scaling in classical statistical mechanics has been reviewed in a number of excellent review chapters [22–24] and is not the subject of this review chapter.

In quantum mechanics, when using variation methods, one encounters the same finite-size problem in studying the critical behavior of a quantum Hamiltonian $\mathscr{H}(\lambda_1, \ldots, \lambda_k)$ as a function of its set of parameters $\{\lambda_i\}$. In this context, critical means the values of $\{\lambda_i\}$ for which a bound-state energy is nonanalytic. In many cases, as in this study, this critical point is the point where a bound state energy becomes absorbed or degenerate with a continuum. In this case, the finite size corresponds not to the spatial dimension but to the number of elements in a complete basis set used to expand the exact wave function of a

given Hamiltonian [10] and the size of a cutoff parameter [26]. The present review chapter is about finite-size scaling in quantum mechanics. Most of the work reviewed here is based on our own work on the development and application of finite-size scaling to atomic and molecular systems.

The review is arranged as follows: In the next section we present some general definitions and results for the critical behavior of quantum one-particle central potentials and few-body systems. In particular, we discuss the near-threshold behavior of quantum N-body Hamiltonians in a D-dimensional space, including the large D-limit approximation. In Section III we briefly review the main ideas of finite-size scaling in Classical Statistical Mechanics. In Section IV we present some very general features of the statistical mechanics of quantum systems and then develop the FSS equations for quantum few-body systems. To illustrate the applications of FSS method in quantum mechanics, we give an example of a short-range potential, the Yukawa potential. Finally in Section IV we examine the main assumption of FSS for quantum systems by showing data collapse for few-body problems. Applications of FSS for atomic and molecular systems is given in Section V. In Section VI we present three different phenomena: resonances, crossover, and multicritical points. We discuss in general the applicability of FSS to resonances, the existence of multicritical points, and the definition of the size of the critical region.

In previous sections, *finite size* corresponds to the number of elements of a complete basis set used in a truncated Rayleigh–Ritz expansion of an exact bound eigenfunction of a given Hamiltonian. In Section VII, we present a different FSS approach, the spatial finite-size scaling. With this method we study the scaling properties by introducing a cutoff radius in the potential. This cutoff changes the critical exponent of the energy, but, for large values of the cutoff radius, the asymptotic behavior of FSS functions is dominated by the exact critical exponent. The method gives accurate values for critical parameters and critical exponents.

To treat quantum phase transitions and critical phenomena, it seems that Feynman's path integral is a natural choice. In this approach, one can show that the quantum partition function of the system in d dimensions looks like a classical partition function of a system in $d+1$ dimensions where the extra dimension is the time [3]. Upon doing so, and allowing the space and time variables to have discrete values, we turn the quantum problem into an effective classical lattice problem. In Section VIII we show how to carry out the mapping between the quantum problem and an effective classical space–time lattice and give an example to illustrate how the approach works. Finally we combine the finite-size scaling method with a multistage real-space renormalization group procedure to examine the Mott metal–insulator transition on a nonpartite lattice and then give discussion and conclusions.

II. SOME GENERAL RESULTS FOR NEAR-THRESHOLD STATES

Weakly bound states represent an interesting field of research in atomic and molecular physics. The behavior of systems near the threshold, which separates bound states from continuous states, is important in the study of ionization of atoms and molecules, molecule dissociation, and scattering collisions. In general, the energy is nonanalytical because a function of the Hamiltonian parameters or a bound state does not exist at the threshold energy. It has been suggested for some time that there are possible analogies between critical phenomena and singularities of the energy [27–29]. In particular, it has been noted that the energy curves of the two-electron atoms as a function of the inverse of the nuclear charge resemble the free energy curves as a function of the temperature for the van der Waals gas [27]. Using the large-dimensional limit model for electronic structure problems, we will show in this section that symmetry breaking of the electronic structure configurations for the many-electron atoms and simple molecular systems can be studied as mean-field problems in statistical mechanics. Then, we will present some general definitions and results for the critical behavior of quantum systems at finite dimensions, in particular at $D = 3$.

A. Phase Transitions at the Large-Dimensional Limit

It is possible to describe stability and symmetry breaking of electronic structure configurations of atoms and molecules as phase transitions and critical phenomena. This analogy was revealed by using the dimensional scaling method and the large-dimensional limit model of electronic structure configurations [7,30–32]. Large-dimensional models were originally developed for specific theories in the fields of nuclear physics, critical phenomena, and particle physics [33,34]. Subsequently, with the pioneering work of Herschbach et al. [29], they found wide use in the field of atomic and molecular physics [35]. In this method, one takes the dimension of space, D, as a variable, solves the problem at some dimension $D \neq 3$ where the physics becomes much simpler, and then uses perturbation theory or other techniques to obtain an approximate result for $D = 3$ [29].

To study the behavior of a given system near the critical point, one has to rely on model calculations that are simple, capture the main physics of the problem, and belong to the same universality class. For electronic structure calculations of atoms and molecules, there are three exactly solvable models: the Thomas–Fermi statistical model (the limit $N \to \infty$ for fixed N/Z, where N is the number of electrons and Z is the nuclear charge); the noninteracting electron model, the limit of infinite nuclear charge ($Z \to \infty$, for fixed N); and the large-dimensional model ($D \to \infty$ for fixed N and Z) [36]. Here we will illustrate the phase transitions and symmetry breaking using the large-dimensional model. In the

application of dimensional scaling to electronic structure, the large-D limit reduces to a semiclassical electrostatic problem in which the electrons are assumed to have fixed positions relative to the nuclei and to each other in the D-scaled space [29]. This configuration corresponds to the minimum of an effective potential which includes Coulomb interactions as well as centrifugal terms arising from the generalized D-dependence kinetic energy. Typically, in the large-D regime the electronic structure configuration undergoes symmetry breaking for certain ranges of nuclear charges or molecular geometries [37].

In order to illustrate the analogy between symmetry breaking and phase transitions, we briefly review the main results for the two-electron atoms in the Hartree–Fock (HF) approximation [7]. In the HF approximation at the $D \to \infty$ limit, the dimensional-scaled effective Hamiltonian for the two-electron atom in an external weak electric field $\mathscr{E}$ can be written as [38,39]

$$\mathscr{H}_\infty = \frac{1}{2}\left(\frac{1}{r_1^2}+\frac{1}{r_2^2}\right) - Z\left(\frac{1}{r_1}+\frac{1}{r_2}\right) + \frac{1}{\left(r_1^2+r_2^2\right)^{1/2}} - \mathscr{E}(r_1 - r_2) \qquad (1)$$

where r_1 and r_2 are the electron–nucleus radii and Z is the nuclear charge. The ground-state energy at the large-D limit is then given by

$$E_\infty(Z,\mathscr{E}) = \min_{\{r_1,r_2\}} \mathscr{H}_\infty \qquad (2)$$

In the absence of an external electric field, $\mathscr{E} = 0$, Goodson and Hershbach [40] have found that these equations have a symmetric solution with the two electrons equidistant from the nucleus, with $r_1 = r_2 = r$.

This symmetric solution represents a minimum in the region where all the eigenvalues of the Hessian matrix are positive, $Z \geq Z_c = \sqrt{2}$. For values of Z smaller than Z_c, the solutions become unsymmetrical with one electron much closer to the nucleus than the other ($r_1 \neq r_2$). In order to describe this symmetry breaking, it is convenient to introduce new variables (r, η) of the form

$$r_1 = r, \qquad r_2 = (1-\eta)r \qquad (3)$$

where $\eta = (r_1 - r_2)/r_1 \neq 0$ measures the deviation from the symmetric solution.

By studying the eigenvalues of the Hessian matrix, we have found that the solution is a minimum of the effective potential for the range, $1 \leq Z \leq Z_c$. We now turn to the question of how to describe the system near the critical point. To answer this question, a complete mapping between this problem and critical phenomena in statistical mechanics is readily feasible with the following analogies:

- Nuclear charge $Z \leftrightarrow$ temperature T
- External electric field $\mathscr{E} \leftrightarrow$ ordering field h
- Ground-state energy $E_\infty(Z, \mathscr{E}) \leftrightarrow$ free energy $f(T, h)$
- Asymmetry parameter $\eta \leftrightarrow$ order parameter m
- Stability limit point $(Z_c, \mathscr{E} = 0) \leftrightarrow$ critical point $(T_c, h = 0)$

Using the above scheme, we can define the critical exponents (β, $\hat{\alpha}$[1], δ, and γ) for the electronic structure of the two electron atom in the following way:

$$\begin{aligned} \eta(Z, \mathscr{E} = 0) &\sim (-\Delta Z)^{\beta}, \qquad \Delta Z \to 0^- \\ E_\infty(Z, \mathscr{E} = 0) &\sim |\Delta Z|^{2-\hat{\alpha}}, \qquad \Delta Z \to 0 \\ \mathscr{E}(Z_c, \eta) &\sim \eta^{\delta}\mathrm{sgn}(\eta), \qquad \eta \to 0 \\ \left.\frac{\partial \eta}{\partial \mathscr{E}}\right|_{\mathscr{E}=0} &\sim |\Delta Z|^{-\gamma}, \qquad \Delta Z \to 0 \end{aligned} \tag{4}$$

where $\Delta Z \equiv Z - Z_c$. These critical exponents describe the nature of the singularities in the above quantities at the critical charge Z_c. The values obtained for these critical exponents are known as classical or mean-field critical exponents with

$$\beta = \frac{1}{2}, \qquad \hat{\alpha} = 0_{dis}, \qquad \delta = 3, \qquad \gamma = 1 \tag{5}$$

The results of the asymmetry parameter η as a function of nuclear charge at $\mathscr{E} = 0$ is shown in Fig. 1. This curve of the asymmetry parameter shown is completely analogous to curves representing the behavior of magnetization as a function of the temperature in mean field models of ferromagnetic systems [41] as shown in Fig. 2.

The above approach, the analogy between symmetry breaking and phase transitions, was generalized to treat the large-dimensional model of the N-electron atoms [30], simple diatomic molecules [31,42], both linear and planar one-electron systems [32], and three-body Coulomb systems of the general form ABA [43].

The above simple large-D picture helps to establish a connection to phase transitions. However, the questions which remain to be addressed are: How to carry out such an analogy to the N-electron atoms at $D = 3$ and what are the physical consequences of this analogy? These questions will be examined in the following sections by developing the finite size scaling method for atomic and molecular systems.

[1] In statistical mechanics the Greek letter α is used for this exponent. We reserve α for the exponent of the energy; therefore, $\hat{\alpha} = 2 - \alpha$.

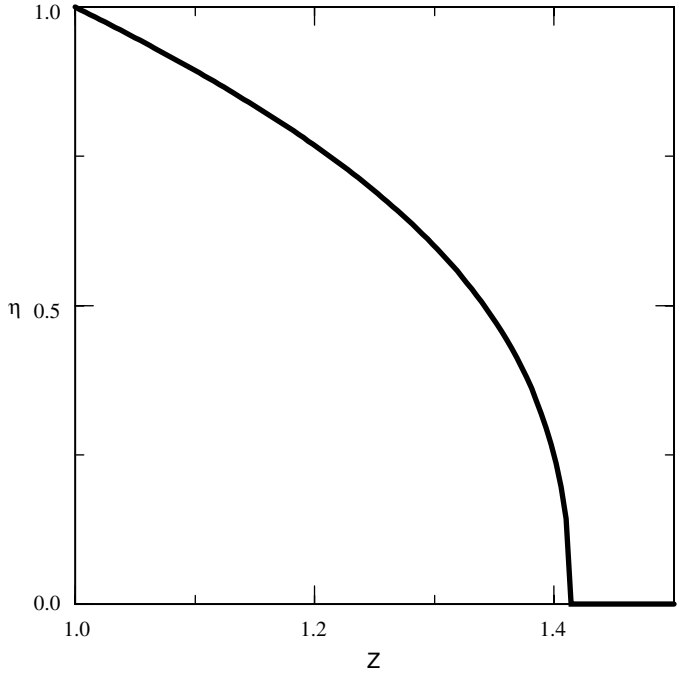

Figure 1. The asymmetry parameter η as a function of the nuclear charge Z for the Hartree–Fock two-electron atom at the large D limit.

B. Critical Phenomena in Spaces of Finite Dimensions

In this section, we will discuss the near-threshold behavior of quantum N-body Hamiltonians in a D-dimensional space. In particular we will study Hamiltonians of the form

$$\mathscr{H}(\lambda;\vec{x}_1,\ldots,\vec{x}_N) = -\frac{1}{2}\sum_{i=1}^{N}\nabla_D^2 + \lambda\, V(\vec{x}_1,\ldots,\vec{x}_N) \tag{6}$$

for different values of N and D. We will assume without loss of generality that the threshold energy is zero, and it is reached from the right $\lambda = \lambda_c > 0$:

$$E(\lambda_c) = \lim_{\lambda\to\lambda_c^+} E(\lambda) = 0 \tag{7}$$

where $E(\lambda)$ is an isolated bound-state energy for $\lambda > \lambda_c$.

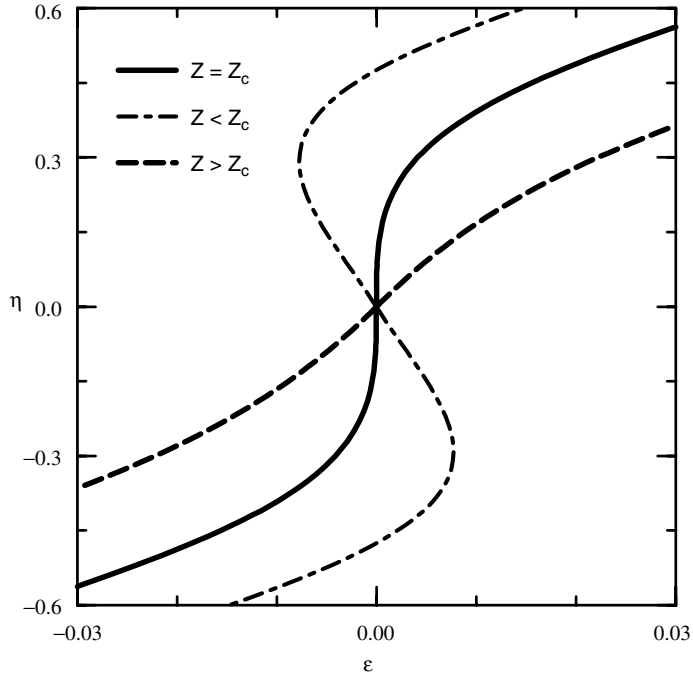

Figure 2. The asymmetry parameter η as a function of the external electric field for three values of the nuclear charge for the Hartree–Fock two-electron atom at the large D limit.

The relevant questions to be addressed at this point are related to the calculation of λ_c, the determination of the leading term in the asymptotic behavior of $E(\lambda)$ near λ_c, and the existence of a square-integrable eigenfunction at the threshold. In the forthcoming sections we will develop the finite-size scaling as a powerful method to obtain accurate numerical estimations of critical parameters. Here we will present some exact results.

Let us introduce the useful concept of a critical exponent. A function $f(x)$ has critical exponent μ at $x = x_0$ if

$$f(x) \sim (x - x_0)^{\mu} \qquad \text{for} \quad x \to x_0 \tag{8}$$

It means that the leading term obeys a power law. Sometimes the leading order is not a power law and might be logarithmic or exponential behavior. From Eq. (8) we have

$$\lim_{x \to x_0} \frac{\ln(f(x))}{\ln(x - x_0)} = \mu \tag{9}$$

For an asymptotic behavior of the form

$$f(x) \sim (x - x_0)^{\mu} \ln^{\delta}(x - x_0) \qquad \text{for} \quad x \to x_0 \tag{10}$$

the limit, as in Eq. (9), is also equal to μ. For an exponential behavior

$$f(x) \sim \exp(\pm c/(x - x_0)^{\delta}) \qquad \text{for} \quad x \to x_0 \tag{11}$$

we have

$$\lim_{x \to x_0} \frac{\ln(f(x))}{\ln(x - x_0)} = \pm\infty \tag{12}$$

We will say that a function with asymptotic behavior like Eq. (10) has a critical exponent $\mu_{\log}$ and that for a function that obeys Eq. (12), the exponent is $\mu = \mp\infty$. It is clear that these definitions of critical exponents are just a useful notation. It means that the function does not obey a power law near a given point, but has logarithmic corrections in the first case and it goes faster than any power of $(x - x_0)$ in the second case.

With these definitions we can go a step beyond Eq. (7) and define the critical exponent α for the near-threshold behavior of the bound-state energy

$$E(\lambda) \sim (\lambda - \lambda_c)^{\alpha} \qquad \text{for} \quad \lambda \to \lambda_c^{+} \tag{13}$$

There are few rigorous results for near-threshold behavior in quantum few-body systems, and most of them are one-particle central potentials.

1. *One-Particle Central Potentials*

The D-dimensional Hamiltonian for a one-particle system is given by

$$\mathscr{H}_D = -\frac{1}{2}\nabla_D^2 + \lambda V(r) \tag{14}$$

where $r = \| \vec{x} \|^{1/2}$, $\vec{x} = (x_1, x_2, \ldots, x_D)$, and the Laplacian operator is given by

$$\nabla_D^2 = \frac{1}{r^{D-1}} \frac{\partial}{\partial r} \left(r^{D-1} \frac{\partial}{\partial r} \right) - \frac{\mathscr{L}_{D-1}^2}{r^2} \tag{15}$$

where $\mathscr{L}_{D-1}^2$ is the total squared angular momentum operator in a D-dimensional space.

The Schrödinger equation is separable by writing the wave function as

$$\Psi(\vec{x}) = \psi(r)\, \mathscr{Y}_{D-1}(\Omega) \tag{16}$$

where $\mathscr{Y}_{D-1}(\Omega)$ is the hyperspherical harmonic, which is an eigenfunction of the generalized angular momentum operator [44]

$$\mathscr{L}^2_{D-1}\mathscr{Y}_{D-1}(\Omega) = l\,(l+D-2)\,\mathscr{Y}_{D-1}(\Omega) \tag{17}$$

and ψ obeys the equation

$$\left\{-\frac{1}{2r^{D-1}}\frac{\partial}{\partial r}\left(r^{D-1}\frac{\partial}{\partial r}\right)+\frac{l(l+D-2)}{2r^2}+\lambda V(r)\right\}\psi(r) = E(\lambda)\psi(r) \tag{18}$$

By incorporating the square root of the Jacobian into the wave function via

$$\psi(r) = r^{-(D-1)/2}\Phi(r) \tag{19}$$

Eq. (18) can be transformed to a simpler form where the centrifugal energy separates out from other kinetic terms. The resulting Hamiltonian has the following form:

$$\left\{-\frac{1}{2}\frac{\partial^2}{\partial r^2}+\frac{(\delta-1)(\delta-3)}{8r^2}+\lambda V(r)\right\}\Phi = E(\lambda)\,\Phi \tag{20}$$

where $\delta = D + 2l$. Note that the boundary condition $\Phi(r=0)=0$ excludes the even eigenfunctions in $D=1$, but there is nothing new in this case and the corresponding results are mentioned below. Equation (20) shows the very well known equivalence between D-dimensional s waves and three-dimensional $l=(D-3)/2$ waves.

At this point we can establish one of the few general results for the critical exponent α in near-threshold studies due to Simon [45]; here we present it in a more restricted form with a simple proof:

Theorem. *If square-integrable solution of Eq. (20) exists at the threshold* $\Phi(\lambda_c; r)$ *with* $\|\Phi(\lambda_c; r)\| = 1$, *then* $\alpha = 1$.

Proof. Because the energy at the threshold is zero, we have

$$\begin{aligned} E(\lambda) = \langle T\rangle + \lambda\,\langle V\rangle \le 0 \quad \text{and} \quad \langle T\rangle = \frac{1}{2}\int |\hat{p}\Phi(\lambda; r)|^2\, dr > 0 \Rightarrow \\ \langle V\rangle(\lambda) < 0\ \forall\ \lambda \ge \lambda_c \end{aligned} \tag{21}$$

where $\hat{p}$ *is the operator momentum. Using the Hellmann–Feynman theorem and Eq. (21) we have*

$$\left.\frac{dE(\lambda)}{d\lambda}\right|_{\lambda=\lambda_c} = \langle V\rangle(\lambda_c) < 0 \tag{22}$$

On the other hand, it is straightforward to show, using variational arguments, that $E(\lambda)$ is a monotonic decreasing function of $\lambda \geq \lambda_c$. Then the Tauberian theorem for differentiation of asymptotic expression [46] holds, and from Eq. (13) we obtain

$$\frac{dE(\lambda)}{d\lambda} \sim (\lambda - \lambda_c)^{\alpha-1} \qquad \text{for} \quad \lambda \to \lambda_c^+ \tag{23}$$

Equations (22) and (23) imply $\alpha - 1 = 0$. Note that the theorem is still applicable to the N-body Hamiltonian Eq. (6), and Eq. (23) is valid even when a square-integrable wave function does not exist at the threshold.

In order to obtain the critical behavior of Eq. (20), it is necessary to study short- and long-range potentials. We will define a potential as long-range if $\lim_{r\to\infty} V(r) \sim r^{-\beta}, \beta > 0$, and as short-range if $\lim_{r\to\infty} r^n V(r) \to 0 \; \forall \; n > 0$. This last case includes the important cases of exponential fall-off and compact support potentials [i.e., $V(r) = 0$ for $r > R > 0$]. In both cases we will assume regularity at $r = 0$.

Short-Range Potentials: The problem of the energy critical exponent for D-dimensional short-range central potential was studied by Klaus and Simon [47], and their main results are summarized in Table I.

It is interesting to note that for a given value of the angular momentum $l = 0$ or 1, there is a marginal dimension with logarithmic deviation from a power law, $\alpha = 1_{\log}$ and $\alpha = 1$ for all dimension D greater than the marginal dimension. The case $l \geq 2$ is equivalent to s waves in a space dimension bigger than 4, the marginal dimension for $l = 0$, and therefore the value of the critical exponent does not depend on the spatial dimension. Actually, Eq. (20) does not have two independent parameters D and l, but just δ. The exponent α depends

TABLE I
Critical Exponent α and Wave Function for Short-Range Central Potentials

Dimension D	Angular Momentum l	Critical Exponent α	Square-Integrable Wave Function at Threshold
1	0, 1	2	No
2	0	∞ (exp)	No
	1	1 (log)	No
	≥ 2	1	Yes
3	0	2	No
	≥ 1	1	Yes
4	0	1 (log)	No
	≥ 1	1	Yes
≥ 5	≥ 0	1	Yes

Source: Ref. 47.

on δ for values smaller than the marginal value $\delta_m = 4$, where it has logarithmic corrections, and it does not depend on δ for $\delta > \delta_m = 4$. We can study Eq. (20) by treating δ as a continuous parameter. Lasaut et al. [48] studied Eq. (20) for $\delta > 2$ (they considered $l > -1/2$ as continuous variable in the three-dimensional space). They have found that the critical exponent α varies continuously with l for $-1/2 < l < 1/2$. Using the symmetry of the potential at $\delta = 2$, we have

$$\alpha = \begin{cases} \infty & \delta = 2 \\ \frac{2}{|\delta - 2|} & 0 < \delta < 2 \text{ or } 2 < \delta < 4 \\ 1_{\log} & \delta = 0, 4 \\ 1 & \delta < 0 \text{ or } \delta > 4 \end{cases} \tag{24}$$

and a square-integrable wave function at the threshold exists only for values of δ corresponding to $\alpha = 1$.

For the scaling of other magnitudes, we do not have rigorous results even for one-dimensional or central potentials, but there are some exactly solvable problems that are very useful for testing the numerical methods.

A standard set of solvable potentials with critical behavior can be found in many text books on quantum mechanics [49,50], like the usual square-well potentials and other piecewise constant potentials. Also there are many potentials that are solvable only at $d = 1$ or for three-dimensional s waves like the Hulthén potential, the Eckart potential, and the Pösch–Teller potential. These potentials belong to a class of potentials, called shape-invariant potentials, that are exactly solvable using supersymmetric quantum mechanics [51,52]. There are also many approaches to make isospectral deformation of these potentials [51,53]; therefore it is possible to construct nonsymmetrical potentials with the same critical behavior as that of the original symmetric problem.

Exact solutions are useful to look for new scaling laws. For example, an interesting question is about the scaling law of the amplitude of probability. The asymptotic behavior of the normalized wave function at fixed value of the radius r_0 defines a new scaling exponent μ:

$$\Phi(\lambda; r_0) \sim (\lambda - \lambda_c)^{\mu} f(r_0) \qquad \text{for} \quad \lambda \to \lambda_c^+ \tag{25}$$

where r_0 is an arbitrary value of r except a possible node of the wave function. This exponent tells us about the localization of the particle for $\lambda \sim \lambda_c$, and therefore it is also relevant in scattering problems. Recently [54], based on the near-threshold behavior of the analytic expression for s-wave functions of the exactly solvable potentials, the Hellmann–Feynman theorem, and numerical FSS results, we assumed that the exponent μ is given by the relation

$$\mu = \frac{\alpha - 1}{2} \tag{26}$$

For short-range central potentials we will prove this relation using asymptotic expressions of the wave function. That is, assuming the short-range potential is negligible for $r > R$, we replace the potential $V(r)$ in Eq. (20) by the compact support potential

$$V_R(r) = \begin{cases} V(r) & \text{if} \quad r < R \\ 0 & \text{if} \quad r > R \end{cases} \tag{27}$$

Then we can calculate μ for a large values of $r_0 > R$.

The external wave function with the potential (27) is proportional to the exact external solution of the square-well potential. The solution, which is continuous at $r = R$, is given by

$$\Phi_R(\lambda, k; r) = \begin{cases} \mathcal{N}\, \phi_<(\lambda, k; r) & \text{if } r < R \\ \mathcal{N}\, \phi_<(\lambda, k; R) \sqrt{\dfrac{r}{R}} \dfrac{K_{\frac{\delta-2}{2}}(kr)}{K_{\frac{\delta-2}{2}}(kR)} & \text{if } r > R \end{cases} \tag{28}$$

where $K_\nu(z)$ is the modified Bessel function of the third kind [55], $k = \sqrt{-2E}$, and $\mathcal{N}$ is the normalization constant. For $E < 0$ the wave function is square-integrable and the norm of $\phi_<$ is arbitrary; in particular, we choose

$$\int_0^R |\phi_<(\lambda, k; r)|^2 \, dr = 1 \tag{29}$$

Note that the specific value of R is unimportant, except that it cannot be a node of the wave function; but nodes are always localized in a finite region. Thus, we can choose R in the region where the wave function does not have nodes. The continuity of the logarithmic derivative gives the condition for the energies. Of course we need the explicit expression of the function $\phi_<$ to obtain the eigenvalues; but for our purpose, it is enough to assume that an isolated eigenvalue becomes equals to zero at $\lambda = \lambda_c$.

Equations (25) and (28) tell us that the exponent μ is defined by the asymptotic behavior of the normalization constant $\mathcal{N}$ near λ_c, and $\mathcal{N}$ is given by the usual condition $\int_0^\infty |\Phi_R|^2 dr = 1$; using Eq. (29), we obtain

$$\mathcal{N} = \frac{k\sqrt{R}\, K_{\frac{\delta-2}{2}}(kR)}{\left[k^2 R\, K^2_{\frac{\delta-2}{2}}(kR) + \phi^2_<(\lambda, k; R) \int_{kR}^\infty x\, K^2_{\frac{\delta-2}{2}}(x)\, dx\right]^{1/2}} \tag{30}$$

The function $K_\nu(z)$ [55] has no singularities for $z > 0$, and the asymptotic behavior for $z \to 0$ is

$$K_0(z) \sim -\ln(z) \quad \text{and} \quad K_\nu(z) \sim \frac{1}{2}\Gamma(\nu)\left(\frac{2}{z}\right)^\nu \qquad \text{for} \quad \nu > 0 \tag{31}$$

and for $z \to \infty$ it is

$$K_\nu(z) \sim \sqrt{\frac{\pi}{2z}} e^{-z} \tag{32}$$

As it was pointed out before, the problem is symmetrical around $\delta = 2$; thus we could analyze the asymptotic behavior of $\mathcal{N}$ for $\delta \geq 2$.

From the asymptotic behavior of the Bessel function K_ν, the leading term for $k \to 0$ of the integral in the denominator of Eq. (30) is given by Eq. (31):

$$\int_{kR}^{\infty} x\, K^2_{\frac{\delta-2}{2}}(x)\, dx \sim \begin{cases} A_1 & 2 \leq \delta < 4 \\ A_2\, \ln(k) & \delta = 4 \\ A_3\, k^{-(\delta-4)} & \delta > 4 \end{cases} \quad \text{for} \quad k \to 0 \tag{33}$$

where A_i, $i = 1, 2, 3$, are positive finite constants.

Therefore, for $\delta < 4$ the leading term of $\mathcal{N}$ is governed by the numerator in Eq. (30). Thus, for $\delta = 2$ we have $\mathcal{N} \sim k \ln(k)$, and then it goes to zero faster than any power of $\lambda - \lambda_c$. For such a behavior we say that the value of $\mu = \infty$ as predicted by Eq. (24). For $2 < \delta < 4$, the asymptotic behavior of $\mathcal{N}$ is $\mathcal{N} \sim k^{(4-\delta)/2} \Rightarrow \mu = \frac{1}{\delta-2}\frac{(4-\delta)}{2} = \frac{\alpha-1}{2}$.

For $\delta \geq 4$, the asymptotic behavior in the denominator of $\mathcal{N}$ is dominated by the divergence in the integral given by Eq. (33). For $\delta = 4$, we have $\lim_{k\to 0} k\, K_1(k\, R) \sim$ constant; thus $\mathcal{N} \sim \ln k \sim \ln(\lambda - \lambda_c) \Rightarrow \mu = 0_{\log}$, according to the value $\alpha = 1_{\log}$ for $\delta = 1$.

Finally, the proof is completed by studying the behavior of $\mathcal{N}$ for $\delta > 4$. From Eqs. (30) and (33) we obtain that $\mathcal{N}$ is a finite constant at $k = 0$; thus the critical exponent is $\mu = 0$. This last result can be obtained using the fact that for $\delta > 4$ ($\alpha = 1$) a normalized wave function at the threshold exists [47]. Therefore, if r_0 is not equal to a node, we have $\lim_{E\to 0} \Phi_\lambda(E; r_0) = \Phi_{\lambda_c}(0; r_0) \neq 0 \Rightarrow \mu = 0$ as predicted by Eq. (26).

Long-Range Potentials: For potentials of the general form

$$V(r) = -\frac{C}{r^\beta}, \qquad C, \beta > 0 \tag{34}$$

it is known [56] that Eq. (20) always support an infinite number of bound states for $\beta < 2$. $\beta = 2$ is a marginal case with pathological behavior. In this case, there is no bound states for $C < ((\delta - 2)/2)^2$, and for $C > ((\delta - 2)/2)^2$ there are square-integrable wave functions for all negative values of the energy. Requiring orthogonality between eigenfunctions, a quantization rule emerges, but the spectrum is not bounded from below (for a renormalized solution of this problem,

see Ref. 18). For $\beta > 2$ the strong singularity of the potential at $r = 0$ causes the solution to have an unclear physical meaning. If the potential V is positive, these conclusions do not necessarily hold.

Stillinger [57] presented an exact solution for a potential of the form

$$V(r) = -\frac{3}{32r^2} + \frac{b}{8r^{1/2}} - \frac{c}{8r}, \qquad b, c > 0 \tag{35}$$

By studying the ground-state energy as a function of b at a fixed value of c, he showed that there exists a critical point, the wave function is normalized at the threshold, and the critical exponent for the energy is $\alpha = 1$. A set of long-range potentials exactly solvable only at $E = 0$ ($\alpha = 1$) is discussed in Ref. 58.

The interesting case of potentials with tails falling off like $1/r^{\beta}$ was recently treated by Mortiz et al. [59]. They reported many aspects of the near-threshold properties for these potentials. However, they did not give values of the critical parameters λ_c and α. There is no general solution of the Schrödinger equation for power-law potentials, but for tails going to zero faster than $1/r^2$ and $E(\lambda_c) = 0$, the solutions are Bessel functions [60] that can be normalized for $\delta > 4$.

2. *Few-Body Potentials*

There are only few rigorous results on critical phenomena for many-body systems, and most of them are variational bounds. As an example, for N-electron atoms, experimental results [61] and numerical calculations [62] rule out the stability of doubly charged atomic negative ions in the gas phase. However, a rigorous proof exists only for the instability of doubly charged hydrogen negative ions [63].

Exact values of critical exponents are more difficult to obtain, because variational bounds do not give estimations of the exponents. Then the result presented by M. Hoffmann-Ostenhof et al. [64] for the two-electron atom in the infinite mass approximation is the only result we know for N-body problems with $N > 1$. They proved that there exists a minimum (critical) charge where the ground state degenerates with the continuum, there is a normalized wave function at the critical charge, and the critical exponent of the energy is $\alpha = 1$.

Finally, there are a series of interesting papers dealing with rigorous results, including accurate estimations for the critical lines and for the ground-state energy of three- and four-charge systems, but without mentioning the problem of the critical exponent [for more details, see a recent review article (Ref. 65) and references therein].

In Section V, we will apply FSS to the three-body Coulomb system. Therefore, it is convenient to present some rigorous results for this problem. Let

us consider the stability and phase transitions of the three-body *ABA* Coulomb systems with charges (Q,q,Q) and masses (M,m,M). This system has as unique possible threshold of $AB + A$. With the scale transformation $r \to fr$, where $f = \mu|Qq|$ and $\mu = mM/(m+M)$ is the reduced mass, the scaled Hamiltonian, $\mathscr{H} \to \mu\mathscr{H}/(f)^2$, reads [11,66]

$$\mathscr{H} = -\frac{\nabla_1^2}{2} - \frac{\nabla_2^2}{2} - \frac{1}{r_1} - \frac{1}{r_2} - \kappa\,\nabla_1 \cdot \nabla_2 + \lambda\frac{1}{r_{12}} \tag{36}$$

where $0 \le \lambda = |\frac{Q}{q}| \le \infty$ and $0 \le \kappa = \frac{1}{1+\frac{m}{M}} \le 1$. Here we have formally separated the motion of the center of mass, and the reference particle is the one with mass m. With this scaling transformation, the Hamiltonian depends linearly on the parameters λ and κ.

Some theorems, valid in particular for the Hamiltonian (36), are presented by Thirring [67]. The main results of interest to our discussion can be summarized as follows:

i. If $\mathscr{H}(\beta)$ is a linear function of β, then $E_0(\beta)$ is a concave function of β.
ii. The ground-state energy of the Hamiltonian Eq. (36) is an increasing function of λ.
iii. For small values of κ (first-order perturbation result) we have $E_0(\kappa = 0) \le E_0(\kappa)$.

We are interested in the critical line that separates the regions where the three-body system *ABA* is stable (bounded) with the region $AB + A$. Using i–iii, we can prove the following:

Lemma. *$\lambda_c(\kappa)$ is a convex function of κ.*

Proof. *$0 \le \kappa_1 < \kappa_2 \le 1$ and $\lambda_1 = \lambda(\kappa_1)$; $\lambda_2 = \lambda(\kappa_2)$. Now define a line in the κ–λ plane beginning at (κ_1, λ_1) and ending at (κ_2, λ_2). A parameterized expression of such a line is*

$$(\kappa, \lambda) = (t\kappa_2 + (1-t)\kappa_1,\ t\lambda_2 + (1-t)\lambda_1), \qquad t \in [0,1]$$

By i, for the ground-state energy over this line holds

$$E_0(t) \ge t\,E_0(t=0) + (1-t)\,E_0(t=1)$$

But $t = 0$ and $t = 1$ belong to the critical curve; thus

$$E_0(t=0) = E_0(t=1) = E_{th} = -\frac{1}{2}$$

Therefore, $E_0(t) \geq E_{th} = -\frac{1}{2}$ *together with ii yield*

$$\lambda_c(\kappa(t)) \leq t\lambda_c(\kappa_2) + (1-t)\lambda_c(\kappa_1)$$

Remarks:

- *If* $\lambda_c(\kappa)$ *is a convex function, then the critical curve has one (and only one) minimum for* $\kappa \in [0,1]$.
- *If* $\nexists\ \kappa^* \in (0,1) / \frac{\partial \lambda_c}{\partial \kappa^*} = 0$, *then the minimum is located at* $\kappa = 0$ *or* $\kappa = 1$.
- *From iii we have* $\frac{\partial \lambda_c}{\partial \kappa}|_{\kappa=0} \leq 0$.
- *The exact s-state eigenfunctions of Hamiltonian Eq. (36) has the functional form*

$$\Psi_s(\vec{r_1}, \vec{r_2}) = \Psi_s(r_1, r_2, r_{12})$$

For this functional form, the correlation of fluctuations in position and momentum spaces takes the form

$$\Gamma_s(\vec{r_1}, \vec{r_2}) = \langle (\vec{r_1} - \langle \vec{r_1} \rangle_s) \cdot (\vec{r_2} - \langle \vec{r_2} \rangle_s) \rangle_s = \langle \vec{r_1} \cdot \vec{r_2} \rangle_s$$

and

$$\Gamma_s(\vec{p_1}, \vec{p_2}) = \langle (\vec{p_1} - \langle \vec{p_1} \rangle_s) \cdot (\vec{p_2} - \langle \vec{p_2} \rangle_s) \rangle_s = \langle \vec{p_1} \cdot \vec{p_2} \rangle_s$$

- *Using* $E_0(\lambda_c(\kappa), \kappa) = E_{th} = -\frac{1}{2}\ \forall\ \kappa \in [0,1]$, *we obtain*

$$\frac{dE_0(\lambda_c(\kappa), \kappa)}{d\kappa} = 0 = \frac{\partial E_0(\lambda_c(\kappa), \kappa)}{\partial \kappa} + \frac{\partial E_0(\lambda_c(\kappa), \kappa)}{\partial \lambda} \frac{\partial \lambda_c}{\partial \kappa}$$

If there exists a minimum in the critical line, $(\kappa^*, \lambda_c(\kappa^*))$, $0 < \kappa^* < 1$, *at this minimum we have*

$$\frac{\partial \lambda_c}{\partial \kappa} = 0 \Rightarrow \partial \frac{E_0}{\partial \kappa}\Big|_* = 0$$

and using Hellman–Feynman theorem, we obtain

$$\langle \nabla_1 \cdot \nabla_2 \rangle|_{(\kappa^*, \lambda_c(\kappa^*))} = 0$$

We will see in Section V that the last result plays an important role in the classification of three-body system to atom-like or to molecule-like systems.

III. FINITE-SIZE SCALING IN CLASSICAL STATISTICAL MECHANICS

In statistical mechanics, the existence of phase transitions is associated with singularities of the free energy per particle in some region of the thermodynamic space. These singularities occur only in the *thermodynamic limit* [68,69]; in this limit the volume (V) and particle number (N) go to infinity in such a way that the density ($\rho = N/V$) stays constant. This fact could be understood by examining the partition function. For a finite system, the partition function is a finite sum of analytical terms, and therefore it is itself an analytical function. It is necessary to take an infinite number of terms in order to obtain a singularity in the thermodynamic limit [68,69].

In practice, real systems have large but finite particle numbers ($N \sim 10^{23}$) and volume, and phase transitions are observed. Even more dramatic is the case of numerical simulations, where sometimes systems with only a few number (hundreds, or even tens) of particles are studied, and "critical" phenomena are still present. The question of why finite systems apparently describe phase transitions, along with the relation of this phenomenon with the true phase transitions in infinite systems, is the main subject of finite-size scaling theory [22]. However, finite-size scaling is not only a formal way to understand the asymptotic behavior of a system when the size tends to infinity. In fact, the theory gives us numerical methods capable of obtaining accurate results for infinite systems even by studying the corresponding small systems (see Refs. 23–25 and references therein).

For readers who desire more details on the development of the theory and applications, there are many excellent review articles and books on this subject in the literature [22–25]. However, in this review chapter we are going to present only the general idea of finite-size scaling in statistical mechanics, which is closely related to the application of these ideas in quantum mechanics.

In order to understand the main idea of finite-size scaling, let us consider a system defined in a D-dimensional volume V of a linear dimension L ($V = L^D$). In a finite-size system, if quantum effects are not taken into consideration, there are in principle three length scales: The finite geometry characteristic size L, the correlation length ξ, which may be defined as the length scale covering the exponential decay $e^{-r/\xi}$ with distance r of the correlation function, and the microscopic length a which governs the range of the interaction. Thus, thermodynamic quantities may depend on the dimensionless ratios ξ/a and L/a. The finite-size scaling hypothesis assumes that, close to the critical point, the microscopic length drops out.

If in the thermodynamic limit, $L \to \infty$, we consider that there is only one parameter T in the problem and the infinite system has a second-order phase transition at a critical temperature T_c, a quantity K develops a singularity as a

function of the temperature T in the form

$$K(T) = \lim_{L\to\infty} K_L(T) \sim |T - T_c|^{-\rho} \tag{37}$$

whereas if it is regular in the finite system, $K_L(T)$ has no singularity.

When the size L increases, the singularity of $K(T)$ starts to develop. For example, if the correlation length diverges at T_c as

$$\xi(T) = \lim_{L\to\infty} \xi_L(T) \sim |T - T_c|^{-\nu} \tag{38}$$

then $\xi_L(T)$ has a maximum that becomes sharper and sharper, and the FSS ansatz assumes the existence of scaling function F_K such that

$$K_L(T) \sim K(T) F_K\left(\frac{L}{\xi(T)}\right) \tag{39}$$

where $F_K(y) \sim y^{\rho/\nu}$ for $y \sim 0^+$. Since the FSS ansatz, Eq. (39), should be valid for any quantity that exhibits an algebraic singularity in the bulk, we can apply it to the correlation length ξ itself. Thus the correlation length in a finite system should have the form [25]

$$\xi_L(T) \sim L\phi_\xi(L^{1/\nu}|T - T_c|) \tag{40}$$

The special significance of this result was first realized by Nightingale [70], who showed how it could be reinterpreted as a renormalization group transformation of the infinite system. The phenomenological renormalization (PR) equation for finite systems of sizes L and L' is given by

$$\frac{\xi_L(T)}{L} = \frac{\xi_{L'}(T')}{L'} \tag{41}$$

and has a fixed point at $T^{(L,L')}$. It is expected that the succession of points $\{T^{(L,L')}\}$ will converge to the true T_c in the infinite size limit.

The finite-size scaling theory combined with transfer matrix calculations had been, since the development of the phenomenological renormalization in 1976 by Nightingale [70], one of the most powerful tools to study critical phenomena in two-dimensional lattice models. For these models the partition function and all the physical quantities of the system (free energy, correlation length, response functions, etc) can be written as a function of the eigenvalues of the transfer matrix [71]. In particular, the free energy takes the form

$$f(T) = -T \ln \lambda_1 \tag{42}$$

and the correlation length is

$$\xi(T) = -\frac{1}{\ln(\lambda_2/\lambda_1)} \tag{43}$$

where λ_1 and λ_2 are the largest and the second largest eigenvalues of the transfer matrix. In this context, critical points are related with the degeneracy of these eigenvalues. For finite transfer matrix, the Perron–Frobenius theorem [72] asserts that the largest eigenvalue is isolated (nondegenerated) and phase transitions can occur only in the limit $L \to \infty$ where the size of the transfer matrix goes to infinity and the largest eigenvalues can be degenerated. It is important to note that in the Perron–Frobenius theorem all the matrix elements are positive.

For quasi-one-dimensional systems of size L, it is possible to calculate all the eigenvalues of finite transfer matrix; and therefore, using scaling ansatz like phenomenological renormalization Eq. (41), it is possible to obtain critical parameters and critical exponents for bidimensional systems. Transfer matrix with finite-size scaling theory was successfully applied to the study of a wide variety of bidimensional lattice system like magnetic models [73], modulated phases [74], percolation and self-avoiding random walks [75–81], long-range interactions [82], and many other problems of critical behavior in statistical physics of geometric nature (see Cardy [25] and the references therein).

IV. FINITE-SIZE SCALING IN QUANTUM MECHANICS

A. Quantum Statistical Mechanics and Quantum Classical Analogies

In this section, we present briefly some very general features of the statistical mechanics of quantum systems. For a given system with a Hamiltonian H, the main quantity of interest is the partition function $Z(\beta)$, where β is the inverse temperature

$$Z(\beta) = Tr\, e^{-\beta H} \tag{44}$$

From this one can calculate the expectation values of any arbitrary operator $\mathcal{O}$ by

$$\langle \mathcal{O} \rangle = \frac{1}{Z} Tr(\mathcal{O} e^{-\beta H}) \tag{45}$$

In the limit $T \to 0$, the free energy of the system, $F = -k_B T \ln Z$, becomes the ground-state energy and the various thermal averages become ground-state expectation values.

To do quantum mechanics, one starts with an orthonormal and complete set of states $|n\rangle$ that have the properties

$$I = \sum_n |n\rangle\langle n|, \qquad \langle n \mid m \rangle = \delta_{nm} \tag{46}$$

and a trace operation is given by

$$\text{Tr } \mathcal{O} = \sum_n \langle n|\mathcal{O}|n\rangle \tag{47}$$

Note that the density matrix operator $e^{-\beta H}$ is the same as the time evolution operator $e^{-iH\tau/\hbar}$ if we assign the imaginary value $\tau = -i\hbar\beta$ to the time interval over which the system evolves. Thus, the partition function takes the form of a sum of imaginary time transition amplitudes for the system to start and return to the same state after an imaginary time interval τ,

$$Z(\beta) = \text{Tr } e^{-\beta H} = \sum_n \langle n|e^{-\beta H}|n\rangle \tag{48}$$

We see that calculating the thermodynamics of a quantum system is the same as calculating transition amplitudes for its evolution in imaginary time [83].

Many problems in D-dimensional statistical mechanics with nearest-neighbor interactions can be converted into quantum mechanics problems in $(D-1)$ dimensions of space and one dimension of time [84]. The quantum theory arises here in a Feynman path integral formulation [85].

In the path integral approach, the transition amplitude between two states of the system can be calculated by summing amplitudes for all possible paths between them. By inserting a sequence of sums over sets of intermediate states into the expression for the partition function, Eq. (48) becomes

$$Z(\beta) = \sum_n \sum_{k_1,k_2,k_3,\ldots,k_N} \langle n|e^{-\delta\tau H/\hbar}|k_1\rangle\langle k_1|e^{-\delta\tau H/\hbar}|k_2\rangle \ldots \langle k_N|e^{-\delta\tau H/\hbar}|n\rangle \tag{49}$$

where $\delta\tau$ is a time interval and N is a large integer chosen such that $N\delta\tau = \hbar\beta$. This expression for the partition function has the form of a classical partition function, which is a sum over configurations expressed in terms of a transfer matrix $\langle k_i|e^{-\delta\tau H/\hbar}|k_j\rangle$, with the imaginary time as an additional dimension [3]. Thus a quantum system existed in D dimensions, and the expression for its partition function looks like a classical partition function for a system with $(D+1)$ dimensions. The extra time dimension is in units of $\hbar\beta$; when taking the limit $\beta \to \infty$, we get a truly $(D+1)$-dimensional effective classical system. Thus, one can solve many problems in one-dimensional statistical mechanics calculating partition functions; averages and correlation functions in terms of their quantum analogs as presented in Table II. This analogy opens the door to use very powerful methods developed in statistical classical mechanics to study quantum phase transitions and critical phenomena [4].

TABLE II
Quantum Classical Analogies

Quantum	Classical
D space and 1 time dimensions	$(D+1)$ space dimensions
Quantum Hamiltonian H	Transfer matrix
Generating functional	Partition function
Ground state	Equilibrium state
Expectation values	Ensemble averages
Ground state of H	Free energy
Coupling constant	Temperature
Propagators	Correlation functions
Mass gap of H $(1/\Delta E)$	Correlation length (ξ)

B. Finite-Size Scaling Equations in Quantum Mechanics

In order to apply the FSS to quantum mechanics problems, let us consider the following Hamiltonian of the form [10]

$$\mathscr{H} = \mathscr{H}_0 + V_\lambda \tag{50}$$

where $\mathscr{H}_0$ is λ-independent and V_λ is the λ-dependent term. We are interested in the study of how the different properties of the system change when the value of λ varies. A critical point λ_c will be defined as a point for which a bound state becomes absorbed or degenerate with a continuum.

Without loss of generality, we will assume that the Hamiltonian, Eq. (50), has a bound state E_λ for $\lambda > \lambda_c$ which becomes equal to zero at $\lambda = \lambda_c$. As in statistical mechanics, we can define some critical exponents related to the asymptotic behavior of different quantities near the critical point. In particular, for the energy we can define the critical exponent α as

$$E_\lambda \underset{\lambda \to \lambda_c^+}{\sim} (\lambda - \lambda_c)^\alpha \tag{51}$$

For general potentials of the form $V_\lambda = \lambda\, V$, we have shown in the previous section that the critical exponent α is equal to one if and only if $\mathscr{H}(\lambda_c)$ has a normalizable eigenfunction with eigenvalue equal to zero [45]. The existence or absence of a bound state at the critical point is related to the type of the singularity in the energy. Using statistical mechanics terminology, we can associate ''first-order phase transitions'' with the existence of a normalizable eigenfunction at the critical point. The absence of such a function could be related to ''continuous phase transitions'' [10].

In quantum calculations, the Rayleigh–Ritz variational method is widely used to approximate the solution of the Schrödinger equation [86]. To obtain exact results, one should expand the exact wave function in a complete basis set

and take the number of basis functions to infinity. In practice, one truncates this expansion at some order N. In the present approach, the finite size corresponds not to the spatial dimension, as in statistical mechanics, but to the number of elements in a complete basis set used to expand the exact eigenfunction of a given Hamiltonian. For a given complete orthonormal λ-independent basis set $\{\Phi_n\}$, the ground-state eigenfunction has the following expansion:

$$\Psi_\lambda = \sum_n a_n(\lambda)\Phi_n \tag{52}$$

where n represents the set of quantum numbers. In order to approximate the different quantities, we have to truncate the series, Eq. (52), at order N. Then the Hamiltonian is replaced by $M(N) \times M(N)$ matrix $\mathscr{H}^{(N)}$, with $M(N)$ being the number of elements in the truncated basis set at order N. Using the standard linear variation method, the Nth-order approximation for the energies are given by the eigenvalues $\{\Lambda_i^{(N)}\}$ of the matrix $\mathscr{H}^{(N)}$,

$$E_\lambda^{(N)} = \min_{\{i\}}\{\Lambda_i^{(N)}\} \tag{53}$$

In order to obtain the value of λ_c from studying the eigenvalues of a finite-size Hamiltonian matrix, one has to define a sequence of pseudocritical parameters, $\{\lambda^{(N)}\}$. Although there is no unique recipe to define such a sequence, in this review we used three methods: The first-order method (FOM) can be applied if the the threshold energy is known [8,76]. In this method one defines $\lambda^{(N)}$ as the value in which the ground-state energy in the Nth-order approximation, $E_0^{(N)}(\lambda)$, is equal to the threshold energy E_T,

$$E_0^{(N)}(\lambda^{(N)}) = E_T(\lambda^{(N)}) \tag{54}$$

The second approach is the phenomenological renormalization (PR) [24,70] method, where the sequence of the pseudocritical values of λ can be calculated by knowing the first and the second lowest eigenvalues of the $\mathscr{H}$ matrix for two different orders, N and N'. The critical λ_c can be obtained by searching for the fixed point of the phenomenological renormalization equation for a finite-size system [70],

$$\frac{\xi_N(\lambda^{(N)})}{N} = \frac{\xi_{N'}(\lambda^{(N')})}{N'} \tag{55}$$

where the correlation length of the classical pseudosystem is defined as

$$\xi_N(\lambda) = -\frac{1}{\log(E_1^{(N)}(\lambda)/E_0^{(N)}(\lambda))} \tag{56}$$

and $E_0^{(N)}(\lambda)$ and $E_1^{(N)}(\lambda)$ are the ground state and the first excited eigenvalues of a sector of given symmetry of the $\mathscr{H}$ matrix [8,9,87].

The third method is a direct finite-size scaling approach to study the critical behavior of the quantum Hamiltonian without the need to make any explicit analogy to classical statistical mechanics [54,88]. The truncated wave function that approximate the eigenfunction Eq. (52) is given by

$$\Psi_\lambda^{(N)} = \sum_n^{M(N)} a_n^{(N)}(\lambda)\Phi_n \tag{57}$$

where the coefficients $a_n^{(N)}$ are the components of the ground-state eigenvector. In this representation, the expectation value of any operator $\mathscr{O}$ at order N is given by

$$\langle \mathscr{O} \rangle_\lambda^{(N)} = \sum_{n,m}^{N} a_n^{(N)}(\lambda)^* a_m^{(N)}(\lambda)\, \mathscr{O}_{n,m} \tag{58}$$

where $\mathscr{O}_{n,m}$ are the matrix elements of $\mathscr{O}$ in the basis set $\{\Phi_n\}$. In general, the mean value $\langle \mathscr{O} \rangle$ is not analytical at $\lambda = \lambda_c$, and we can define a critical exponent, $\mu_{\mathscr{O}}$, by the relation

$$\langle \mathscr{O} \rangle_\lambda \underset{\lambda \to \lambda_c^+}{\sim} (\lambda - \lambda_c)^{\mu_{\mathscr{O}}} \tag{59}$$

In statistical mechanics, the singularities in thermodynamic functions associated with a critical point occur only in the thermodynamic limit. In the variation approach, singularities in the different mean values will occur only in the limit of infinite basis functions [88].

As in the FSS ansatz in statistical mechanics [24,77], we will assume that there exists a scaling function for the truncated magnitudes such that

$$\langle \mathscr{O} \rangle_\lambda^{(N)} \sim \langle \mathscr{O} \rangle_\lambda F_{\mathscr{O}}(N|\lambda - \lambda_c|^\nu) \tag{60}$$

with a different scaling function $F_{\mathscr{O}}$ for each different operator but with a unique scaling exponent ν.

Now we are in a position to obtain the critical parameters by defining the following function [88]:

$$\Delta_{\mathscr{O}}(\lambda; N, N') = \frac{\ln\left(\langle \mathscr{O} \rangle_\lambda^{(N)} / \langle \mathscr{O} \rangle_\lambda^{(N')}\right)}{\ln(N'/N)} \tag{61}$$

At the critical point, the mean value depends on N as a power law, $\langle \mathcal{O} \rangle \sim N^{-\mu_{\mathcal{O}}/\nu}$; thus one obtains an equation for the ratio of the critical exponents

$$\Delta_{\mathcal{O}}(\lambda_c; N, N') = \frac{\mu_{\mathcal{O}}}{\nu} \tag{62}$$

which is independent of the values of N and N'. Thus, for three different values N, N', and N'' the curves defined by Eq. (61) intersect at the critical point

$$\Delta_{\mathcal{O}}(\lambda_c; N, N') = \Delta_{\mathcal{O}}(\lambda_c; N'', N) \tag{63}$$

In order to obtain the critical exponent α, which is associated with the energy, we can take $\mathcal{O} = \mathscr{H}$ in Eq. (62) with $\mu_{\mathcal{O}} = \alpha$:

$$\frac{\alpha}{\nu} = \Delta_{\mathscr{H}}(\lambda_c; N, N') \tag{64}$$

By using the Hellmann–Feynman theorem [86] we obtain

$$\frac{\partial E_\lambda}{\partial \lambda} = \left\langle \frac{\partial \mathscr{H}}{\partial \lambda} \right\rangle_\lambda = \left\langle \frac{\partial V_\lambda}{\partial \lambda} \right\rangle_\lambda \tag{65}$$

Taking $\mathcal{O} = \partial V_\lambda / \partial \lambda$ in Eq. (62) gives an equation for $(\alpha - 1)/\nu$ that, together with Eq. (64), gives the exponents α and ν. Now, we can define the following function:

$$\Gamma_\alpha(\lambda; N, N') = \frac{\Delta_{\mathscr{H}}(\lambda; N, N')}{\Delta_{\mathscr{H}}(\lambda; N, N') - \Delta_{\partial \mathscr{V}_\lambda / \partial \lambda}(\lambda; N, N')} \tag{66}$$

which is also independent of the values of N and N' at the critical point $\lambda = \lambda_c$ and gives the critical exponent α:

$$\alpha = \Gamma_\alpha(\lambda_c; N, N') \tag{67}$$

From Eq. (64) the critical exponent ν is readily given by

$$\nu = \frac{\alpha}{\Delta_{\mathscr{H}}(\lambda_c; N, N')} \tag{68}$$

The FSS equations are valid only as an asymptotic expression, $N \to \infty$; but with a finite basis set, unique values of λ_c, α, and ν can be obtained as a succession of values as a function of N, N', and N''. The relation between N, N', and N'' was extensively studied in FSS in statistical mechanics [24], and it is

known that the fastest convergence is obtained when the difference between these numbers is as small as possible. In our work [10] we took $\Delta N = 1$, and when there are parity effects we used $\Delta N = 2$. In order to obtain the extrapolated values for $\lambda^{(N)}$, $\alpha^{(N)}$, and $\nu^{(N)}$ at $N \to \infty$, we used the algorithm of Bulirsch and Stoer [89] with $N' = N + \Delta N$ and $N'' = N - \Delta N$. This algorithm was also studied in detail and gives very accurate results for both statistical mechanics problems [90] and electronic structure critical parameters [10].

C. Extrapolation and Basis Set Expansions

To illustrate the applications of the FSS method in quantum mechanics, let us give an example of a short-range interaction, the Yukawa potential. This potential is spherically symmetric, and therefore the critical behavior can be studied for zero and nonzero angular momentum.

In atomic units the Hamiltonian of the screened Coulomb potential can be written as

$$\mathscr{H}(\lambda) = -\frac{1}{2}\nabla^2 - \lambda\frac{e^{-r}}{r} \tag{69}$$

It is well known that the perturbation expansion in $\sigma = 1/\lambda$ around the Coulombic limit, $\sigma = 0$, is asymptotic with zero radius of convergence [91]. This Hamiltonian has bound states for large values of λ and has the exact value of the critical exponent $\alpha = 2$ for states with zero angular momentum and $\alpha = 1$ for states with nonzero angular momentum [47].

A convenient orthonormal basis set that can be used is given by [88]

$$\Phi_{n,l,m}(r,\Omega) = \frac{1}{\sqrt{(n+1)(n+2)}} e^{-\frac{r}{2}} L_n^{(2)}(r) Y_{l,m}(\Omega) \tag{70}$$

where $L_n^{(2)}(r)$ is the Laguerre polynomial of degree n and order 2 and $Y_{l,m}(\Omega)$ is the spherical harmonic function of solid angle Ω [55].

In this basis set, one has to calculate the lowest eigenvalue and eigenvector of the finite Hamiltonian matrix. The matrix elements of the kinetic energy operator can be calculated analytically, and therefore the problem reduces to calculate the matrix elements of the particular potential. Now, in order to obtain the numerical values for λ_c, α, and ν we can use Eqs. (63), (64), and (68) or we can simply use $\Gamma_\alpha(\lambda; N, N')$, Eq. (66), which is independent of the values of N and N' at the critical point $\lambda = \lambda_c$. Plotting $\Gamma_\alpha(\lambda; N, N')$ as a function of λ gives a family of curves with an intersection at λ_c. At the point $\lambda = \lambda_c$, one can read the critical exponent α and the critical exponent ν is readily given by Eq. (68).

For the ground state, the curves of $\Gamma_\alpha(\lambda; N, N-2)$ as a function $1/N$ for even values of N are shown in Fig. 3 for $4 \leq N \leq 100$. From this figure, one can

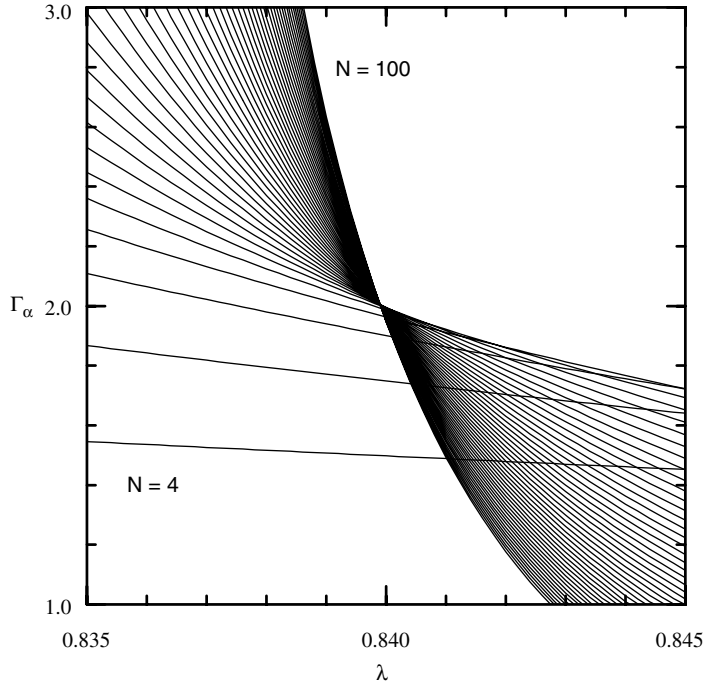

Figure 3. $\Gamma_\alpha(\lambda; N, N-2)$ as a function of λ for the ground state of the Yukawa potential for even values of $4 \leq N \leq 100$.

obtain the values of λ_c and the critical exponent α. The curves of $\lambda^{(N)}$, and $\alpha^{(N)}$ as a function of $1/N$ for $10 \leq N \leq 100$ are shown in Figs. 4 and 5. It seems that a reasonable large-N regime was obtained when $N > 20$; and finally, obtain the extrapolated values as $N \to \infty$ by using the algorithm of Bulirsch and Stoer [89]. The extrapolated values calculated with the points corresponding to $20 \leq N \leq 100$ for $l = 0$ are $\lambda_c = 0.8399039$ and $\alpha = 2$, in excellent agreement with the exact numerical value of $\lambda_c = 0.839908$ [92] and the exact value for $\alpha = 2$ [47].

The behavior of the ground-state energy, $E_0^{(N)}$, as a function of λ for different values of N is different from the state with $l = 1$. For $l = 0$ the energy curve goes smoothly to zero as a function of λ, but the second derivative function develops a discontinuity in the neighborhood of the critical point, $\lambda_c \simeq 0.8399$ and the critical exponent $\alpha = 2$. For $l = 1$, the energy curve bends sharply to zero at the critical point $\lambda_c \simeq 4.5409$ with a critical exponent $\alpha = 1$. As one should expect, there is a discontinuity in the first derivative as a function of λ [88].

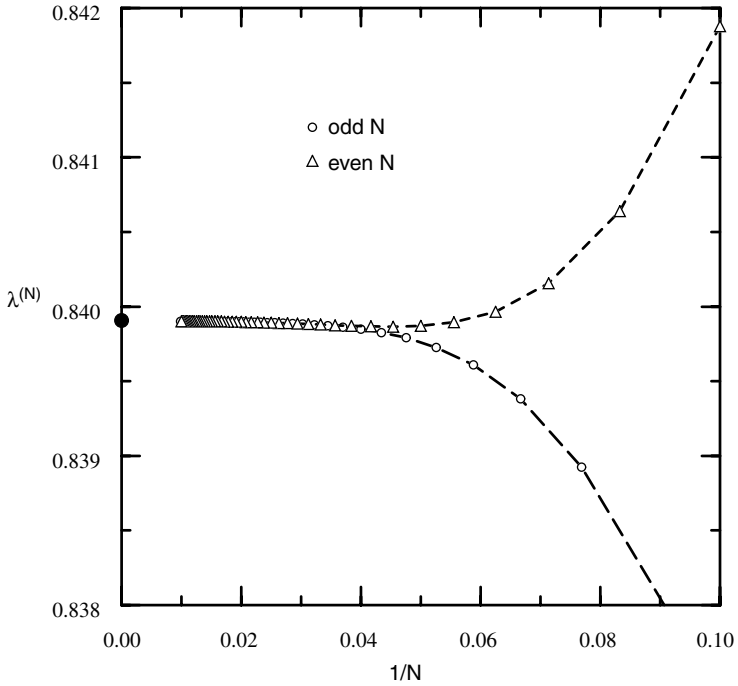

Figure 4. $\lambda^{(N)}$ as a function of $1/N$ for the ground state of the Yukawa potential. The extrapolated values are shown by dots.

D. Data Collapse for the Schrödinger Equation

In order to show the data collapse for quantum few-body problems, let us examine the main assumption we have made in Eq. (60) for the existence of a scaling function for each truncated magnitude $\langle \mathcal{O} \rangle_{\lambda}^{(N)}$ with a unique scaling exponent ν.

Since the $\langle \mathcal{O} \rangle_{\lambda}^{(N)}$ is analytical in λ, then from Eqs. (59) and (60) the asymptotic behavior of the scaling function must have the form

$$F_{\mathcal{O}}(x) \sim x^{-\mu_{\mathcal{O}}/\nu} \tag{71}$$

Eqs. (60) and (71) have the scaling form as presented in Ref. [93]. For our purposes, it is convenient to write this in a slightly different form. From Eqs. (60) and (71) we have

$$\langle \mathcal{O} \rangle^{(N)}(\lambda_c) \sim N^{-\mu_{\mathcal{O}}/\nu} \tag{72}$$

for large values of N.

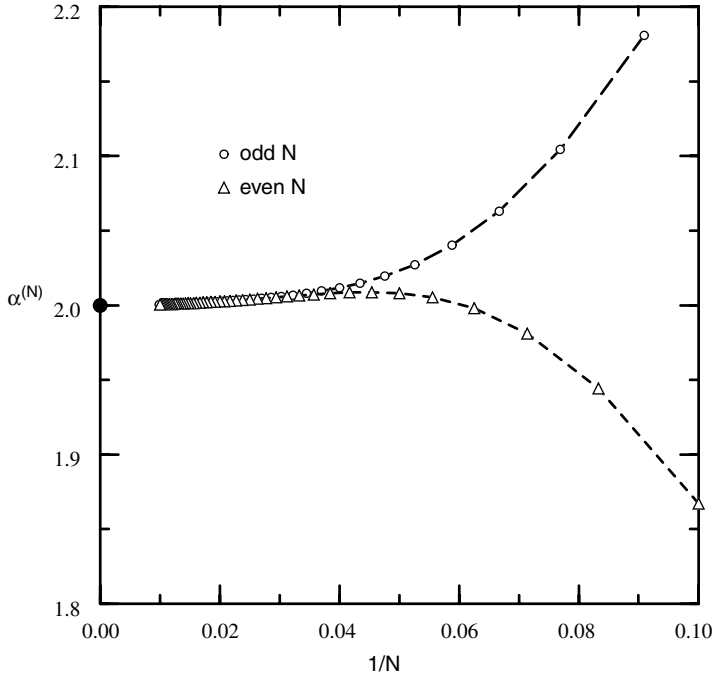

Figure 5. $\alpha^{(N)}$ as a function of $1/N$ for the ground state of the Yukawa potential. The extrapolated values are shown by dots.

Because the same argument of regularity holds for the derivatives of the truncated expectation values, we have that

$$\left.\frac{\partial^m \langle \mathcal{O} \rangle^{(N)}}{\partial \lambda^m}\right|_{\lambda=\lambda_c} \sim N^{-(\mu_{\mathcal{O}}-m)/\nu} \tag{73}$$

$\langle \mathcal{O} \rangle^{(N)}$ is analytical in λ; then using Eq. (73), the Taylor expansion could be written as [93]

$$\langle \mathcal{O} \rangle^{(N)}(\lambda) \sim N^{-\mu_{\mathcal{O}}/\nu} G_{\mathcal{O}}(N^{1/\nu}(\lambda - \lambda_c)) \tag{74}$$

where $G_{\mathcal{O}}$ is an analytical function of its argument.

This equivalent expression for the scaling of a given expectation value has a correct form to study the data collapse in order to test FSS hypothesis in quantum few-body Hamiltonians. If the scaling Eq. (60) or Eq. (74) holds, then

near the critical point the physical quantities will collapse to a single universal curve when plotted in the appropriate form $\langle \mathcal{O} \rangle^{(N)} N^{\mu_{\mathcal{O}}/\nu}$ against $N^{1/\nu}\,(\lambda - \lambda_c)$ [93].

In order to check FSS assumptions, let us show the data collapse for the one-body Yukawa potential Eq. (69). The advantage of studying this simple model is that there exist rigorous theorems that give the exact values for energy-critical α-exponents [47] and accurate values for the critical screening length and the universal exponent ν [88] for both zero and nonzero angular momentum.

As a complete basis set, we have used the Laguerre polynomials and the spherical harmonic as given in Eq. (70). We applied the data collapse method to the ground-state energy and the lowest $l = 1$ energy. Results are shown in Fig. 6a for $l = 0$ and in Fig. 6b for $l = 1$ [93]. One can see clearly that all data for $N = 20, 40, 60, 80, 100$ collapse on one curve.

We note that in analogy with statistical mechanics, each block ($l = 0$ and $l = 1$) of the Hamiltonian matrix could be interpreted as a transfer matrix of a classical pseudosystem. Within this analogy, the lowest eigenvalue is associated with the free energy and the critical point as a first-order phase transition for

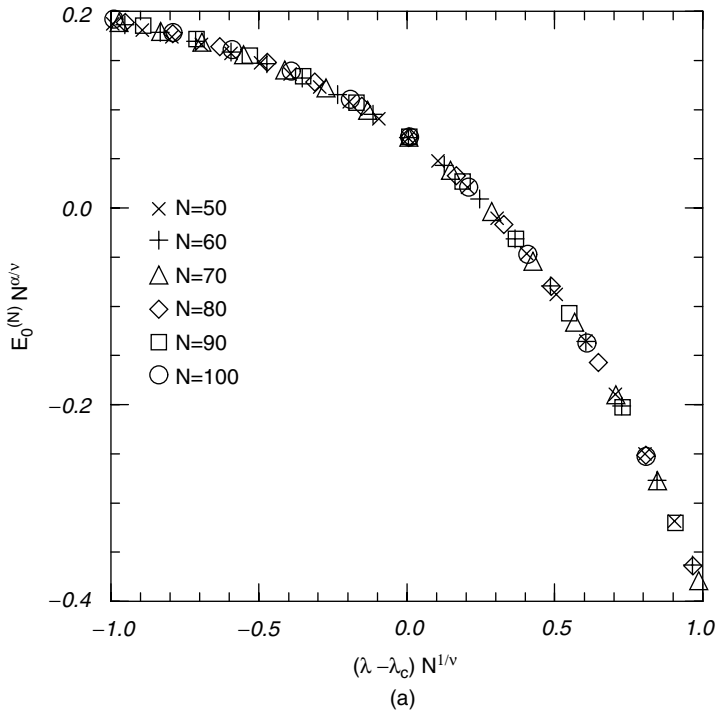

Figure 6. Data collapse for the energy of the Yukawa potential. (a) For the ground state with $\alpha = 2$ and $\nu = 1$. (b) For the lowest $l = 1$ level with $\alpha = 1$ and $\nu = 1/2$.

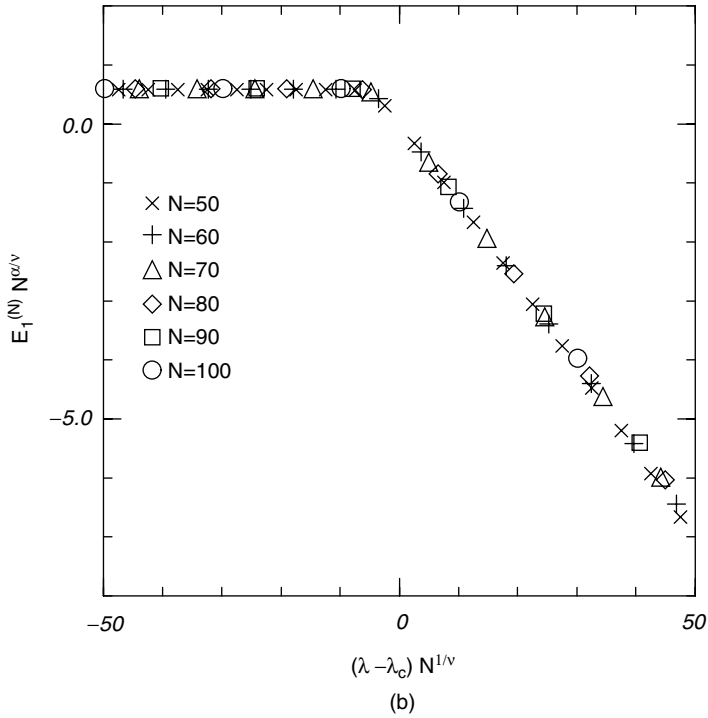

Figure 6 (*Continued*)

$\alpha = 1$ (remember that the α exponent is related to the statistical mechanics $\widehat{\alpha}$ exponent for the specific heat by the relation $\hat{\alpha} = \alpha - 2$), or as a continuous phase transition for $\alpha > 1$. As a result of this analogy, we can use scaling laws from statistical mechanics to be applied to the classical pseudosystem. In particular, for continuous phase transitions we can calculate the spatial dimension d of the pseudosystem using the hyperscaling relation [94]:

$$4 - \alpha = d\nu \tag{75}$$

where d is the spatial dimension of the pseudosystem. Then for $\alpha = 2$ and $\nu = 1$ it gives a spatial dimension $d = 2$. For $l = 1$ there is a first-order phase transition; therefore the relation between the ν exponent and the spatial dimension of the pseudosystem is $d = 1/\nu$ [95], which gives again $d = 2$. The excellent collapse of the curves gives a strong support to the FSS arguments in quantum mechanics [93].

V. QUANTUM PHASE TRANSITIONS AND STABILITY OF ATOMIC AND MOLECULAR SYSTEMS

In this section we will apply the FSS method to obtain critical parameters for few-body systems with Coulombic interactions. Thus, FSS approach can be used to explain and predict stability of atomic and molecular systems.

A. Two-Electron Atoms

In this section we plan to review the analytical properties of the eigenvalues of the Hamiltonian for two-electron atoms as a function of the nuclear charge. This system, in the infinite-mass nucleus approximation, is the simplest few-body problem that does not admit an exact solution, but has well-studied ground-state properties. The Hamiltonian in the scaled variables [96] has the form

$$\mathscr{H}(\lambda) = -\frac{1}{2}\nabla_1^2 - \frac{1}{2}\nabla_2^2 - \frac{1}{r_1} - \frac{1}{r_2} + \frac{\lambda}{r_{12}} = \mathscr{H}_0 + \lambda V \tag{76}$$

where $\mathscr{H}_0$ is the unperturbed hydrogenic Hamiltonian, V is the Coulomb interelectronic repulsion, and λ is the inverse of the nuclear charge Z. For this Hamiltonian, a critical point means the value of the parameter, λ_c, for which a bound-state energy becomes absorbed or degenerate with the continuum.

An eigenvalue and an eigenvector of this Hamiltonian, Eq. (76), can be expressed as a power series in λ. Kato [97] showed that these series have a nonzero radius of convergence. This radius is determined by the distance from the origin to the nearest singularity in the complex plane λ^*. The study of the radius of convergence, λ^*, and whether or not this is the same as the critical value of λ_c, has a long history with controversial results [98–101]. Recently, Morgan and co-workers [102] have performed a 401-order perturbation calculation to resolve this controversy over the radius of convergence of the $\lambda = 1/Z$ expansion for the ground-state energy. They found numerically that $\lambda_c = \lambda^* \sim 1.09766$, which confirms Reinhardt's analysis of this problem using the theory of dilatation analyticity [101]. Ivanov [103] has applied a Neville–Richardson analysis of the data given by Morgan and co-workers and obtained $\lambda_c = 1.09766079$.

The Hamiltonian (76) commutes with the total angular momentum operator $\vec{\mathscr{L}} = \vec{\mathscr{L}}_1 + \vec{\mathscr{L}}_2$. Using a complete λ-independent basis set $\{\Phi_{\mathscr{K},\ell}\}$ with the property

$$\mathscr{L}^2 \Phi_{\mathscr{K},\ell} = \ell(\ell+1)\Phi_{\mathscr{K},\ell} \tag{77}$$

where $\mathscr{K}$ represents all the quantum numbers but ℓ, we can study the spectrum of $\mathscr{H}(\lambda)$ at each block of fixed ℓ. This will allow us to study excited states of the lowest symmetry of each block.

To carry out the FSS procedure, one has to choose a convenient basis set to obtain the two lowest eigenvalues and eigenvectors of the finite Hamiltonian matrix. As basis functions for the FSS procedure, we choose the following basis set functions [104–106]:

$$\Phi_{ijk,\ell}(\vec{x}_1,\vec{x}_2) = \frac{1}{\sqrt{2}}\left(r_1^i\, r_2^j\, e^{-(\gamma r_1+\delta r_2)} + r_1^j r_2^i\, e^{-(\delta r_1+\gamma r_2)}\right) r_{12}^k\, F_\ell(\theta_{12},\mathbf{\Omega}) \qquad (78)$$

where γ and δ are fixed parameters, we have found numerically that $\gamma = 2$ and $\delta = 0.15$ are a good choice for the ground state [87], r_{12} is the interelectronic distance, and $F_\ell(\theta_{12},\mathbf{\Omega})$ is a suitable function of the angle between the positions of the two electrons θ_{12} and the Euler angles $\mathbf{\Omega} = (\Theta,\Phi,\Psi)$. This function F_ℓ is different for each orbital block of the Hamiltonian. For the ground state we have $F_0(\theta_{12},\mathbf{\Omega}) = 1$, and for the $2p^2\ ^3P$ state we have $F_1(\theta_{12},\mathbf{\Omega}) = \sin(\theta_{12})\cos(\Theta)$. These basis sets are complete for each ℓ-subspace [105,106]. The complete wave function is then a linear combination of these terms multiplied by variational coefficients determined by matrix diagonalization [87]. In the truncated basis set at order N, all terms are included such that $N \geq i+j+k$, so the number of trial functions $M(N)$ is

$$M(N) = \frac{1}{12}N^3 + \frac{5}{8}N^2 + \frac{17}{12}N + a_N \qquad (79)$$

where a_N is 1 $(\frac{7}{8})$ if N is even (odd).

By diagonalizing the finite Hamiltonian matrix, one can obtain the lowest two energy eigenvalues as a function of the order of the truncated basis set, $E_0^{(N)}$ and $E_1^{(N)}$. Using the PR equation, Eq. (55), one can look for its fixed point by taking the ratio of these two eigenvalues raised to a power N as a function of λ [8]. Figure 7 shows the crossing points, which are the fixed points of Eq. (55), for $N = 6,7,8,\ldots,13$. The values of the fixed points as a function of N can be extrapolated to the limit $N \to \infty$ by using the Bulirsch and Stoer algorithm [89], which is widely used for FSS extrapolation [4]. The extrapolated values of $\lambda_c = 1.0976 \pm 0.0004$ is in excellent agreement with the best estimate of $\lambda_c = 1.09766079$ [103].

The behavior of the ground-state energy, $E_0^{(N)}$, as a function of λ for different values of N is shown in Fig. 8a. When the value of N approaches the limit, $N \to \infty$, the true ground-state energy bends over sharply at λ_c to becomes degenerate with the lowest continuum at $E_0 = -\frac{1}{2}$. This behavior can be seen in the finite-order approximation: The larger the value of N, the more the energy curve bends toward a constant energy. In virtue of this behavior, we expect the first derivative of the energy with respect to λ to develop a step-like discontinuity at λ_c. The first derivative is shown in Fig. 8b for $N = 6,7,8,\ldots,13$.

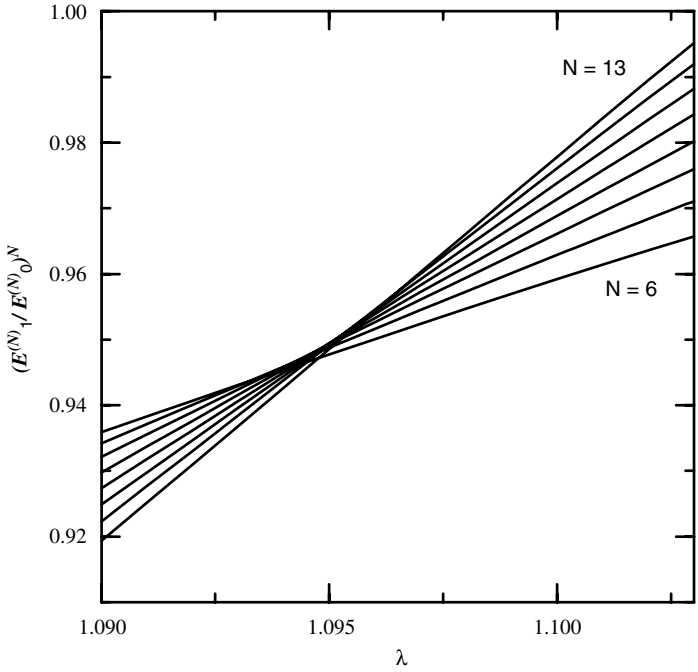

Figure 7. The ratio between the ground-state energy and the second lowest eigenvalue of the two-electron atom raised to a power N as a function of λ for $N = 6, 7, \ldots, 13$.

As expected, the second derivative will develop a delta-function-like behavior as N is getting larger, as shown in Fig. 8c.

The behavior of the ground-state energy and its first and second derivatives resembles the behavior of the free energy at a first-order phase transition. For the two-electron atoms, when $\lambda < \lambda_c$ the nuclear charge is large enough to bind two electrons; this situation remains until the system reaches a critical point λ_c, which is the maximum value of λ for which the Hamiltonian has a bound state or the minimum charge necessary to bind two electrons. For $\lambda > \lambda_c$, one of the electrons jumps to infinity with zero kinetic energy [87].

The convergence law of the results of the PR method is related to the corrections to the finite-size scaling. From Eq. (55) we expect that at the critical value of nuclear charge the correlation length is linear in N. In Fig. 9 we plot the correlation length of the finite pseudosystem (evaluated at the exact critical point λ_c) as a function of the order N. The linear behavior shows that the asymptotic equation [Eq. (60)] for the correlation length holds for very low values of N [87].

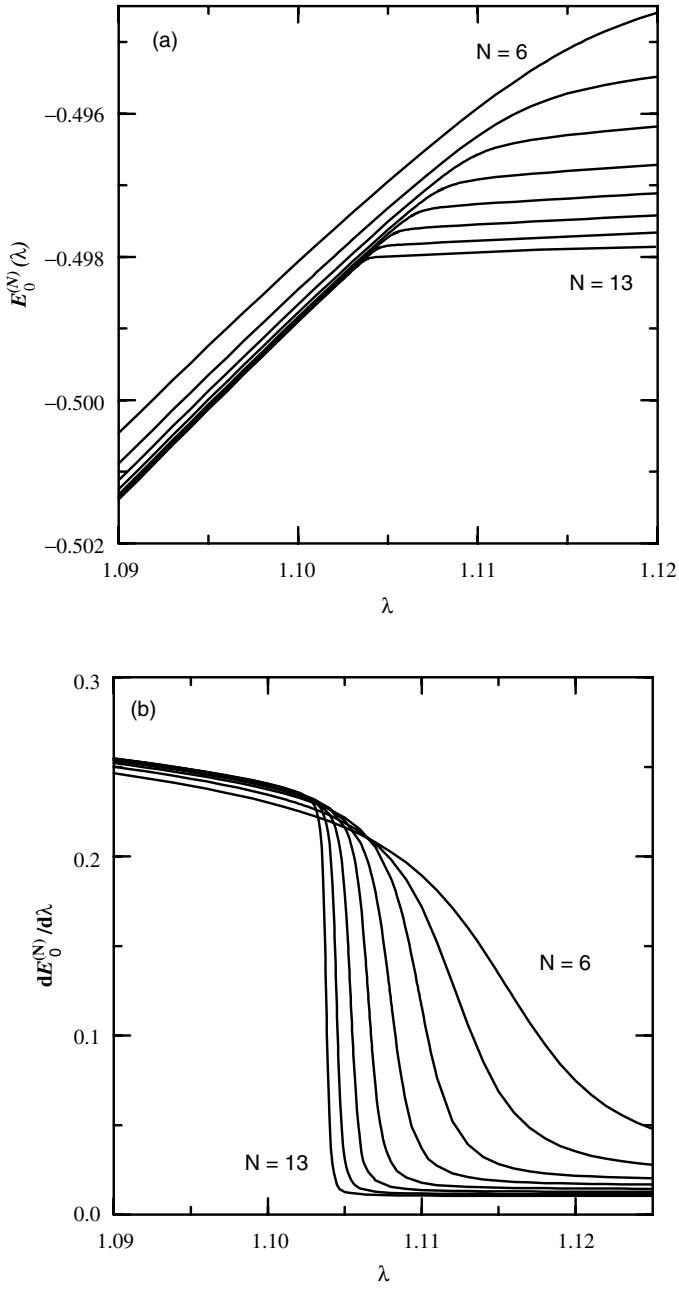

Figure 8. The two-electron atom: Variational ground-state energy (a), first derivative (b), and second derivative (c) as a function of λ for $N = 6, 7, \ldots, 13$.

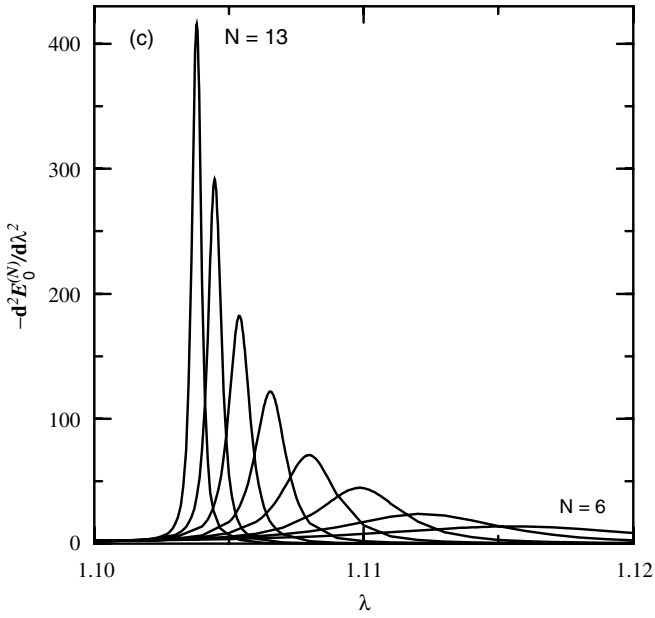

Figure 8 (*Continued*)

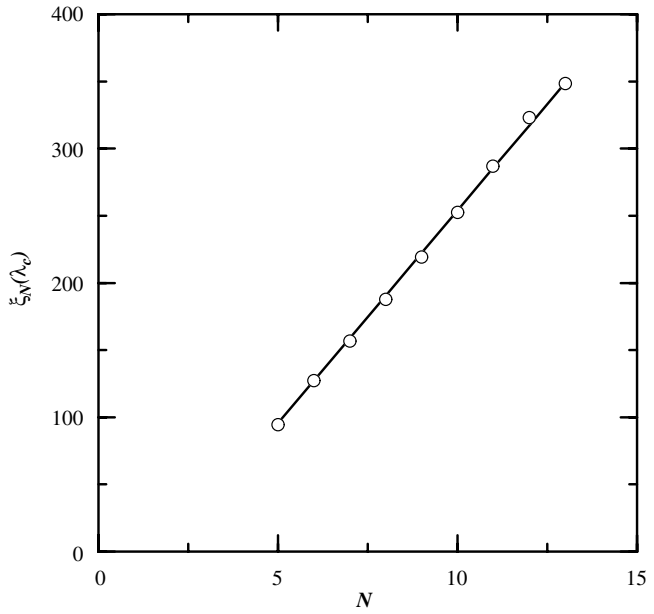

Figure 9. Correlation length for the two-electron atom evaluated at the critical point λ_c as a function of N.

The classical critical exponent ν that describes the asymptotic behavior of ξ at λ_c can be obtained for two different values of N and N' [87]:

$$\frac{1}{\nu} = \frac{\log\left[\left(\frac{d\xi_N}{d\lambda} \Big/ \frac{d\xi_{N'}}{d\lambda}\right)_{\lambda=\lambda^{(N,N')}}\right]}{\log(N/N')} - 1 \tag{80}$$

Using Eq. (80), we can estimate the critical exponent ν. The extrapolated value is $\nu = 1.00 \pm 0.02$, and the correlation length diverges as $\xi \sim |\lambda - \lambda_c|^{-\nu}$.

Hoffmann-Ostenhof et al. [64] have proved that $\mathscr{H}(\lambda_c)$ has a square-integrable eigenfunction corresponding to a threshold energy $E(\lambda_c) = -\frac{1}{2}$. They noted that the existence of a bound state at the critical coupling constant λ_c implies that for $\lambda < \lambda_c$, $E(\lambda)$ approaches $E(\lambda_c) = -\frac{1}{2}$ linearly in $(\lambda - \lambda_c)$ as $\lambda \to \lambda_c^-$. Morgan and co-workers [102] confirmed this observation by their $1/Z$ perturbation calculations. They show that $E(\lambda)$ approaches $E(\lambda_c) = -\frac{1}{2}$ as

$$E(\lambda) = E(\lambda_c) + 0.235(\lambda - \lambda_c) \tag{81}$$

From the FSS equation, Eq. (64), we obtain the ratio of the critical exponents α/ν. The extrapolated value of $\alpha = 1.04 \pm 0.07$, which is in agreement with the observation of Hoffmann-Ostenhof et al. [64].

Having reviewed the results for the critical behavior of the ground-state energy of the helium isoelectronic sequence, we may now consider other excited states. The ground state is symmetric under electronic exchange and has a natural parity, which means that its parity $\mathscr{P} = \mathscr{P}_1\mathscr{P}_2 = (-1)^{\ell_1}(-1)^{\ell_2}$ is equal to $(-1)^{\ell}$ [107], where ℓ_i is the angular momentum number of the ith particle and $|\ell_1 - \ell_2| \le \ell \le \ell_1 + \ell_2$. All the S states have this parity because $\ell_1 = \ell_2 = \ell = 0$. States with $\mathscr{P} = (-1)^{\ell+1}$ will be called *states of unnatural parity*. The triplet $2p^2\ ^3P$ has an unnatural parity.

For the H^- ion, Hill [108] proved that there is only one bound state with natural parity. This result, along with Kato's proof [109] that the Helium atom has an infinite number of bound states, seems to suggest that the critical point for the excited natural states is $\lambda = 1$ [87].

For the unnatural states of the H^- ion, we know from the work of Grosse and Pitner [107] that there is just one unnatural bound state $2p^2\ ^3P$ for $\lambda = 1$. An upper bound of $-0.12535\,a.u.$, which is below the threshold energy $E_T^P = -\frac{1}{8}$, was estimated for this state by Midtdal [100] and Drake [110].

From the variational calculations, the behavior of the energy for the triplet $2p^2\ ^3P$ state as a function of λ is very similar to the one found for the ground state. The curves start to bend over sharply to a constant values as N gets larger.

The true excited-state energy, in the limit $N \to \infty$, bends over sharply at λ_c^P to become degenerate with the lowest continuum at $E_T^P = -\frac{1}{8}$ [87].

Now, the PR equation, Eq. (55), can be applied for the excited state $2p^2\ ^3P$ to obtain a sequence of pseudocritical λ as a function on N, $\{\lambda_P^{(N,N')}\}$. The extrapolated value of this sequence gives $\lambda_c^P = 1.0058 \pm 0.0017$. As far as we know, the only estimate of λ_c for this triplet state is the one given by Brändas and Goscinski [111]. By applying a Darboux function ansatz [112,113] to the E_n's of Midtdal et al. [100] for n up to 27, they found $\lambda_c \sim 1.0048$, which is in good agreement with the FSS result $\lambda_c^P = 1.0058 \pm 0.0017$.

B. Three-Electron Atoms

Using the finite-size scaling method, study of the analytical behavior of the energy near the critical point shows that the open-shell system, such as the lithium-like atoms, is completely different from that of a closed-shell system, such as the helium-like atoms. The transition in the closed-shell systems from a bound state to a continuum resemble a ''first-order phase transition,'' while for the open-shell system the transition of the valence electron to the continuum is a ''continuous phase transition'' [9].

To examine the behavior of open-shell systems, let us consider the scaled Hamiltonian of the lithium-like atoms:

$$\mathscr{H}(\lambda) = \sum_{i=1}^{3}\left[-\frac{1}{2}\nabla_i^2 - \frac{1}{r_i}\right] + \lambda \sum_{i<j=1}^{3} \frac{1}{r_{ij}} \tag{82}$$

where r_{ij} are the interelectron distances and λ is the inverse of the nuclear charge [9].

As a basis function for the FSS procedure, we used the Hylleraas-type functions [105] as presented by Yan and Drake [114]:

$$\Psi_{ijklmn}(\vec{x}_1, \vec{x}_2, \vec{x}_3) = \mathscr{C}\,\mathscr{A}\left(r_1^i\, r_2^j\, r_3^k r_{12}^l\, r_{23}^m\, r_{31}^n\; e^{-\alpha(r_1+r_2)} e^{-\beta r_3}\; \chi_1\right) \tag{83}$$

where the variational parameters, $\alpha = 0.9$ and $\beta = 0.1$, were chosen to obtain accurate results near the critical charge $Z \simeq 2$, χ_1 is the spin function with spin angular moment 1/2

$$\chi_1 = \alpha(1)\beta(2)\alpha(3) - \beta(1)\alpha(2)\alpha(3) \tag{84}$$

$\mathscr{C}$ is a normalization constant, and $\mathscr{A}$ is the usual three-particle antisymmetrizer operator [114].

The finite order of the basis set is allowed to be $i + j + k + l + m + n \leq N$. The maximum value of N was taken to be $N = 8$, which gives a 1589×1589 Hamiltonian matrix [9].

The general algorithm of Bulirsch and Stoer [89] was used to obtain the extrapolated value of the sequences $\lambda^{(N)}$ for lithium-like atoms. The extrapolated value from the PR method was found to be $\lambda_c = 0.48 \pm 0.03$ [9]. In the neighborhood of the critical charge, the ionization energy for lithium-like atoms, $I = E_{Li} - E_{He}$, goes smoothly to zero as a function of λ as shown in Fig. 10. In virtue of the behavior of the energy curves, the first derivative of the ionization energy with respect to λ remain continuous. This behavior is different from that of our previous results for the helium-like atoms [87] where the ionization energy bends sharply to zero at the helium critical $\lambda_c^{(He)} \simeq 1.0976$. The different behavior of the energy as a function of the Hamiltonian parameter, λ, suggests, in analogy with standard phase transitions in statistical mechanics,

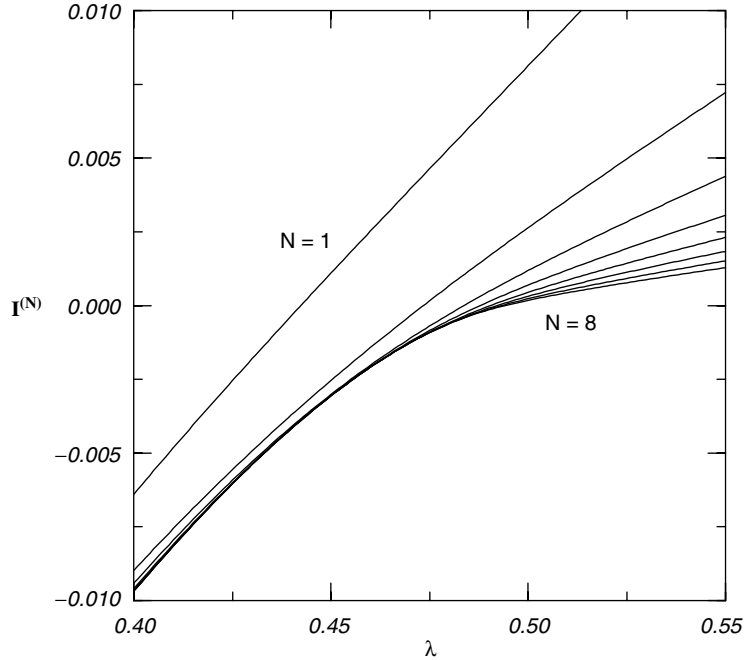

Figure 10. Ionization energy, $I^{(N)}$, for three-electron atoms as a function of λ for $N = 1, 2, \ldots, 8$. ($N = 1$ means that 5 basis functions were used in the calculations, and $N = 8$ means that 1589 basis functions were used.)

that the transition from a ground bound state to a continuum in the helium-like atoms resemble "first-order phase transitions," while for lithium-like atoms the transition is continuous.

In the previous section we showed that for the helium-like atoms the critical exponent for the energy, $E \simeq (\lambda_c - \lambda)^{\alpha}$, $\lambda \to \lambda_c^-$, is equal to one, $\alpha = 1$ [87]. For three-electron atoms, $\alpha \simeq 1.64 \pm 0.05$ and the Hamiltonian does not have a square-integrable wave function at the bottom of the continuum [9]. The behavior of the correlation length $\xi^{(N)}$ for the associated classical pseudo-system [87] as a function of λ is shown in Fig. 11. In this figure, the behavior of the correlation length is characteristic of a continuous phase transition using finite-size scaling method, which goes like an inverse power law in $(\lambda - \lambda_c)$.

Now, let us use the data collapse method to test the hypothesis of finite-size scaling used to obtain the critical parameter for this system and estimate the critical exponent ν for the lithium-like atoms. Using data collapse to the ionization energy of the three-electron atom in its ground state, $I_3(\lambda) = E_0^{Li}(\lambda) -$

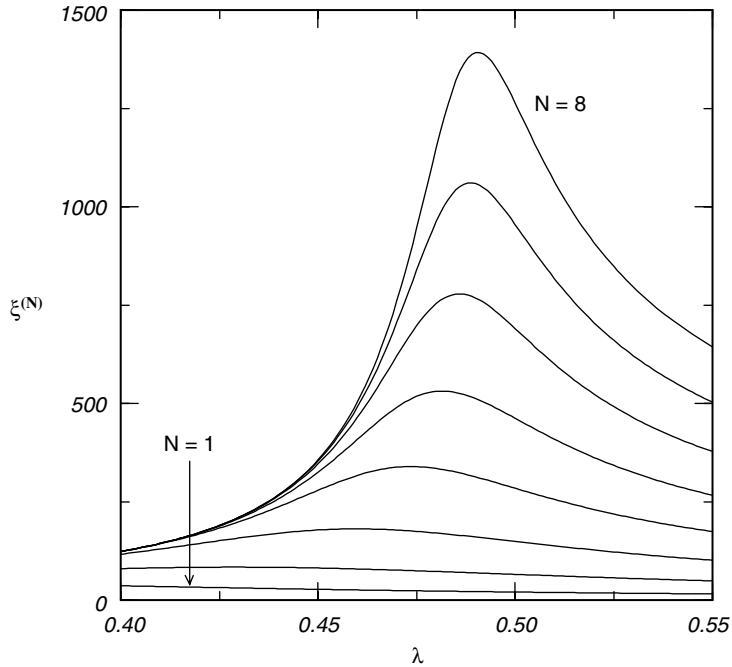

Figure 11. The correlation length, $\xi^{(N)}$, as a function of λ for the three-electron atoms for $N = 1, 2, \ldots, 8$.

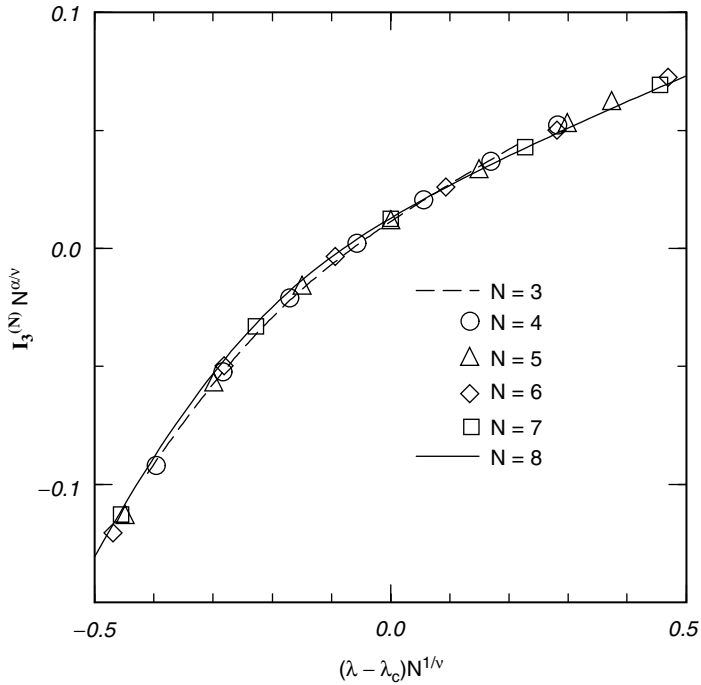

Figure 12. Data collapse for the ionization energy of the three-electron atom with $\alpha = 1.64$ and $\nu_3 = 0.8$.

$E_0^{He}(\lambda)$, one obtains $\nu = 0.8 \pm 0.1$ [93]. The calculations were done with a Hylleraas basis set with $N = 3, 4, \ldots, 8$, which represents up to 1589 Hylleraas functions. The excellent collapse of the curves for I_3 gives a strong support to the FSS hypothesis [93] as shown in Fig. 12.

C. Critical Nuclear Charges for *N*-Electron Atoms

For N-electron atoms, Lieb [115] proved that the number of electrons, N_c, that can be bound to an atom of nuclear charge, Z, satisfies $N_c < 2Z + 1$. With this rigorous mathematical result, only the instability of the dianion H^{2-} has been demonstrated [115]. For larger atoms, $Z > 1$, the corresponding bound on N_c is not sharp enough to be useful in ruling out the existence of other dianions. However, Herrick and Stillinger estimated the critical charge for a neon isoelectronic sequence, $Z_c \simeq 8.77$. Cole and Perdew [116] also confirmed this

result for $N = 10$ by density functional calculations and ruled out the stability of O^{2-}. Using Davidson's tables of energies as a function of Z for atoms up to $N = 18$ [117], one can estimate the critical charges from the equality [118], $E(N, Z_c) = E(N-1, Z_c)$. However, Hogreve used large and diffuse basis sets and multireference configuration interaction to calculate the critical charges for all atoms up to $N = 19$ [119].

Let us consider an N-electron atom with a nuclear charge Z. In atomic units, the potential of interaction between the loose electron and an atomic core consisting of the nucleus and the other $N-1$ electrons tends to $-Z/r$ at small r and to $(-Z+N-1)/r$ at large r. After the scaling transformation $r \to Zr$, the potential of interaction between two electrons is λ/r_{ij} with $\lambda = 1/Z$, and the potential of interaction between an electron and the nucleus is $-1/r_i$. In these scaled units the potential of interaction between a valence electron and a core tends to $-1/r$ at small r and tends to $(-1+\gamma)/r$ with $\gamma = (N-1)\lambda$ at large r. It is easy to see that the model of the form [62]

$$V(r) = -\frac{1}{r} + \frac{\gamma}{r}\left(1 - e^{-\delta r}\right) \tag{85}$$

correctly reproduces such an effective potential both at small r and at large r.

This model has one free parameter that was fitted to meet the known binding energy of the neutral atom and its isoelectronic negative ion [62]. The critical charges are found for atoms up to Rn ($N = 86$). The critical charges are found from the following condition:

$$E_1(\lambda_c) = 0, \qquad Z_c = 1/\lambda_c \tag{86}$$

where E_1 is the extrapolated ionization energy. Results agree (mostly within an accuracy of 0.01 [62]) with both the ab initio multireference configuration interaction calculations of Hogreve [119] and the critical charges extracted by us from Davidson's figures of isoelectronic energies [117].

The goal here is to perform a systematic check of the stability of atomic dianions. In order to have a stable doubly negatively charged atomic ion, one should require the surcharge, $S_e(N) \equiv N - Z_c(N) \geq 2$. We have found that the surcharge never exceeds two as shown in Fig. 13. The maximal surcharge, $S_e(86) = 1.48$, is found for the closed-shell configuration of element Rn and can be related to the peak of electron affinity of the element $N = 85$. Experimental results for negative ions of lanthanides remain unreliable [120,121]. We did not calculate critical charges for lanthanides. Since the electron affinities of lanthanides are relatively small $\leq 0.5\,\text{eV}$ [122,123], we expect that the surcharges will be small.

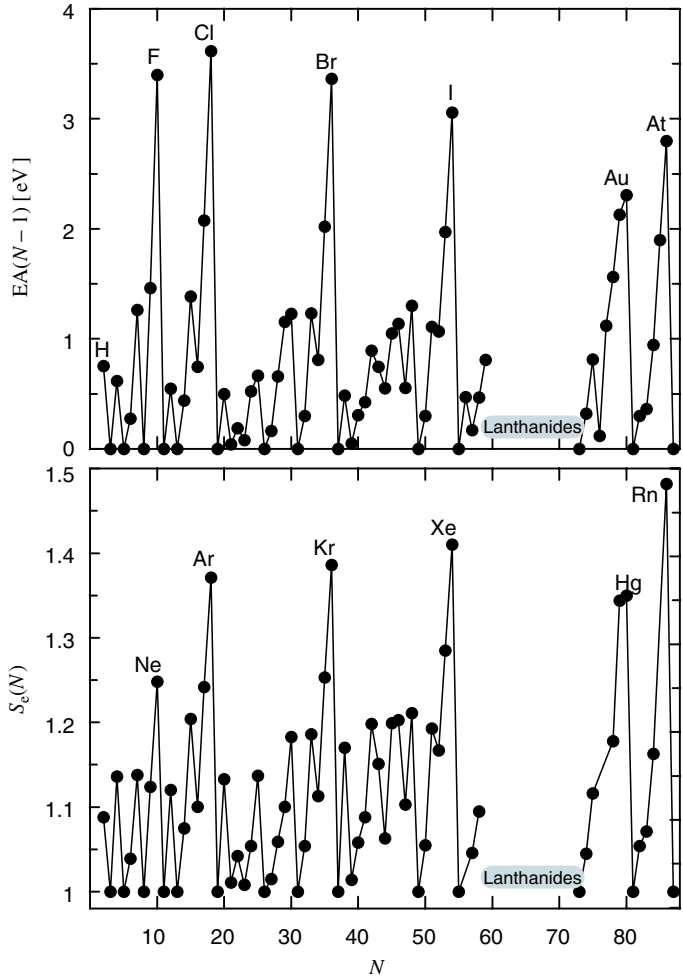

Figure 13. The calculated surcharge, $S_e = N - Z_c$, compared with the experimental electron affinity, $EA(N-1)$, as a function of the number of electrons, N.

Calculation of the critical charges for N-electron atoms is of fundamental importance in atomic physics since this will determine the minimum charge to bind N electrons. Already Kato [97] and Hunziker [124] show that an atom or ion has infinitely many discrete Rydberg states if $Z > N - 1$, and the results of Zhislin [125] show that a negative ion has only finitely many discrete states if $Z \leq N - 1$. Because experiment has yet to find a stable doubly negative atomic ion, Morgan and co-workers [102] concluded that the critical charge obeys the

following inequality: $N-2 \leq Z_c \leq N-1$. The numerical results [62] confirmed this inequality and show that, at most, only one electron can be added to a free atom in the gas phase. The second extra electron is not bound by a singly charged negative ion because of the combined action of the repulsive potential surrounding the isolated negative ion and the Pauli exclusion principle [126]. However, doubly charged atomic negative ions might exist in a strong magnetic field of the order of a few atomic units, where 1 a.u. $= 2.3505 \times 10^9 G$ [62].

Recently, there has been an ongoing experimental and theoretical search for doubly charged negative molecular dianions [12,127]. In contrast to atoms, large molecular systems can hold many extra electrons because the extra electrons can stay well-separated [128]. However, such systems are challenging from both theoretical and experimental points of view. Although several authors [129–132] have studied the problem of the stability of diatomic systems as a function of the two nuclear charges, Z_1 and Z_2, there was no proof of the existence or absence of diatomic molecular dianions. The present approach might be useful in predicting the general stability of molecular dianions.

D. Critical Parameters for Simple Diatomic Molecules

Molecular systems are challenging from the critical phenomenon point of view. In this section we review the finite-size scaling calculations to obtain critical parameters for simple molecular systems. As an example, we give detailed calculations for the critical parameters for H_2^+-like molecules without making use of the Born–Oppenheimer approximation. The system exhibits a critical point and dissociates through a first-order phase transition [11].

The general Hamiltonian for A charged point particles under Coulomb interactions is represented in Cartesian coordinates by [11]

$$\mathscr{H} = \sum_{i}^{A} \frac{\mathbf{P}_i^2}{2M_i} + \sum_{i<j}^{A} \frac{Q_i Q_j}{|\mathbf{R}_i - \mathbf{R}_j|} \tag{87}$$

where $\mathbf{P}_i$, $\mathbf{R}_i = [X_i, Y_i, Z_i]$, M_i and Q_i are the momentum operator, column-vector coordinates, mass, and charge of particle i, respectively.

After separation of the translational motion [133] of the center of mass (CM) $M_0 = \sum_i^A M_i$ the Hamiltonian becomes

$$\mathscr{H} = \sum_{i=0}^{a} \frac{\mathbf{p}_i^2}{2\mu_i} + \frac{1}{2M_1} \sum_{i \neq j}^{a} \mathbf{p}_i \cdot \mathbf{p}_j + \sum_{i<j}^{a} \frac{Q_{i+1} Q_{j+1}}{r_{ij}} \tag{88}$$

where i and j go from 0 to $a = A - 1$; the μ_i are the reduced masses with $\mu_0 = M_0$ and $\mu_i = \frac{M_1 M_{i+1}}{M_1 + M_{i+1}}$; $r_{ij} = |\mathbf{r}_{ij}| = |\mathbf{R}_{i+1} - \mathbf{R}_{j+1}|$ and $r_i = |\mathbf{r}_i| = |\mathbf{R}_{i+1} - \mathbf{R}_1|$; $(\mathbf{r_0})$ is the CM vector, and $(\mathbf{r_1}, \mathbf{r_2}, \ldots, \mathbf{r_a})$ are the vectors of internal coordinates of

particle $2, 3, \ldots, A$, respectively, and $(\mathbf{p_0}, \mathbf{p_1}, \mathbf{p_2}, \ldots, \mathbf{p_a})$ are their corresponding momenta.

Now, an explicit form of the Coulombic interactions V for a quantum system including B electrons and C positive-charged centers (protons) may be written as

$$V = \sum_{0=i<j}^{b} \frac{1}{r_{ij}} - \sum_{i=0}^{b} \sum_{k=b+1}^{a} \frac{Z_k}{r_{ik}} + \sum_{b+1=k<l}^{a} \frac{Z_k Z_l}{r_{kl}} \tag{89}$$

where the indices i, j are for electrons and k, l for protons with $b = B - 1$ and $a = A - 1 = B + C - 1$. The potential V includes electron–electron repulsive terms, electron–proton attractive terms and proton–proton repulsive terms.

However, for one-electron system, $B = 1, b = 0$ and $a = C$, the Z^2-scaled Hamiltonian with $\lambda = Z = Z_k$ becomes [11]

$$\mathscr{H} = \sum_{i=1}^{a} \frac{\mathbf{p}_i^2}{2\mu_i} + \frac{1}{2M_1} \sum_{0=i\neq j}^{a} \mathbf{p}_i \cdot \mathbf{p}_j - \sum_{k=1}^{a} \frac{1}{r_{0k}} + \lambda \sum_{1=k<l}^{a} \frac{1}{r_{kl}} \tag{90}$$

Therefore, the Hamiltonian of simple molecular systems can be represented as

$$\mathscr{H}(\lambda) = \mathscr{H}_0 + V_\lambda \tag{91}$$

where $\mathscr{H}_0$ is λ-independent and V_λ is the λ-dependent part. This Hamiltonian has the correct general form obtained in previous sections for the application of the FSS method to determine the critical value of the parameter λ.

Several investigators have performed calculations on the stability of H_2^+-like systems in the Born–Oppenheimer approximation. Critical charge parameters separating the regime of stable, metastable, and unstable binding were calculated using ab initio methods [134–137]. However, using the finite-size scaling approach, one can show that this critical charge is not a critical point [118]. But, without making use of the Born–Oppenheimer approximation the H_2^+-like system exhibits a critical point.

For H_2^+-like systems, Eq. (88) is used with $\lambda = Z$, $a = C = 2$, $\mu = M/(1 + M)$, and $M = 1836.152701$ a.u. The ground-state eigenfunction can be expanded in the following basis set [138] $\Phi_{(n,m,l)}$:

$$\Phi_{(n,m,l)}(r_1, r_2, r_{12}) = N_0 \phi_n(x) \phi_m(y) \phi_l(z) \tag{92}$$

where N_0 is the normalization coefficient and $\phi_n(x)$ is given in terms of Laguerre polynomials $L_n(x)$:

$$\phi_n(x) = L_n(x)e^{-x/2} \tag{93}$$

The coordinates $x, y,$ and z are expressed in the following perimetric coordinates [139]:

$$\begin{aligned} x &= \frac{\theta}{k_x}(r_1 + r_2 - r_{12}) \\ y &= \frac{\theta}{k_y}(-r_1 + r_2 + r_{12}) \\ z &= \frac{\theta}{k_z}(r_1 - r_2 + r_{12}) \end{aligned} \tag{94}$$

where $k_x = 1 = k_y/2 = k_z/2$ and θ is an adjustable parameter that was chosen to be $\theta = 1.5$.

Calculating the matrix elements of the Hamiltonian in this basis set gives a sparse, real, and symmetric $M(N) \times M(N)$ matrix at order N. By systematically increasing the order N, one obtained the lowest two eigenvalues at different basis lengths $M(N)$. For example, $M(N) = 946$ and 20,336 at $N = 20$ and 60, respectively [11]. The symmetric matrix is represented in a sparse row-wise format [140] and then reordered [141] before triangularizations. The Lanczos method [142] of block-renormalization procedure was employed.

For the ground state of H_2^+-like molecules, the critical point λ_c of $\mathscr{H}(\lambda)$ can be obtained from finite-size scaling calculations. Using the finite-size scaling equation directly, one can obtain the fixed point from Eq. (55). Figure 14 shows the curves $E_1^{(N)}(\lambda)/E_0^{(N)}(\lambda)$ as a function of λ for $N = 31$ up to $N = 60$. By virtue of this behavior, one expect that the first derivative of the energy as a function of λ develops a step-like discontinuity at λ_c as shown in Fig. 15. The crossing points between two different sizes N and $N + 1$ give a series for $\{\lambda^{(N)}\}$. By systematically increasing the order N, one can reach a critical point $\lambda_c = 1.2286 \pm 0.0005$. Here λ_c and the error are estimated using the final minimum and maximum values and their difference over $48 < N < 60$. This value is in agreement with the calculation using the first-order method [11].

For the critical exponent α, starting from the series $\{\alpha^{(N)}(\lambda)\}$ and following the direct approach of finite-size scaling Eq. (67), one obtain the series $\alpha^{(N)}(\lambda_c)$. From these data, the estimated energy critical exponent is $\alpha = 1.000 \pm 0.005$.

Moreover, after calculating the critical exponent α, the critical exponent $\{\nu^{(N)}(\lambda)\}$ is readily given by Eq. (68). The results of the calculations for the $\nu^{(N)}(\lambda)$ series show oscillatory behavior. The data do not reach a limit at N

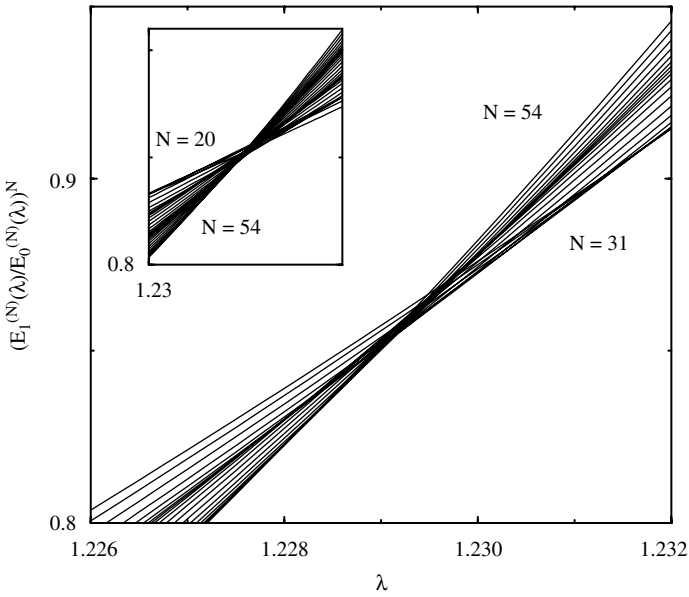

Figure 14. H_2^+-like molecule: The ratio between the ground-state energy and the second lowest eigenvalue raised to a power N as a function of λ $(= Z)$ at $\theta_t = 1.5$ for $N = 31, 32, \ldots, 60$.

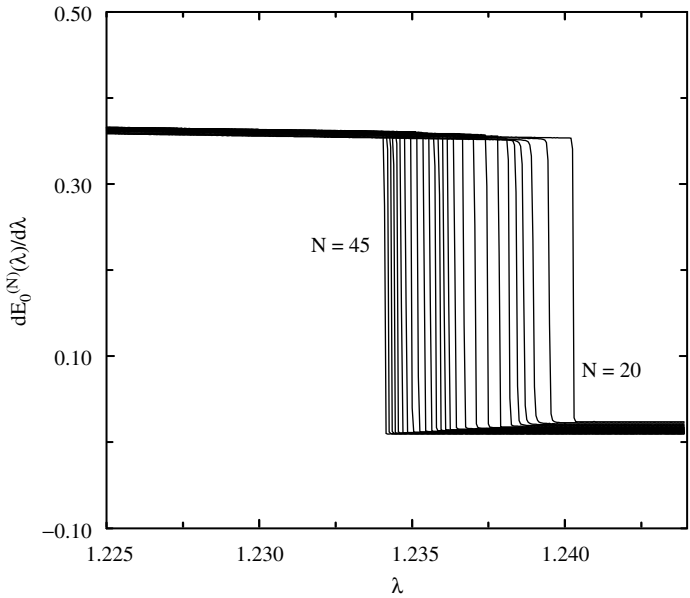

Figure 15. First derivative of the ground-state energy of the ground state of the H_2^+-like molecule as a function of λ $(= Z)$ at $\theta_t = 1.5$ for $N = 20, 21, \ldots, 45$.

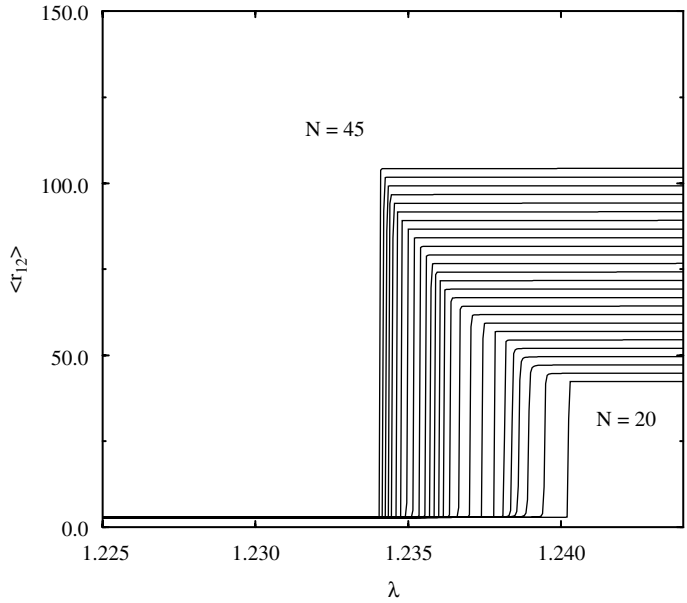

Figure 16. The expectation value of the distance between the two protons $\langle \mathbf{r}_{12} \rangle$ for the H_2^+-like molecule as a function of λ $(= Z)$ at $\theta_t = 1.5$ for $N = 20, 21, \ldots, 45$.

up to 60, but it does show that the correlation exponent is smaller than one and decreases as N increases. The estimated value using the final maximum and minimum points over $48 < N < 60$ is $\nu = 0.3 \pm 0.2$ [11].

From the present calculations, the expectation value of the operator $\mathbf{r}_{12}$ may provide a direct physical picture about the thermodynamic stability and dissociation of H_2^+-like molecules. As shown in Fig. 16, there is a vertical jump of the mean value $\mathbf{r}_{12}$ at λ_c. We note that there are similarities and differences between helium-like atoms and H_2^+-like molecules. In Section V.A of helium-like systems, based on an infinite mass assumption, we show that the electron at the critical point leaves the atom with zero kinetic energy in a first-order phase transition. This limit corresponds to the ionization of an electron as the nuclear charge varies. For the H_2^+-like molecules, the two protons move in an electronic potential with a mass-polarization term. They move apart as λ approaches its critical point and the system approaches its dissociation limit through a first-order phase transition.

Large molecular systems are challenging from the critical phenomenon point of view. In order to apply the finite-size scaling method, one needs to have a complete basis set. The present basis set used for the finite-size scaling calculations is built up on the perimetric coordinates that are only suitable for

the three-body systems, thus restricting the basis set's extension to treat larger molecules. Several types of Gaussian basis sets have been tested. The first one has the following general form:

$$\Psi = (1 + \mathbf{P}_{12}) \sum_{m=1}^{M} e^{-\alpha_m r_1^2 - \beta_m r_2^2 - \gamma_m r_{12}^2} \tag{95}$$

where M is the expansion length, $\mathbf{P}_{12}$ is the exchange operator and α_m, β_m and γ_m are the variational parameters. The finite size scaling results using this basis set were strongly dependent on the initial values of the variational parameters. Another two types of Gaussian basis sets were used have the general form

$$\Psi = (1 + \mathbf{P}_{12}) \left(\sum_{m=1}^{M} e^{-\alpha_m r_1^2 - \beta_m r_2^2 - \gamma_m r_{12}^2} \right) \sum_{k=0}^{N} C_{mk} r_{12}^{2k} \tag{96}$$

where $k \leq N$, N is the order and M is expansion length for a set of given parameters $\{\alpha_m, \beta_m, \gamma_m\}$, and

$$\Psi = (1 + \mathbf{P}_{12}) \left(\sum_{m=1}^{M} e^{-\alpha_m r_1^2 - \beta_m r_2^2 - \gamma_m r_{12}^2} \right) \sum_{i,j,k}^{N} C_{mijk} r_1^{2i} r_2^{2j} r_{12}^{2k} \tag{97}$$

where $i + j + k \leq N$. These Gaussian basis sets are correlated and involve power law terms [133] that are equivalent to the power law terms used in the Laguerre polynomials in Eq. (21). This basis set can be used to recover the previous results and clearly will be suitable for larger diatomic molecules.

Qicun Shi research is still underway to combine FSS with Gaussian basis functions to treat larger molecular systems and also to investigate the effect of external fields on the molecular stability and whether or not one can use this approach to selectively break chemical bonds in polyatomic molecules.

E. Phase Diagram for Three-Body Coulomb Systems

The stability of three-body Coulomb systems is an old problem which has been treated in many particular cases [143–145] and several authors reviewed this problem [146,147]. For example, the He atom $(\alpha e^- e^-)$ and H_2^+ (ppe^-) are stable systems, H^- $(pe^- e^-)$ has only one bound state [108], and the positronium negative ion Ps^- $(e^+ e^- e^-)$ has a bound state [148], while the positron–hydrogen system $(e^- pe^+)$ is unbound and the proton–electron–negative–muon $(pe^- \mu^-)$ is an unstable system [149]. In this section, we show that all three-body *ABA* Coulomb systems undergo a first-order quantum phase transition from the stable phase of *ABA* to the unstable breakup phase of $AB + A$ as their masses and charges varies. Using the FSS method, we calculate the transition line that

separates the two phases. For any combination of the three particles of the form *ABA*, one can read directly from the phase diagram if the system is stable or unstable. Moreover, the transition line has a minimum that leads to a new proposed classification of the *ABA* systems to molecule-like systems and to atom-like systems [66]. This is very important in exploring the resonance spectrum and dynamics of three particles where there is neither an obvious point of reference as the heavy nucleus in H^- nor a line of reference as the internuclear axis in H_2^+. Rost and Wintgen [150] have shown that the resonance spectrum of positronium negative ion Ps^- can be understood and classified with the molecule H_2^+ quantum numbers by treating the internuclear axis of Ps^- as an adiabatic parameter. The current approach gives a systematic classification of all *ABA* systems [66].

Let us consider the stability and quantum phase transitions of the three-body *ABA* Hamiltonian given by Eq. (36). The Hamiltonian, Eq. (36), formally separated the motion of the center of mass and depends linearly on the parameters λ and κ.

We are interested in the study of the critical behavior of the Hamiltonian as a function of both parameters λ and κ. The *ABA* system is stable if its energy is lower than the energy of the dissociation to $AB + A$. The critical behavior and stability of the ground-state energy as a function of λ for $\kappa = 0$ has been previously studied for the two-electron atoms [87] (with $Q = -1$, $M = 1$, $m = \infty$ and $\lambda = 1/q = 1/Z$, where Z is the nuclear charge) and for the hydrogen molecule-like ions [11] (with $q = -1$, $m = 1$, $M = \infty$ and $\lambda = |Q| = Z$).

In order to obtain the stability diagram for the three-body Coulomb systems in the $(\lambda - \kappa)$-plane, one has to calculate the transition line, $\lambda_c(\kappa)$, which separates the stable phase from the unstable one. To carry out the finite-size scaling calculations, the following complete basis set was used [66]:

$$\Phi_{n,m,l}(r_1, r_2, r_{12}) = \phi_n(x)\phi_m(y)\phi_l(z), \qquad \phi_n(x) = L_n(x)e^{-x/2} \tag{98}$$

where L_n is the Laguerre polynomial of degree n and order 0 and $x = \frac{\theta}{k_x}(r_1 + r_2 - r_{12})$, $y = \frac{\theta}{k_y}(-r_1 + r_2 + r_{12})$, and $z = \frac{\theta}{k_z}(r_1 - r_2 + r_{12})$ are the perimetric coordinates [151]. For faster convergence, the parameters $k_x = 1 = k_y/2 = k_z/2$, and $\theta = 1.5$ were chosen.

Solving the Schödinger equation gives a sparse, real, and symmetric $M(N) \times M(N)$ matrix of order N. The symmetric matrix is expressed in a sparse row-wise format, reordered, and LU-decomposed [152]. Then, one employs the block-renormalization Lanczos procedure [153] to obtain the eigenvalues [66]. From the leading two eigenvalues, $E_0^{(N)}(\lambda)$ and $E_1^{(N)}(\lambda)$, one can obtain the correlation length, Eq. (56), for the classical pseudosystem, $\xi_N(\lambda)$. Now we are in a position to apply the phenomenological renormalization equation, Eq. (55), to obtain a sequence of pseudocritical parameters $\lambda_c^{(N)}$ for different values of κ.

The values of the parameter $\kappa = (1 + m/M)^{-1}$ were varied in the interval [0,1] according to the different masses of the combined particles. The values, in atomic units, of the particle masses were taken from Ref. 154: for electron $m_e = 1.0$, for proton $m_p = 1836.1526675$, for deuteron $m_d = 3670.4829550$, for tritium $m_t = 5496.9216179$ [154,155], for muon $m_\mu = 206.7682657$, and for helium $m_{\mathrm{He}} = 7296.299508$.

The numerical results for all *ABA* Coulomb systems show that the ground-state energy is a continuous function of $1.0 \leq \lambda \leq 1.25$ and $0 \leq \kappa \leq 1$, but bends over sharply at λ_c to become degenerate with the scaled lowest continuum at $E_0 = -\frac{1}{2}$. By virtue of this behavior, we expect that the first derivative of the energy with respect to λ to develop a step-like discontinuity at λ_c. $\mathscr{H}(\lambda_c)$ has a square-integrable eigenfunction as κ varies corresponding to a scaled threshold energy $E^{th}(\lambda_c) = -\frac{1}{2}$ [64]. $E(\lambda)$ approaches $E^{th}(\lambda_c)$ linearly in $(\lambda - \lambda_c)$ as $\lambda \to \lambda_c^-$ [64,102].

For the *ABA* Coulomb systems when $1 \leq \lambda \leq \lambda_c$, the ratio of charges is sufficiently small enough to keep the three particles bound and the system at least has one bound state [108]. This situation remains until the system reaches a critical point λ_c, which is the maximum value of λ for which the Hamiltonian has a bound state. For $\lambda \geq \lambda_c$, one of the particles jumps to infinity with zero kinetic energy. In Fig. 17 the transition line, λ_c, is shown as a function of κ. The parameter κ changes between $\kappa = 1$, which corresponds to the H_2^+-like systems in the Born–Oppenheimer approximation, and $\kappa = 0$, which corresponds to the He-like atoms in the infinite mass approximation. Between the two limits $\kappa = 0$ and $\kappa = 1$, there are many stable three-particle systems as shown in the figure. The transition line separates the three-particle systems into stable systems (with at least one bound state) and unstable systems. These numerical results confirm the general properties of the stability domain discussed by Martin [149], and the instability region in the λ–κ plane should be convex. Particularly, the transition curve has a minimum, which occurs at $\kappa_m = 0.35$, and hence all possible bound three-body systems are divided into two branches in the λ–κ plot, one with $0 \leq \kappa < \kappa_m$ and the other with $\kappa_m < \kappa \leq 1$. The two systems closest to κ_m are Ps^- with $\kappa = 0.5$ and $\bar{p}\bar{p}d$ with $\kappa = 0.33$. The window in Fig. 17 shows the two different branches in their ground-state energy as a function of the location of the pseudocritical points $\lambda_c^{(N)}(\kappa)$.

The observation of two different branches leads us to investigate the similarity between the molecule-like systems of the right branch, $\kappa > \kappa_m$, such as the Ps^-, and the atom-like systems of the left branch, $\kappa < \kappa_m$, such as $\bar{p}\bar{p}d$. The parameter κ measures the strength of the mass polarization term, which is due to the motion of the two identical particles with respect to the third particle. The mass polarization term is then a measure of the momentum correlation of the two identical particles with respect to the third particle. If $\kappa \gg \kappa_m$, as in the case of a molecule such as H_2^+, then the light particle with mass m and charge q

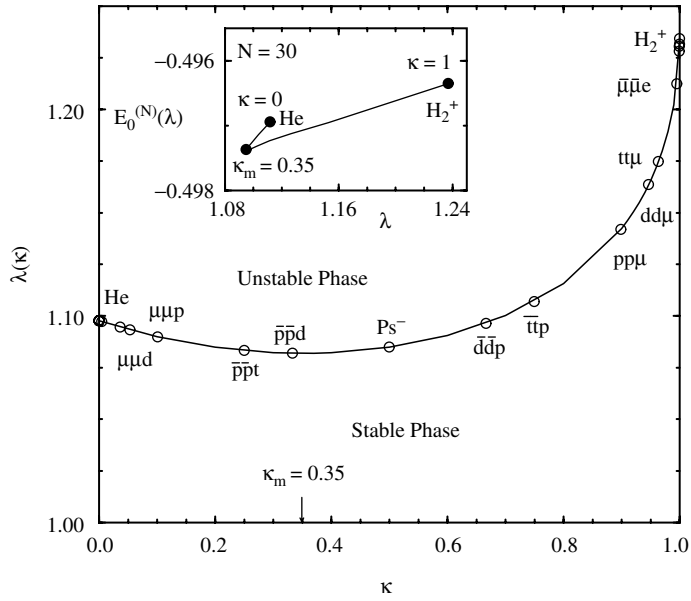

Figure 17. The critical parameter λ_c as a function of κ in the range $0 \leq \kappa \leq 1$. The different three-body systems are shown along the transition line that separates the stable phase from the unstable one. Note the minimum value of $\kappa_m = 0.35$; for $\kappa > \kappa_m$ we have molecule-like systems, while for $\kappa < \kappa_m$ the systems behave like atoms. The inset in this figure shows the two branches in the $(E_0^{(N)} - \lambda)$-plane as κ varies in the interval [0, 1].

tends to stay in the middle of the two heavy particles to achieve bonding, while for $\kappa \ll \kappa_m$, as in the case of the He atom, each light particle with mass M and charge Q is less localized and thus the momentum correlation is smaller. The fact that the resonance spectrum and dynamics of Ps^- $(\kappa = 0.5)$ was understood and classified with the H_2^+ quantum numbers [150] is very encouraging and shows that the above proposed classification might shed some light on a systematic and concise picture of the dynamics of all *ABA* Coulomb systems.

VI. CROSSOVER PHENOMENA AND RESONANCES IN QUANTUM SYSTEMS

In this section we present three different phenomena, resonances, crossover and multicritical points. We will discuss in general the applicability of FSS to resonances, the existence of multicritical points and the definition of the size of the critical region. Application of FSS to a specific Hamiltonian that presents the three phenomena shows the relation between them [156].

A. Resonances

We will study, in particular, resonances that may occur for potentials that have a barrier over the threshold value separating an inner region from an outer region where the potential goes asymptotically to the threshold value. These resonances are known in the literature as *shape-type* [157] or *potential* [158] resonances.

Resonances are not truly bound states, but they are interpreted as metastable states. Because of the boundary conditions of resonances, the problem is not Hermitian even if the Hamiltonian is (that is, for square integrable eigenfunctions). Resonances are characterized by complex eigenvalues (complex poles of the scattering amplitude)

$$E = E_n + \frac{i}{2}\Gamma_n \tag{99}$$

where the real part E_n of an eigenvalue is the energy of the system and the imaginary part Γ_n is the inverse of the lifetime of the corresponding *quasi-bound* state. The corresponding eigenfunctions are nonnormalizable. The classical book by Newton [159] presents an excellent discussion on this subject.

The nature of the resonance states, narrow or broad, crucially depends on the behavior of the corresponding bound eigenvalue in the neighborhood of the threshold. There is no rigorous definition of *narrow* and *broad* resonances, but the former has a long lifetime and is accessible for observation. For a broad resonance, the practical definition of its energy and width becomes a difficult problem [158].

For Hamiltonian (6), as we showed in Section II, if there is a true bound state at the threshold, then the eigenvalue hits the continuum linearly in $(\lambda - \lambda_c)$; that is, in a ''first-order phase transition,'' a bound state and a virtual state coexists at the threshold and a sharp resonance (i.e., $\Gamma_n \ll E_n$) will develop for $\lambda < \lambda_c$. However, if there is no bound state at the threshold, then the eigenvalue merges into the continuum quadratically in $(\lambda - \lambda_c)$—that is, in a ''second-order phase transition.'' The eigenvalue is analytical at $\lambda = \lambda_c$, and a virtual state emerges for $\lambda < \lambda_c$. Therefore, if a resonance appears, it will be a virtual resonance ($E_n < 0$) and will turn to a truly resonance for $\lambda < \lambda_r$, where λ_r is defined by the condition $E_n(\lambda_r) = 0$. Now, $\Gamma(\lambda_r) > 0$ and therefore this kind of resonance comes out broad. That is, for one-dimensional systems and s waves of three-dimensional radial potentials, all resonances, including the most narrow one, are not obtained by a bound–resonance transition mechanism. They are obtained, however, due to the sequence bound–virtual–virtual resonance–resonance transition, where virtual states are associated with (real) negative energies of non-normalizable eigenfunctions and virtual resonances are complex eigenvalues with real parts embedded below the threshold energy; that is, the real parts are negative when the threshold energy is equal to zero.

If a virtual–virtual resonance transition exists, it occurs at λ_v, where $\lambda_r < \lambda_v < \lambda_c$. Such virtual–virtual resonance transition is associated with a branch point with exponent one-half:

$$E_n(\lambda) \sim (\lambda - \lambda_v)^{1/2}, \qquad \lambda \to \lambda_v^+ \tag{100}$$

Note that Eq. (100) is valid only for the real virtual energy.

To illustrate the appearance of resonances when a potential parameter is varied we consider the one-dimensional Hamiltonian [156],

$$\mathscr{H}(a, J) = \frac{p^2}{2} + \left(\frac{x^2}{2} - J\right) e^{-ax^2} \tag{101}$$

where a and J are free parameters (instead λ, we use the usual notation (a, J) for this Hamiltonian [157]). The potential in Eq. (101) exhibits predissociation resonances analogous to those found in diatomic molecules [160,161] and was used as a model potential to check the accuracy of different methods for the calculations of resonances [162,163].

We studied the critical behavior of the eigenfunctions and resonances of the Hamiltonian equation, Eq. (101), using the FSS method described in Section IV. As a basis function for the finite-size scaling procedure, we used the orthonormalized eigenfunctions of the harmonic oscillator with mass equal to 1 and frequency equal to a:

$$\Psi_n(a; x) = \left(\frac{a}{\pi}\right)^{1/4} \frac{1}{\sqrt{2^n n!}} e^{-ax^2/2} H_n(\sqrt{a}x) \tag{102}$$

where $H_n(x)$ are the Hermite polynomials of order n [55].

In order to obtain the matrix elements of the Hamiltonian equation, Eq. (101), we need to calculate the kinetic energy terms

$$\begin{aligned} T_{m,n} &\equiv \langle m \,|\, \frac{p^2}{2} \,|\, n \rangle \\ &= \frac{a}{2}\left[\left(n + \frac{1}{2}\right)\delta_{m,n} - \frac{\sqrt{(n+1)(n+2)}}{2}\delta_{m-2,n} - \frac{\sqrt{(n-1)n}}{2}\delta_{m+2,n}\right] \end{aligned} \tag{103}$$

and the potential energy terms [60]

$$e_{m,n} \equiv \langle m \,|\, e^{-ax^2} | n \rangle = \begin{cases} (-1)^{n+\frac{n+m}{2}} \dfrac{\Gamma\left(\frac{m+n+1}{2}\right)}{\sqrt{2\pi m! n!}}, & m+n \text{ even} \\ 0, & m+n \text{ odd} \end{cases} \tag{104}$$

The other matrix elements, $\langle m \,|\, x^k e^{-ax^2} \,|\, n \rangle$ for any value of k, can be evaluated using the recurrence relations between Hermite polynomials [55]. By diagonalizing the Hamiltonian in the above basis set, we obtained the eigenstates as a function of both parameters a and J.

One of the most powerful tools to study resonances is *complex scaling* techniques (see Ref. 157 and references therein). In complex scaling the coordinate $\vec{x}$ of the Hamiltonian was rotated into the complex plane; that is, $H(\vec{x}) \rightarrow H(\vec{x}\, e^{i\phi/2})$. For resonances that have $\theta_{res} = \tan^{-1}[\mathrm{Im}(E^{(res)})/\mathrm{Re}(E^{(res)})] < \phi$ the wave functions of both the bound and resonance states are represented by square-integrable functions and can be expanded in standard L^2 basis functions.

As an example, the Hamiltonian equation, Eq. (101), with $a = 0.2$ and $J = 0.2$, presents a sharp resonance $E_0^{(res)} \simeq 0.23676931 - i\,0.98613158\,10^{-03}$, and its second resonance is $E_1^{(res)} \simeq 1.2516098 - i\,0.48039784$. Therefore we have $\theta_0 \simeq 0.004 < \pi/10$ and $\pi/10 < \theta_1 \simeq 0.366484 < \pi/5$. In Fig. 18 we

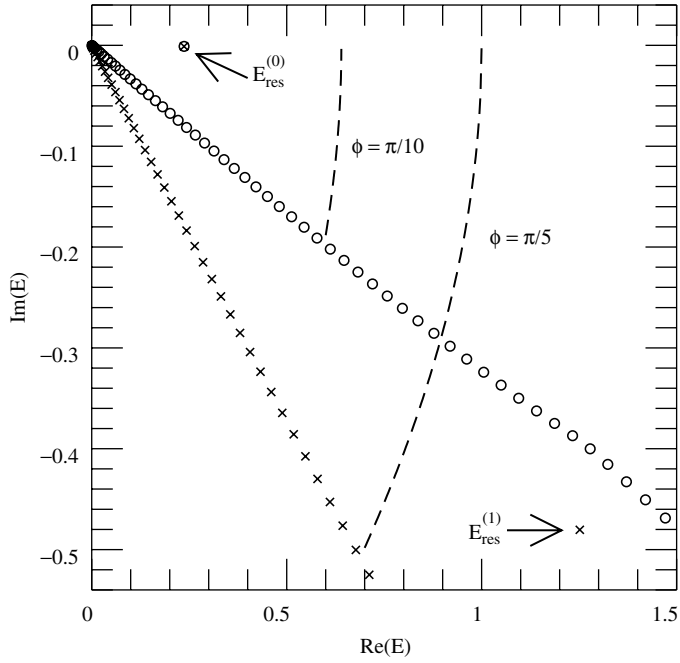

Figure 18. $\mathrm{Im}(E)$ versus $\mathrm{Re}(E)$ for complex-rotated $N = 100$ diagonalization of Hamiltonian equation (101), with $a = 0.2$, $J = 0.2$, $\phi = \pi/10$ (circles), and $\phi = \pi/5$ (crosses). The continuous line occurs for an angle ϕ with the real axis, the first (sharp) resonance appears for both calculations, and the second resonance appears only for $\phi = \pi/5 > \theta_1$.

show all the eigenvalues for $\phi = \pi/10$ and $\phi = \pi/5$ obtained with a complex-rotated 500-function expansion. The rotated continuum forms an angle ϕ with the $\mathrm{Re}(E)$ axis, and two resonances appear as isolated eigenvalues. Note that the sharp resonance appears for both $\phi = \pi/10$ and $\phi = \pi/5$ curves, but the broad resonance cannot be obtained with the $\phi = \pi/10 < \theta_1$ expansion.

It is well known that complex-rotated basis-set expansions give very accurate values for complex energies [157]. But in order to apply FFS to obtain critical exponents, we observe that the scaling function $F_{\mathcal{O}}(x)$ in the scaling relation (60) has to be replaced by a complex function of a ϕ-dependent complex argument for both resonances and bound states. Then it is necessary to introduce new scaling functions and critical exponents. The convergence process with the number N of basis functions is not uniform, and therefore it is very difficult to make extrapolations from the numerical data.

To visualize the phenomenon, the (real) ground-state energy of Hamiltonian (101) with $a = 0.2$ and $J = 1$ is $E_0 \simeq -0.4770651355$. We show in Fig. 19

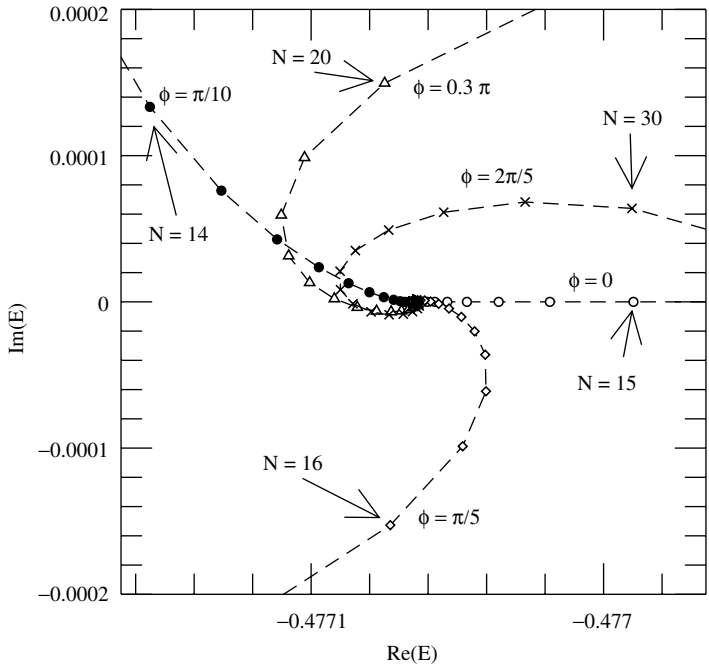

Figure 19. $\mathrm{Im}(E)$ versus $\mathrm{Re}(E)$ for the ground-state energy of Hamiltonian equation (101), with $a = 0.2$, $J = 1$ from complex-rotated diagonalization with $\phi = n\pi/10$; $n = 0(\circ)$, $1(\bullet)$, $2(\diamondsuit)$, $3(\triangle)$, and $4(\times)$ for increasing values of N. The minimum value of N for each angle is indicated by an arrow.

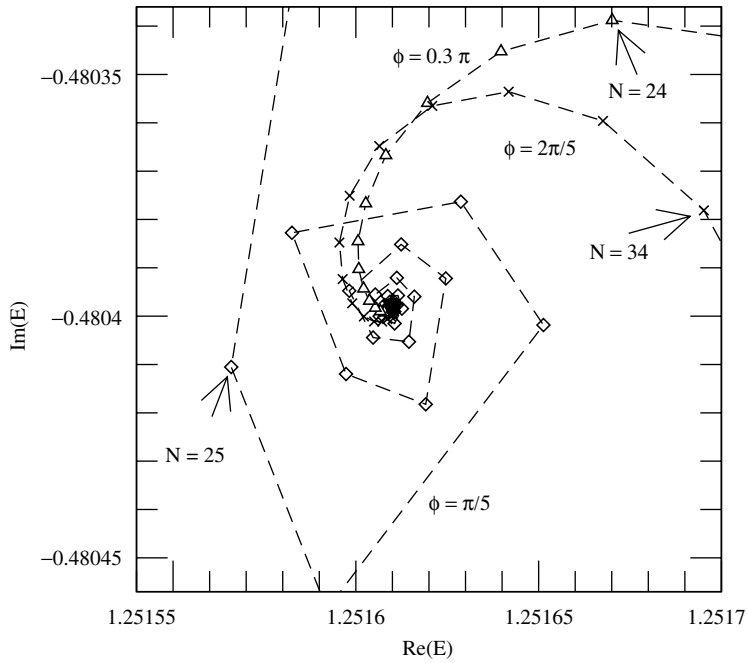

Figure 20. Im(E) versus Re(E) for the second resonance of Hamiltonian Eq. (101) with $a = 0.2$, $J = 0.2$ from complex-rotated diagonalization with $\phi = n\pi/10$; $n = 2(\diamondsuit)$, $3(\triangle)$, and $4(\times)$ for increasing values of N. The minimum value of N for each angle is indicated by an arrow.

Re($E_0^{(N)}$) versus Im($E_0^{(N)}$) for large values of N and five different values of ϕ. It is clear that the process converges, but convergence is not uniform (except for $\phi = 0$) even for $|E_0^{(N)}|^2$. The same picture occurs for resonances, as shown in Fig. 20 for the second resonance $E_2^{(res)} \simeq 1.25161 - i\,0.4803978$ of Hamiltonian (101) with $a = 0.2$ and $J = 0.2$.

To summarize, for our model Hamiltonian, resonances appear after a bound–virtual and a virtual–virtual resonance transition. There is no method to obtain virtual energies using a square-integrable basis set, even in the complex-rotated formalism. Then, at this point we can ask if FSS is a useful method to study this kind of resonance. As we will show in the next subsection, the answer is yes; FSS is a method to obtain near-threshold properties, and with FSS we can characterize the near-threshold resonances by solving the Hermitian (not complex-rotated) Hamiltonian using a real square-integrable basis-set expansion. Moreover, the critical point of the virtual resonance–resonance transition, λ_r, could also be obtained using FSS.

B. Crossover Phenomena

In general, FSS uses scaling laws to describe asymptotic behavior of many-body systems near the threshold energy. An important question is, What is the meaning of the word *near* in the preceding sentence. We will call a crossover phenomena to a phenomena related with the failure of the system to attain its asymptotic scaling regime [94]. Even when crossover phenomena is defined in relation with FSS expansions, as we will see, the *size* of the critical region, where asymptotic regime holds, has possible experimental consequences.

Therefore we are going to examine the critical behavior of the system defined by Hamiltonian (101) using the FSS method described in Section IV. That is, we are going to calculate the values of a and J for which a bound-state energy becomes absorbed or degenerate with a continuum. We define $J_c^{(n)}(a)$ as the value of J for which the n-bound-state energy becomes equal to zero (the threshold energy is set at zero)

$$J_c^{(n)}(a) \equiv \inf_{\{J\}}\{E_n(a,J) < 0\} \tag{105}$$

and the related critical exponent for the energy α_n is given by

$$E_n(a,J) \underset{J\to J_c^{(n)+}}{\sim} (J - J_c^{(n)})^{\alpha_n} \tag{106}$$

The FSS calculation of critical parameters was done using the functions Eq. (102) and the matrix elements Eqs.(103) and (104). The critical line $J_c^{(n)}(a)$ and the critical exponent α_n were calculated using Eqs. (66) and (67).

Figures 21 and 22 show the ''phase diagrams'' $J^{(n)}$ as a function of a for the ground state $n = 0$; and for several states, $n = 0, 1, 2, 3$ and $n = 4$. From a theorem proved by Klaus and Simon [47] valid for Hamiltonian (101), we know that the critical exponent for the energy is $\alpha_n = 2\ \forall n, a > 0$, where n denotes the isolated bound states (see Section II).

In both figures the critical line separates the resonance region from the bound region. As will be shown later, the transition from bound to resonance states go through virtual states. There is no bound states with positive energy for $a > 0$, but there is at least one bound state for $J \geq J^*(a) \equiv 1/(4a)$ [164]. This result shows that the solid line in Fig. 21 does not cross the curve $J^*(a)$ (the Simon line). Numerical results show that $J_c(a)$ goes asymptotically to $J^*(a)$ when $a \to \infty$. For fixed a, the ground state $E_0(J,a)$ is concave, nonincreasing, and continuous as a function of J, and it is decreasing for $J \geq 1/(4a)$ [165].

In the limit $a = 0$, Hamiltonian (101) reduces to the Hamiltonian of a harmonic oscillator with frequency equals one plus a constant J. Then the

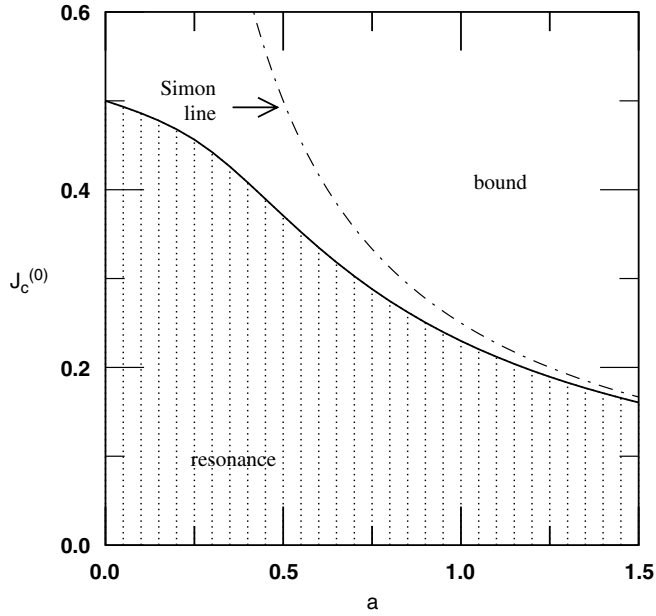

Figure 21. Phase diagram for the ground-state energy of Hamiltonian equation (101), with the critical J as a function of a for $N = 300$. The solid line separates the bound-state energies from the resonance energies. The simon line is shown by the dashed line.

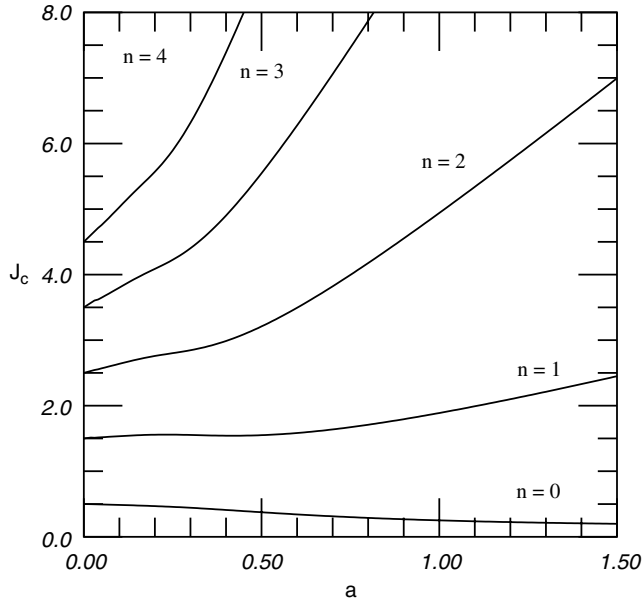

Figure 22. Phase diagram for several energy states of Hamiltonian equation (101), with the critical J as a function of a for $N = 300$.

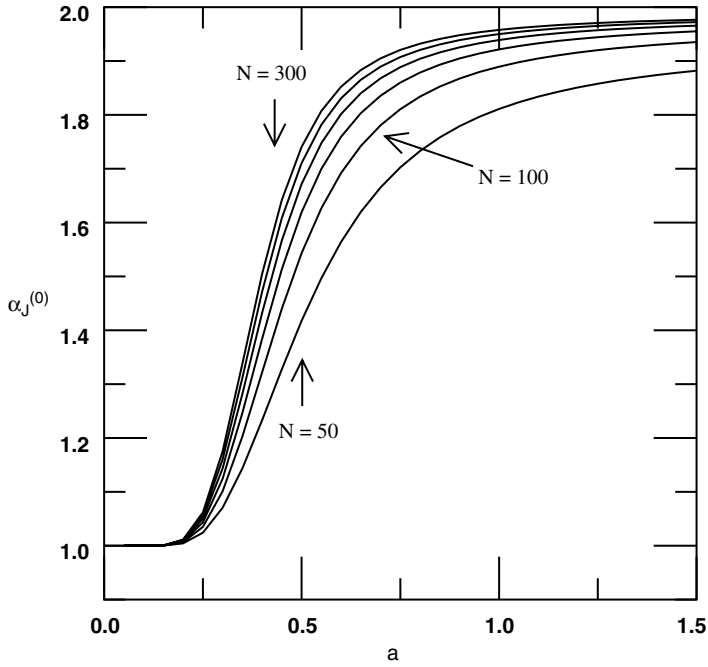

Figure 23. The critical exponent for the ground-state energy of Hamiltonian equation (101) as a function of a for different values of $N = 50, 100, \ldots, 300$.

ground state is $E_0 = 1/2 - J$, and therefore the "critical" value of the parameter is $J_c(a = 0) = 1/2$. Of course, for $a = 0$ there is no "true" critical parameters, because the system has an infinite number of bound states for all values of J. But $J = 1/2$ corresponds to the value of J where the ground-state energy is equal to zero, in agreement with the definition, Eq. (105). For all values of $a > 0$, there are no bound states with positive energy and the phase curve goes continuously to the point $(a = 0, J = 1/2)$ when $a \to 0$. Simple variational bounds show that the slope of the critical line $J_c(a)$ at $a = 0$ is smaller than $-1/8$ (numerical results give a slope value near -0.14).

In Figs. 23 and 24 the critical exponent α is shown as a function of a for the ground state and first even excited state, respectively. A crossover phenomenon appears for this exponent. For large values of a, we obtain $\alpha_n \simeq 2$:

$$E_n(a, J) \underset{J \to J_c^{(n)+}}{\sim} (J - J_c^{(n)})^2, \qquad a \text{ fixed}, \ n = 0, 2 \tag{107}$$

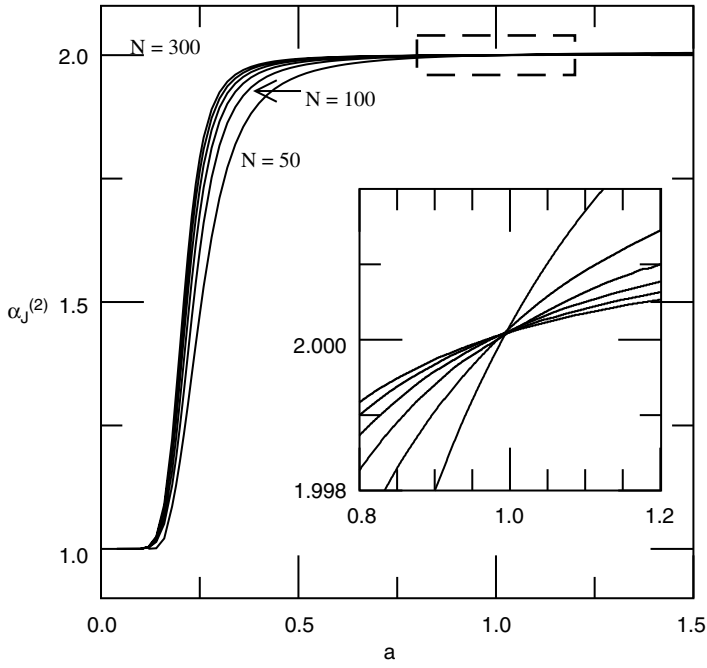

Figure 24. The critical exponent for the first even excited state of Hamiltonian equation (101) as a function of a for different values of $N = 50, 100, \ldots, 300$. Note the appearance of a special point at about $a = 1$.

But for small values of a we have $\alpha_n \simeq 1$

$$E_n(a, J) \underset{J \to J_c^{(n)+}}{\sim} (J - J_c^{(n)}), \qquad a \text{ fixed}, \ n = 0, 2 \tag{108}$$

As a matter of fact, the sharp transition from $\alpha_0 = 2$ to $\alpha_0 = 1$ at $a \sim 0.2$–0.5 in Fig. 23 and at $a \sim 0.1$–0.3 in Fig. 24 is a result of the truncation of the Hamiltonian matrix. As the size of the basis set that is used to represent the Hamiltonian is increased, this transition occurs at $a \to 0$. Namely, the crossover phenomena disappear as the size of the basis set is increased. The exact result for this short-range potential is $\alpha_n = 2$ for $a > 0$, and bound states become virtual states as J is reduced.

For large values of a the exponent is $\alpha = 2$, but for small values of a the exponent is one. The crossover region $\alpha_n: 2 \to 1$ is related to the characteristic length of the finite basis set. The larger the number N of functions, the larger the

region with $\alpha_n^{(N)} \sim 2$. This fact is characteristic of this kind of scaling phenomena. For small values of a the behavior of the system is linear except in a small neighborhood of the critical point, not accessible to a "small" N expansion. This phenomenon has practical consequences: Even the exact transition is continuous with $\alpha = 2$, and for small values of a this asymptotic behavior could not be seen in an experiment if the critical region is smaller than the working appreciation. Therefore an effective exponent $\alpha = 1$ and a sharp resonance with $J_{res} = J_c$ will be observed.

Note that it is not a *true* change in the phase transition (second order to first order). If such a change occurs, a new scaling relation appears and the curves with different N should cross at approximately the same point. This point is a particular case of critical point, called multicritical point in theory of phase transition [25]. Multicritical points in few-body systems is the subject of the next subsection.

C. Multicritical Points

We studied in the previous section several types of phase transition, namely, bound–virtual, bound–resonance, and so on. A characteristic of a phase transition is that two different solutions merge ($\alpha \neq 1$), or coexist at the critical point ($\alpha = 1$). Many-body and multiparameter Hamiltonians could present more complicated transitions, and we will call them multicritical points.

One kind of a multicritical point is a point over a critical line where more than two different states coalesce. The common multicritical points in statistical mechanics theory of phase transition are tricritical points (the point that separates a first order and a continuous line) or bicritical points (two continuous lines merge in a first order line) (see, for example, Ref. 166). These multicritical points were observed in quantum few-body systems only in the large dimension limit approximation for small molecules [10,32]. For three-dimensional systems, this kind of multicritical points was not reported yet.

On the other hand, the two-parameter Hamiltonian, Eq. (101), presents a multicritical point that has, to the best of our knowledge, no classical statistical mechanic analogy [156]. A crossing point appears for α_2 as shown in the window of Fig. 24. This special point is a multicritical point, but with no change in the value of the critical exponent $\alpha_2 = 2$. Even when we are using real square-integrable functions, it is necessary to study virtual and resonances states to explain this crossing point. Because complex rotating methods cannot give the virtual states, we use a numerical integration procedure to solve the Scrhödinger equation.

In order to obtain virtual and resonances states, we have to find eigenfunctions of Hamiltonian (101) which grows up exponentially when $|x| \to \infty$. Using the fact that the potential goes to zero very fast, we can obtain

accurate results for Siegert states [167]. $V(x)$ is assumed to be zero for $|x| > x_0$:

$$V(x) = \begin{cases} \left(\frac{x^2}{2} - J\right)e^{-ax^2}, & |x| < x_0 \\ 0, & |x| > x_0 \end{cases} \tag{109}$$

Following Meyer and Walter [168] instead of the Hamiltonian defined in Eq. (101), we solved the non-Hermitian eigenvalue problem

$$\left[-\frac{1}{2}\frac{d^2}{dx^2} + V(x)\right]\Psi_s(x) = p^2\Psi_s(x) \tag{110}$$

With the energy-dependent boundary conditions at $x = 0, x_0$, we obtain

$$\left.\frac{d\Psi_s}{dx}\right|_{x=0} = 0, \qquad \left.\frac{d\Psi_s}{dx}\right|_{x=x_0} = ik\Psi_s(x_0) \tag{111}$$

where $k = \sqrt{2E}$ and the energy is determinate by the condition

$$p = k \tag{112}$$

Eigenfunction expansions as used in Ref. 168 are not accurate near the critical point. Instead, we developed a shooting point method in order to make a direct numerical integration of Eq. (110) with the condition Eq. (112). Real energies (bound and virtual) were found by bisection methods, and for complex energies it was necessary to combine the Newton–Raphson and grid methods.

As we show in Fig. 25, the multicritical point is related to the crossing of the bound state $n = 2$ line with the resonance $n = 4$ at the critical $\mathrm{Re}(E) = 0$ energy. In this figure we show also the results for $n = 3$. The dashed lines in Fig. 25 describe virtual states. The cusp behavior is a reflection of a transition through a branch point with exponent of one-half from a virtual state associated with a real eigenvalue to a virtual state that is associated with a *complex* eigenvalue.

It is important to emphasize that the $n = 4$ virtual–virtual resonance and resonance curves in Fig. 25 cannot be obtained by using basis-set expansion. Note that the resonance is broad; therefore it cannot be calculated even by using stabilization methods [169]. However, the FSS method gives the localization of the virtual resonance–resonance transition.

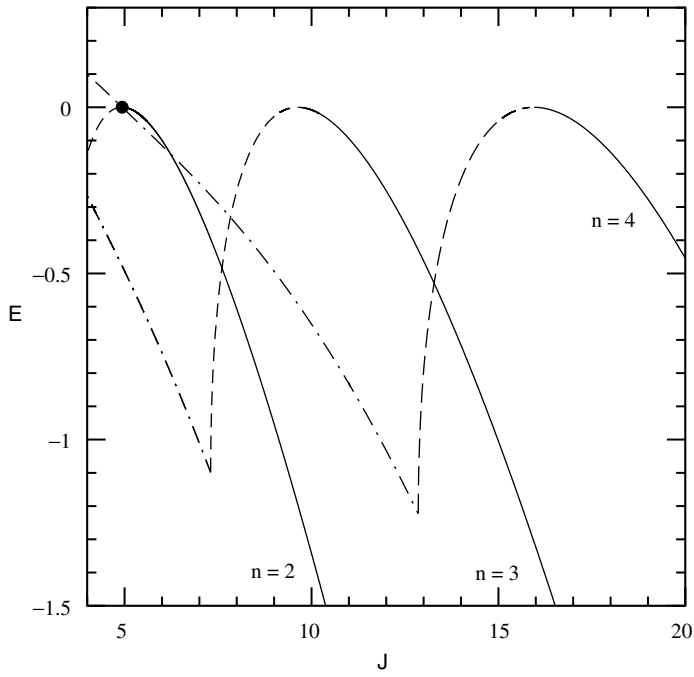

Figure 25. Energies for the states $n = 2$, $n = 3$, and $n = 4$ (continuous line), and virtual state energies (dashed lines) and the real part of the complex energy for $n = 3$ and $n = 4$ (dot–dashed line) of Hamiltonian equation (101), calculated using Eqs. (110) and (111) with $a = a_c = 1.027$, $x_0 = 6$. The multicritical point (•) is located at $(a, J) \sim (1.027, 4.932)$.

VII. SPATIAL FINITE-SIZE SCALING

In previous sections, *finite size* corresponds to the number of elements of a complete basis set used in a truncated Rayleigh–Ritz expansion of an exact bounded eigenfunction of a given Hamiltonian. In this section we present a different FSS approach. In this case, we will confine the system inside a box of size R. The box could be penetrable ($V(r) = 0$ for $r > R$) or impenetrable ($V(r) = \infty$ for $r > R$). Different approaches to solve the Schrödinger equation, for which the system is confined, have been developed from the 1930s to nowadays (Refs. 167 and 170 and references therein). These methods were used as approximations to the corresponding "free system" [170] or to calculate bound states of "true confined systems" [171]. But confining the potential could change drastically the behavior for large value of r; and then, as we see in Section II, the critical properties of the bound states. Therefore these

approximate solutions, capable of giving accurate results for "deep" bound states, could give an erroneous near-threshold behavior even for very large values of R.

We will study the scaling properties by introducing a cutoff radius R in the potential. This cutoff changes the critical exponent of the energy, but, for large values of the cutoff radius, the asymptotic behavior of FSS functions is dominated by the exact critical exponent [26]. The method gives accurate values for critical parameters and critical exponents.

We will develop the theory for one-body central potentials described by Eq. (20), confined to a penetrable box. The main difference between a penetrable and an impenetrable box is the boundary condition at $r = R$. The former has the advantage that it is useful for calculation of bound states, but also for resonance and virtual states.

We will use the fact that the potential goes to zero for $r \to \infty$ to introduce the scaling length R defined for a compact support potential $V_R(\lambda; r)$ as

$$V_R(\lambda; r) = \begin{cases} \lambda V(r) + \dfrac{(\delta - 1)(\delta - 3)}{8r^2} & \text{if } r \leq R \\ 0 & \text{if } r > R \end{cases} \tag{113}$$

Replacing the potential plus the centrifugal term in Eq. (20) by potential (113) gives

$$\mathscr{H}_R(\lambda; r)\Phi_R(\lambda; r) = \left[-\frac{1}{2}\frac{d^2}{dr^2} + V_R(\lambda; r)\right]\Phi_R(\lambda, r) = E_R(\lambda)\Phi_R(\lambda; r) \tag{114}$$

with the boundary conditions $\Phi_R(\lambda; r = 0) = 0$, and $d\ln(\Phi_R(\lambda; r))/dr$ is continuous at $r = R$.

Hamiltonian (114) could be solved with a prefixed precision using the Siegert method [167]. Consequently, the scaling ansatz also gives a powerful numerical tool useful for calculating critical parameters related to the bound states, resonances, and virtual states [167,172].

As we pointed out in Section II, for $\delta = 3$, a Hamiltonian with a compact support potential has a critical exponent $\alpha = 2$ and the energy is analytical at the critical point defined by the condition $E_R(\lambda_R) = 0$. Therefore near the critical point $\lambda = \lambda_R$ of Hamiltonian (114) the asymptotic form of the lowest eigenvalue is

$$E_R(\lambda) \sim a_R\,(\lambda - \lambda_R)^2 \qquad \text{for} \quad \lambda \to \lambda_R,\ a_R \neq 0\ \forall\ R < \infty \tag{115}$$

where $E_R(\lambda)$ corresponds to a bound (virtual) state if $\lambda > (<)\lambda_R$.

We will assume that the ground-state energy of the Hamiltonian (20) has a critical exponent $\alpha \neq 2$ (for example, a short-range potential $V(r)$ and $2 < \delta \neq 3$). The main hypothesis of the spatial finite-size scaling (SFSS) ansatz, which makes the different values of α compatible, is that the coefficient a_R, analytical for finite values of R, has to develop a singularity at the exact critical value λ_c when $R \to \infty$ as

$$a_R \sim -\frac{a}{|\lambda_c - \lambda_R|^{\eta}} \qquad \text{for} \quad R \to \infty \tag{116}$$

where a is a positive constant. Then, the asymptotic behavior of the energy near λ_R for large values of R is

$$E_R(\lambda) \sim -a \frac{(\lambda - \lambda_R)^2}{|\lambda_c - \lambda_R|^{\eta}} \tag{117}$$

Therefore, we can evaluate the asymptotic expression of the energy (117) at $\lambda = \lambda_c$:

$$E_R(\lambda_c) \sim -a\,|\lambda_c - \lambda_R|^{2-\eta} \tag{118}$$

This relation gives us the correction to the finite-size critical exponent obtaining the exact α exponent for Hamiltonian (20) as

$$\alpha = 2 - \eta \tag{119}$$

In a very different context, in statistical mechanics theory of critical phenomena, corrections to classical exponents are calculated using a systematic series of mean field approximations. In this case, the deviation η from the mean-field value of a critical exponent is called *coherent anomaly* [173].

Remember that $E_R(\lambda)$ in Eqs. (115)–(118) corresponds to a bound state if $\lambda_R < \lambda_c$ and corresponds to a virtual state if $\lambda_R > \lambda_c$. Note that there is no other formal difference between bound and virtual states other than the sign in the logarithmic derivate of the wave function at $r = R$. Therefore there are no technical problems related with this fact. A relation between λ_R and λ_c can be established for compact support potentials. In this case, using variational arguments, we obtain

$$\lambda_R(\delta) \begin{cases} > \lambda_c & \text{if } \delta < 3 \\ = \lambda_c & \text{if } \delta = 3 \\ < \lambda_c & \text{if } \delta > 3 \end{cases} \tag{120}$$

Generally, η, λ_c, λ_R, and a in Eqs. (118) and (119) are unknown parameters. In order to calculate them, we will study asymptotic expressions of diverse magnitudes for large values of the cutoff radius R.

We assume that the critical parameter for Hamiltonian (114) goes to the exact critical parameter for Hamiltonian (20) for large values of R in the form

$$\lambda_R \sim \lambda_c - \frac{\Delta}{R^{\mu}} \qquad \text{for} \quad R \to \infty \tag{121}$$

where Δ is a positive constant and μ is an unknown scaling exponent. The energy at $\lambda = \lambda_c$ Eq. (118) takes the form

$$E_R(\lambda_c) \sim -\frac{\text{constant}}{R^{(2-\eta)\mu}} \qquad \text{for} \quad R \to \infty \tag{122}$$

We can calculate the energy for two different values of R, and the logarithm of the quotient gives

$$\ln\left(\frac{E_{R_1}(\lambda_c)}{E_{R_2}(\lambda_c)}\right) \sim (2-\eta)\mu \ln\left(\frac{R_2}{R_1}\right) \qquad \text{for} \quad R_1, R_2 \to \infty \tag{123}$$

In order to obtain a second relation between the exponents α and μ using the Hellmann–Feynman theorem, Eqs. (23) and (117), we have

$$\frac{\partial E_R(\lambda)}{\partial \lambda} = \left\langle \frac{\partial \mathscr{H}_R}{\partial \lambda} \right\rangle \sim -2a \frac{(\lambda - \lambda_R)}{|\lambda_c - \lambda_R|^{\eta}} \tag{124}$$

In a similar way, we calculate this quantity for different values of R, and the quotient gives

$$\ln\left(\frac{\frac{\partial}{\partial\lambda} E_{R_1}(\lambda)}{\frac{\partial}{\partial\lambda} E_{R_2}(\lambda)}\right)\Bigg|_{\lambda=\lambda_c} \sim (1-\eta)\mu \ln\left(\frac{R_2}{R_1}\right) \qquad \text{for } R_1, R_2 \to \infty \tag{125}$$

Now, we can eliminate the exponent μ by defining a function $\Gamma(R_1, R_2; \lambda)$ as

$$\Gamma(R_1, R_2; \lambda) = \ln\left(\frac{E_{R_1}(\lambda)\left(\frac{\partial}{\partial\lambda} E_{R_2}(\lambda)\right)^2}{E_{R_2}(\lambda)\left(\frac{\partial}{\partial\lambda} E_{R_1}(\lambda)\right)^2}\right) \Bigg/ \ln\left(\frac{E_{R_1}(\lambda)\,\frac{\partial}{\partial\lambda} E_{R_2}(\lambda)}{E_{R_2}(\lambda)\,\frac{\partial}{\partial\lambda} E_{R_1}(\lambda)}\right) \tag{126}$$

In particular, for $\lambda = \lambda_c$ we have

$$\Gamma(R_1, R_2; \lambda_c) = \eta \qquad \text{for} \quad R_1, R_2 \to \infty \tag{127}$$

independent of the values of R_1 and R_2. Therefore, two curves calculated with different values of R will cross at the same point $\lambda = \lambda_c$. The value of the function Γ at this point is the critical exponent η. Actually, this is an asymptotic result, and we will have to calculate a set of values $\{\lambda_c^{(i)}, \eta^{(i)}\}_{i=1,N}$ for different values of R. Final estimation of (λ_c, η) has to be obtained by performing an extrapolation of the data for $1/R \to 0$ as we did in previous sections.

The numerical approach is as follows: Take $\{R_i\}$ $i = 1, \ldots, N$ an arbitrary set of (large) values of R, and let $\Delta \ll R_i$ be a fixed parameter. We can obtain a set of values $\{\lambda_c^{(i)}, \eta^{(i)}\}_{i=1,N}$ by using Eq. (127) as

$$\Gamma(R_i - \Delta, R_i; \lambda_c^{(i)}) = \Gamma(R_i, R_i + \Delta; \lambda_c^{(i)}) = \eta^{(i)} \tag{128}$$

In previous sections the FSS parameter was a discrete variable, the number of functions in a basis-set expansion. In this case the most accurate results were obtained by searching for crossing points of curves with minimum difference between the FSS parameters (in general, 1; or 2 for problems with parity effects). In the present case, the parameter R is a real variable. Therefore, the minimum difference between parameters is given by the limit $\Delta \to 0$. This limit introduces derivatives of the functions $E_R(\lambda)$ and $\partial E_R(\lambda)/\partial\lambda$ with respect to R. In practice the derivatives have to be calculated numerically, and then it is convenient to use a finite value of Δ, which is fixed by numerical stability studies.

To illustrate the method, we apply SFSS to the usual spherical square well of width $r_0 = 1$ and depth equal to -1, and then the potential Eq. (113) takes the form

$$V_R(\lambda; r) = \begin{cases} -\lambda + \dfrac{(\delta-1)(\delta-3)}{8r^2} & \text{if } r \le 1 \\ \dfrac{(\delta-1)(\delta-3)}{8r^2} & \text{if } 1 < r \le R \\ 0 & \text{if } r > R \end{cases} \tag{129}$$

In this case, the exponent is $\alpha = 2$ for finite values of R and for all values of δ. The exact critical exponent α for $R = \infty$ obeys Eq. (24).

According to Eq. (120), we have to calculate bound-state energies for $\delta > 3$ and virtual-state energies for $2 < \delta < 3$. The Siegert method [167] assumes the exact boundary conditions at $r = 0$ and $r = R$ and gives exact results for the Hamiltonian equation (114). A Siegert state is a solution of the Schrödinger equation (114) defined for $0 \le r \le R$ with the boundary conditions $\Phi_R(\lambda; r = 0) = 0$ and $\Phi_R(\lambda; r = R) = \mp k\Phi'_R(\lambda; r = R)$, where $k = \sqrt{-2E_R}$ and the upper (lower) sign is for bound (virtual) states.

The usual technique is to perform a numerical integration of Eq. (114) using boundary conditions at $r = 0$ and searching for the eigenvalue $E_R(\lambda)$ by the shooting method applied iteratively until the boundary condition at $r = R$ is obtained. For the potential equation (129), we will write down the exact transcendental equation for the energy for all values of R, δ, and λ, and no numerical integration is needed.

The (unnormalized) lowest-energy wave function of Hamiltonian (114) with the potential (129) is

$$\Phi_R(\lambda; r) = \begin{cases} \sqrt{r}\, J_{\frac{\delta-2}{2}}(\kappa r) & \text{if } r \leq 1 \\ \sqrt{r}\left(A\, I_{\frac{\delta-2}{2}}(kr) + B\, K_{\frac{\delta-2}{2}}(kr)\right) & \text{if } 1 < r \leq R \end{cases} \tag{130}$$

where $\kappa = \sqrt{2(\lambda + E_R)}$ and $J_\nu(z)$, $I_\nu(z)$, and $K_\nu(z)$ are Bessel functions of the first kind and modified Bessel functions of the first and third kind, respectively [55]. Continuity of the logarithmic derivative at $r = 1$ plus the Siegert boundary condition at $r = R$ give the transcendental equation for the eigenvalues

$$\begin{aligned} &\left[I_{\frac{\delta-2}{2}}(kR) + 2kR\left(\pm I_{\frac{\delta-2}{2}}(kR) + I'_{\frac{\delta-2}{2}}(kR)\right)\right]\left[kK'_{\frac{\delta-2}{2}}(k)\, J_{\frac{\delta-2}{2}}(\kappa) - \kappa\, J'_{\frac{\delta-2}{2}}(\kappa) K_{\frac{\delta-2}{2}}(k)\right] \\ &\quad = \left[K_{\frac{\delta-2}{2}}(kR) + 2kR\left(\pm K_{\frac{\delta-2}{2}}(kR) + K'_{\frac{\delta-2}{2}}(kR)\right)\right] \\ &\qquad \times \left[kI'_{\frac{\delta-2}{2}}(k)\, J_{\frac{\delta-2}{2}}(\kappa) - \kappa\, J'_{\frac{\delta-2}{2}}(\kappa) I_{\frac{\delta-2}{2}}(k)\right] \end{aligned} \tag{131}$$

where the prime ($'$) means derivatives with respect to the argument, the upper signs give bound-state energies, and the lower signs give virtual state energies. The critical parameter λ_R is obtained taking the limit $E_R \to 0$ in Eq. (131). Using standard relations between Bessel functions and their derivatives [55], we get

$$(\delta - 1)\, R^{\delta-2} J_{\frac{\delta-4}{2}}\left(\sqrt{2\lambda_R}\right) - (\delta - 3)\, J_{\frac{\delta}{2}}\left(\sqrt{2\lambda_R}\right) = 0 \tag{132}$$

We look for numerical solutions of Eq. (128) with different values of Δ. Results are numerically stable in an acceptable range, and the plots we show here were done with $\Delta = 1$.

SFSS gives corrections to critical exponents and also very accurate estimations of the critical parameter λ_c. In Fig. 26 we plot λ_c, $\lambda_{R=10}$, and $\lambda_c^{R=10}$ versus δ for small values of δ. Note the discrepancy between the exact $R = \infty$ and $R = 10$ lines; the curve obtained from SFSS with $R = 10$ is indistinguishable from the exact $R = \infty$ line at the graphic resolution.

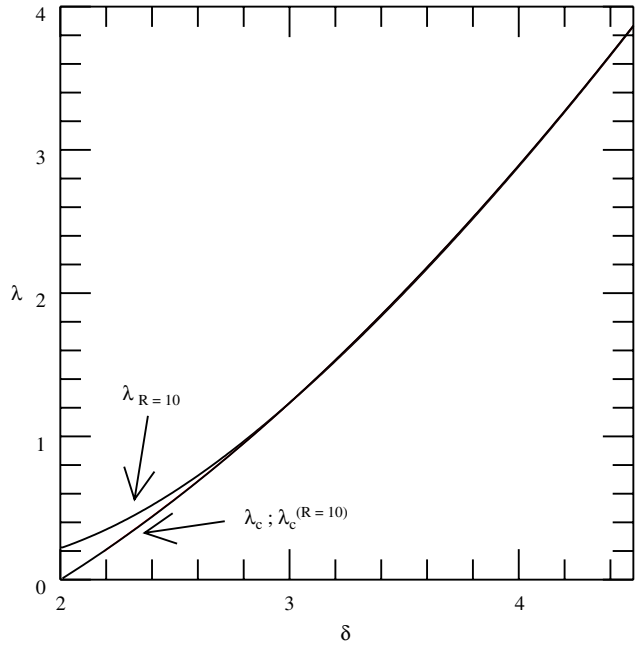

Figure 26. Exact values of λ_c for $R = \infty$ and SFSS calculations of $\lambda_c^{(R=10)}$ (indistinguishable lines) and $\lambda_{R=10}$ as a function of δ for the minimum energy state of the square-well potential.

In Fig. 27 we compare the exact values of the exponent $\alpha(\delta)$ given in Eq. (24) and $\alpha^{(R=20)}$. As expected, we obtained good numerical results except near $\delta = 4$, where the exact exponent has logarithmic deviations and the curve is nondifferentiable. This zone around $\delta = 4$ is magnified in Fig. 28, comparing the exact exponent with the approximations obtained with $R = 10, 20, 30, 40,$ 50. Note from Fig. 26 that the values obtained for $\lambda_c^{(R)}$ are accurate even near $\delta = 4$.

For the important case of odd values of δ, corresponding to three-dimensional l waves $l = 0, 1, 2, \ldots$ for $\delta = 3, 5, 7, \ldots$, the Bessel functions reduce to the usual trigonometric and hyperbolic functions times powers of r [55]. In this case, everything but the solution of the transcendental equation for the energy can be done analytically. The advantage is that we can go further to very large values of R, and the convergence for $R \to \infty$ could be studied without any extrapolation process.

In particular, we study the case $\delta = 5$ corresponding to the three-dimensional ($l = 1$) waves. The exact values of the critical parameters are $\lambda_c = \pi^2/2 \simeq 4.9348022$ and $\alpha = 1$.

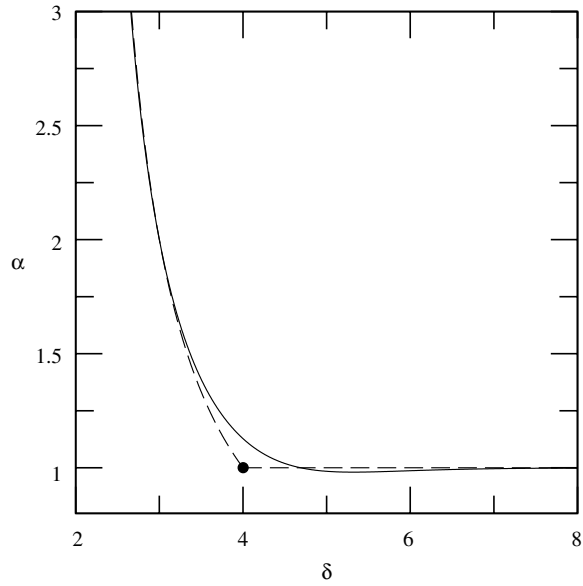

Figure 27. Exact values of α for $R = \infty$ (dashed line) and SFSS calculations of $\lambda^{(R=20)}$ (continuous line) as a function of δ for the minimum energy state of the square-well potential. The point where the exponent has a logarithmic deviation $\alpha(\delta = 4) = 1_{\log}$ is shown by a dot.

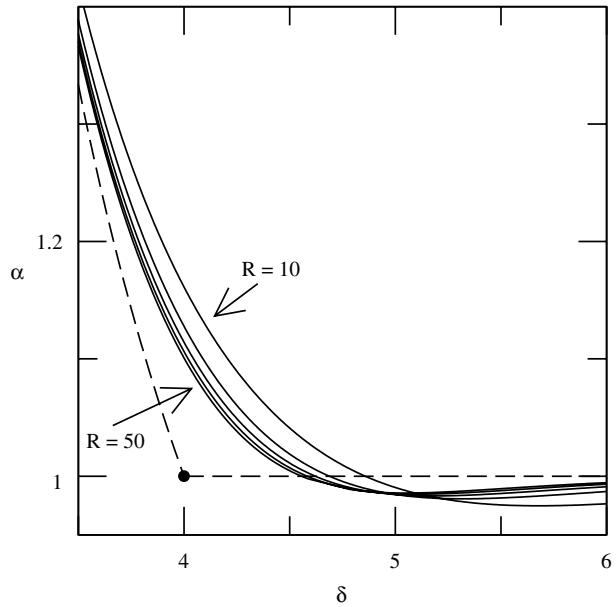

Figure 28. Exact values of α for $R = \infty$ (dashed line) and SFSS calculations of $\lambda^{(R)}$ for $R = 10, 20, 30, 40, 50$ (continuous lines) as a function of δ for the minimum energy state of the square-well potential. The point where the exponent has a logarithmic deviation $\alpha(\delta = 4) = 1_{\log}$ is shown by a dot.

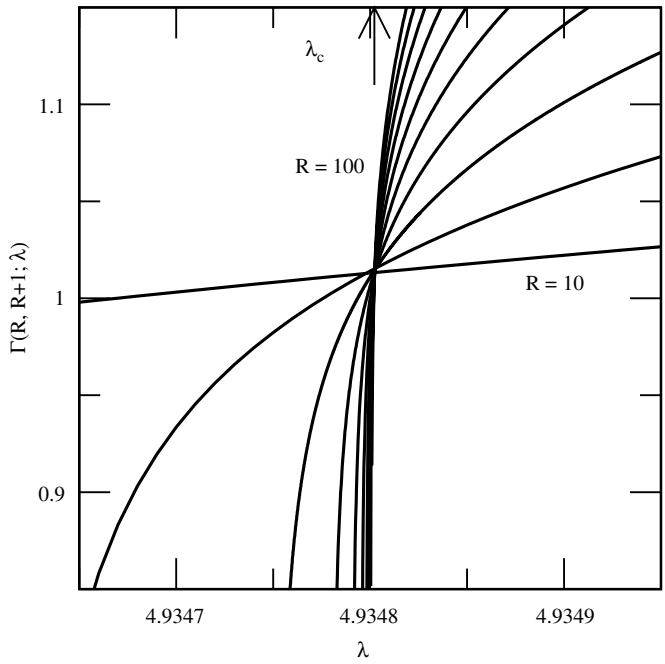

Figure 29. $\Gamma(R, R+1; \lambda)$ as a function of λ for the minimum $\delta = 5$ ($l = 1$) bound state of the square-well potential for values of $R = 10, 20, \ldots, 100$.

In Fig. 29, we show $\Gamma(R, R+1; \lambda)$ against λ for $R = 10, 20, \ldots, 100$ for the lowest-energy $\delta = 5$ ($l = 1$) bound state. As the asymptotic result, Eq. (127) predicts the curves cross at (approximately) the same point.

In Fig. 30 the critical point $\lambda_c^{(R)}$ for finite values of R is plotted against $1/R$, obtaining an excellent agreement with the exact value showed in the plot by a dot. Finally, $\alpha^{(R)}$ against $1/R$ is shown in Fig. 31. Note the minimum occur at $R \simeq 25$. Figures 30 and 31 also show that, as usual in FSS [10,24], the convergence process is faster for the critical parameter calculation than for the critical exponent calculation.

In summary, in this section we presented a SFSS approach to study the critical behavior of bound and virtual states of the radial Schrödinger equation. The scaling is done by introducing a cutoff radius in the potential. This cutoff changes the critical exponent of the energy, but, for large values of the cutoff radius, the asymptotic behavior of FSS functions is dominated by the exact critical exponent. The method gives accurate values for critical parameters and critical exponents, even when the eigenfunctions are not square-integrable.

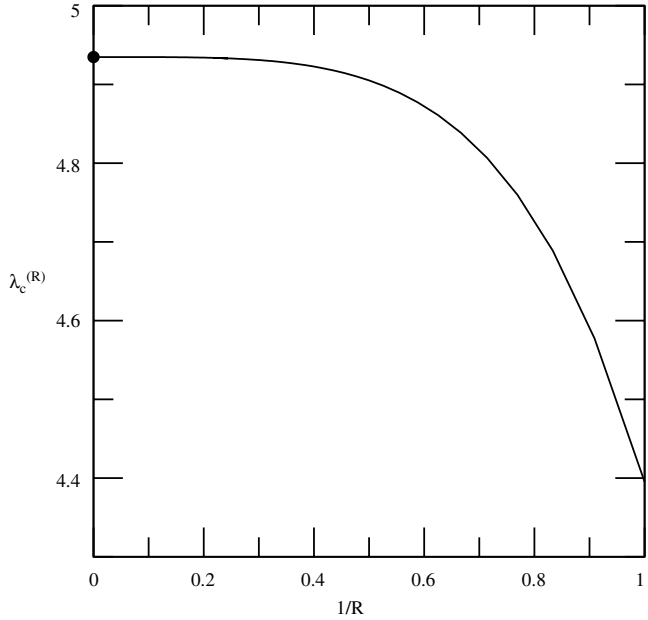

Figure 30. $\lambda_c^{(R)}$ versus $1/R$ for the minimum $\delta = 5$ ($l = 1$) bound state of the square-well potential. The exact value of $\lambda_c = \pi^2/2$ is also shown by a dot.

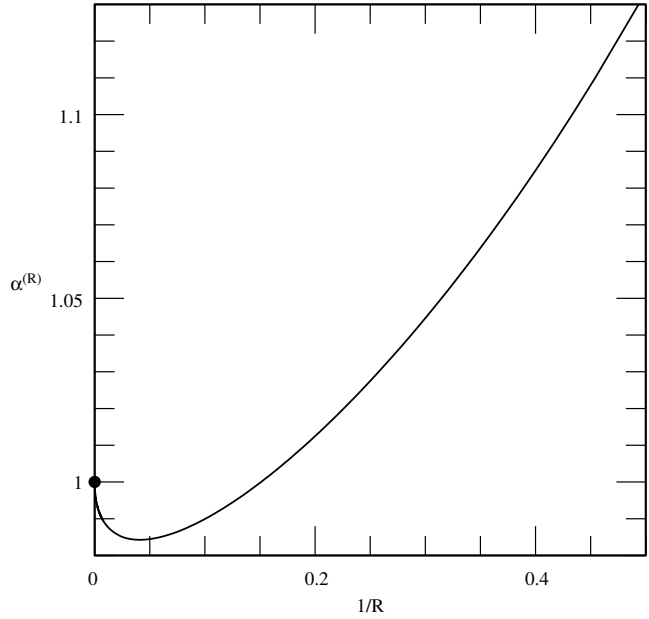

Figure 31. $\alpha^{(R)}$ versus $1/R$ for the minimum $\delta = 5$ ($l = 1$) bound state of the square-well potential. The exact value of $\alpha = 1$ is also shown by a dot.

The main idea of SFSS is similar to the other FSS approaches presented in this review, but the SFSS ansatz is not supported by variational principles and does not use basis-set expansions. It is more difficult to apply it to many-body systems, but it still might be a powerful tool to study bound–virtual–resonance transitions [156] and other analytical properties of the complex energy plane.

VIII. FINITE-SIZE SCALING AND PATH INTEGRAL APPROACH FOR QUANTUM CRITICALITY

In Section IV.A, we have shown that the quantum partition function in D dimensions looks like a classical partition function of a system in $(D+1)$ dimensions, with the extra dimension being the time. With this mapping and allowing the space and time variables to have discrete values, we turn the quantum problem into an effective classical lattice problem.

Having a classical pseudosystem connected to the original quantum problem allows us to go further in the phase transition analogies by realizing that the divergences in thermodynamic quantities are consequences of a more fundamental phenomena [174]. The divergence of the correlation length when the system is critical is due to the fact that the classical lattice shows fractal patterns; in other words, the classical lattice becomes self-similar in all length scales. Thus it is not necessary to limit the phase transition analogies to the search for points where the correlation length diverges. Any quantity that changes its scaling behavior in a phase transition can be used.

A. Mapping Quantum Problems to Lattice Systems

In the path integral approach, the analytical continuation of the probability amplitude to imaginary time $t = -i\tau$ of closed trajectories, $x(t) = x(t')$, is formally equivalent to the quantum partition function $Z(\beta)$, with the inverse temperature $\beta = -i(t' - t)/\hbar$. In path integral discrete time approach, the quantum partition function reads [175–177]

$$Z(\beta) = \lim_{\Delta\tau\to 0}\left(\frac{m}{2\pi\Delta\tau\hbar}\right)^{N_\tau/2}\int\prod_{\ell=0}^{N_\tau} dx_\ell \times \exp\left[-\frac{\Delta\tau}{\hbar}\left(\sum_{\ell=0}^{N_\tau-1} m\frac{(x_{\ell+1}-x_\ell)^2}{2(\Delta\tau)^2} + \lambda\sum_{\ell=0}^{N_\tau-1}\frac{V(x_{\ell+1})+V(x_\ell)}{2}\right)\right] \quad (133)$$

where λ is the strength of the one-dimensional potential $V(x)$, $\Delta\tau = \beta/N_\tau$ is the regular grid spacing between N_τ points along the imaginary time axis indexed by $\ell = 0, 1, \ldots, N_\tau$. The closed path is made by a periodic boundary condition in the time direction such that $x_{N_\tau} = x_0$.

In order to obtain a connection with statistical mechanics lattice systems, we discretize the position space. The position in time slice ℓ is given by

$$x_{i_\ell} = x_0 + i_\ell \Delta L, \qquad \text{with} \quad i_\ell = 1, 2, \ldots, N_q \tag{134}$$

where ΔL is the regular grid spacing of the position axis which has a total of N_q points and q_0 is a constant used to adjust the origin of the coordinate system. Moreover, the size of the space is limited by $L = N_q \, \Delta L$.

Now we to concentrate on the properties of the two-dimensional lattice, the space–time lattice. The partition function, Eq. (133), shows that there is coupling only in the time direction and only between nearest-neighbor time slices. This allows us to use the statistical mechanics technique of writing the partition function Z of the finite system as the trace of a matrix T to the power N_τ.

$$Z(\Delta L, \Delta\tau)_{N_q, N_\tau} = \mathrm{Tr}(T^{N_\tau}) \tag{135}$$

The matrix T is called the transfer matrix. Its elements are given by

$$T(i_\ell, i_{\ell+1}) = \Delta L \left(\frac{m}{2\pi\hbar\Delta\tau}\right)^{1/2} \tag{136}$$

$$\times \exp\left\{ -\frac{\Delta\tau}{\hbar} \left[\frac{m}{2} \left(\frac{\Delta L}{\Delta\tau} \right)^2 (i_{\ell+1} - i_\ell)^2 + \lambda \frac{V_{i_{\ell+1}} + V_{i_\ell}}{2} \right] \right\} \tag{137}$$

where $V_{i_\ell} = V(q_\ell)$ is the potential energy of time slice ℓ evaluated at the space point i_ℓ.

The above transfer matrix can be seen as a transfer matrix of a classical pseudosystem. One can draw the analogy between this classical pseudosystem and a polymer that is constrained to lie in a two-dimensional lattice, each time slice being a polymer bead as shown in Fig. 32. The Hamiltonian of the pseudosystem reads

$$\mathscr{H} = \sum_{\ell=1}^{N_\tau} \mathscr{H}_{\ell,\ell+1} \tag{138}$$

where

$$\mathscr{H}_{\ell,\ell+1} = \frac{m}{2} \left(\frac{\Delta L}{\Delta\tau} \right)^2 (i_{\ell+1} - i_\ell)^2 + \lambda \frac{V_{i_{\ell+1}} + V_{i_\ell}}{2} + C \tag{139}$$

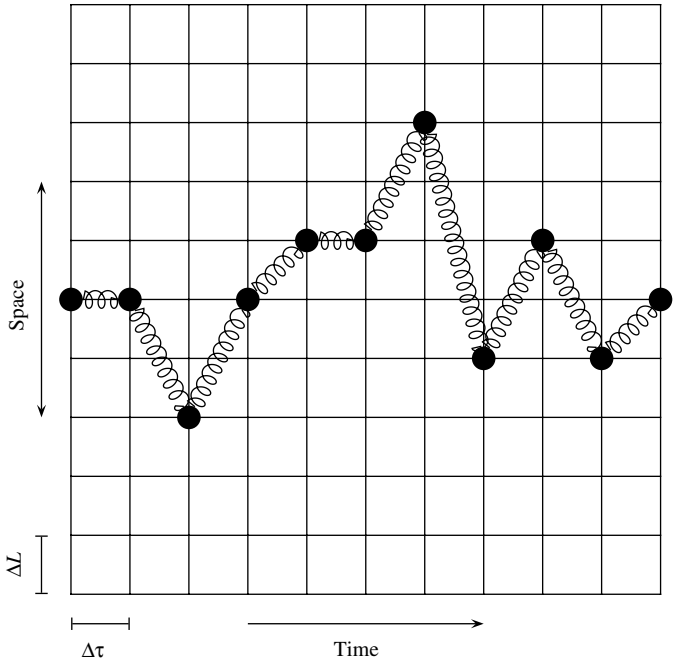

Figure 32. Mapping the quantum problem to a space–time lattice. The analogy to a polymer that is constrained to lie in a two-dimensional lattice is shown. Thus each time slice represents a polymer bead while the coupling between neighbor beads is connected by springs. For each time slice there is only one possible bead.

with $C = -\hbar \ln\{[m/(2\pi\hbar\Delta\tau)]^{1/2}\Delta L\}/\Delta\tau$ being a constant independent of the state of the lattice. With the above polymer analogy, the first term represents the harmonic coupling between neighboring beads connected by a spring and the second term is the interaction of each bead with some "local external field."

The partition function of the classical pseudosystem becomes

$$T(i_\ell, i_{\ell+1}) = \exp[-(\Delta\tau/\hbar)\mathscr{H}_{\ell,\ell+1}] \tag{140}$$

If the classical pseudosystem Hamiltonian were independent of $\Delta\tau$, the classical pseudosystem would behave as a statistical mechanics lattice system with inverse temperature $\Delta\tau/\hbar$.

In order to complete the mapping between the quantum problem and the classical pseudosystem, one must address the problems of both the continuum and the infinite limits. The ground-state properties of the original system are obtained by taking both the continuum limit, $(\Delta\tau, \Delta L \to 0)$, and the thermodynamic limit, $(\beta, L \to \infty)$ [174].

B. Quantum Criticality

In the path integral lattice definition, the time t is defined only in the sites of a regular time lattice with lattice constant $\Delta T = T/N_T$. The initial lattice point is $t_0 = t'$, the last one is $t_{N_T} = t''$, and any intermediate instant is given by $t_j = t' + j\Delta T,\ j = 0, 1, \ldots, N_T$. The position in each instant is given by $x_j = x(t_j)$. In the absence of the potential, the path integral summation is a summation over Brownian paths. Given the position x_{j-1} and the time interval ΔT, the increment $y_j = x_j - x_{j-1}$ is a random variable with probability proportional to $e^{-my^2/(2\hbar\Delta T)}$. The Brownian paths have a fractal nature and are self-similar as long as one scales the space and time direction with [178]

$$x \to bx, \qquad t \to b^2 t \tag{141}$$

where the scale factor b is any real positive number.

The classical system, whose states are given by the Brownian paths (the system can be also interpreted as a Gaussian polymer [179]) can be rescaled by the relations given in Eq. (141) to preserve the same structure. This fact makes the time lattice critical in the sense of renormalization group theory [25,180]. When the strength of the attractive potential is $\lambda \to \infty$, the particle must be bound and the contribution to the path integral summation of the Brownian paths are weighted by the factor $\exp(-\frac{1}{\hbar}\int_{t'}^{t''} V(x(t);\lambda)\, dt)$. Thus, the paths in the neighborhood of the origin contribute much more than paths filling uniformly the whole space. The system is not scaling-invariant anymore because we can devise two regions in the space, one where the particle is likely to be localized and the other where it is not. If the system is scale-invariant, the system is in a critical phase. If the scaling invariance is broken by the potential, we have a noncritical phase. The transition between these two phases at a finite value of lambda ($\lambda = \lambda_c$) will be properly called a *phase transition*.

The numerical study of the phase transition is made by fixing the grid spacing ΔL and ΔT and the discretization number N_L, which sets the rank of the transfer matrix to be diagonalized. The numerical calculation in a discrete and finite system gives an estimate of the actual values of all observable. The ground-state energy $E_L^{(0)}$ is given by

$$e^{-N_T \Delta T E_L^{(0)}/\hbar} = Z = \mathrm{Tr}[\mathrm{T}^{N_T}] \tag{142}$$

where the transfer matrix T is defined as

$$T(x_j, x_{j-1}) = \left(\frac{m\Delta L^2}{2\pi\hbar\Delta T}\right)^{1/2} \exp\left[-\frac{1}{\hbar}\left(\frac{m}{2\Delta T}(x_j - x_{j-1})^2 + \Delta T V(x_j;\lambda)\right)\right] \tag{143}$$

For a large N_T, the trace is dominated by the leading eigenvalue of the transfer matrix $Z \approx (a_L^{(0)})^{N_T}$ and the ground-state energy is given by

$$E_L^{(0)} = -\frac{\hbar}{\Delta T}\ln(a_L^{(0)}) \tag{144}$$

where $a_L^{(0)}$ is the leading eigenvalue of the transfer matrix. Having the leading eigenvector of the transfer matrix, one can evaluate any other ground-state expectation value. Because all geometric properties of the fractal Brownian paths are preserved in the critical region, the root mean square displacement $R_L = \langle x^2 \rangle^{1/2}$ must scale with the macroscopic dimension L. If the particle is bound, R_L must achieve a finite value independent of L. Hence R_L has a different scaling behavior if the particle is free or bound. This in principle can be used to determine the phase transition point.

The correlation length ξ along the imaginary time direction is the other quantity we can use to determine the critical region. The correlation length is defined as the asymptotic behavior of the correlation function

$$C(j\Delta T) = \langle x_0 x_j \rangle - \langle x_0 \rangle^2 \approx \exp\left(-\frac{j\Delta T}{\xi}\right), \qquad j \to \infty \tag{145}$$

The correlation length can be written in terms of the two leading eigenvalues $a_L^{(0)}$ and $a_L^{(1)}$ of the transfer matrix

$$\xi_L = -\Delta T \frac{1}{\ln(a_L^{(1)}/a_L^{(0)})} \tag{146}$$

When the system is critical, the quantum states must be correlated in all length scales along the time direction and thus the correlation length must scale with $\xi \sim T$. Hence in the true free particle case with $T \to \infty$ and $L \to \infty$ the correlation length diverges. Since L is finite, one cannot have a true divergence, but the scaling relations presented in Eq. (141) should still apply if L is finite and sufficiently large. Thus, the correlation length must scale as $\xi \sim L^2$ in the critical region.

For a given value of the critical parameter λ, we perform calculations with different system sizes. If $\xi_L(\lambda)$ scales with L^2 and $R_L(\lambda)$ scales with L, we call the system critical because the particle behaves like a free particle. When the strength of the potential breaks down this scaling behavior, the system is not critical and the particle is bound. The value of $\lambda = \lambda_c$ is the transition point.

As an example to illustrate this method, we study the case of a single particle in the presence of the Pöschl–Teller potential [181]

$$V(x;\lambda) = -\lambda(\lambda-1)/\cosh^2(x), \qquad \lambda \geq 1 \tag{147}$$

This problem has an exact solution [50]

$$E_n = -(\lambda - 1 - n)^2, \qquad n \leq \lambda - 1, \quad n = 0, 1, 2, \ldots \tag{148}$$

In the one-dimensional case, there is always a bound solution unless $\lambda = 1$ when the potential vanishes, and the particle is free. In three dimensions the behavior is much more interesting. Regardless of the presence of an attractive potential in the interval $1 < \lambda < 2$, there is no bound solution until $\lambda \geq 2$. Hence there is a finite value of the potential strength parameter, $\lambda_c = 2$, that defines the stability limit of the bound solution. In the present approach, this point can be obtained by investigating the scaling properties of the correlation length ξ_L and the mean radial distance R_L.

The one-dimensional case is a straightforward application of Eq. (143). The lattice in the position space is defined by picking evenly spaced points in the interval $x \in [-L/2, L/2]$. The results are obtained by exact diagonalization of the transfer matrix for every system size defined by $L = N_L \Delta L$. To investigate the trivial transition at $D = 1$, it is enough to consider only one grid spacing $\Delta L = 0.03$. For the remainder of this section we return the atomic units particle mass equal to one. Thus the values of ξ_L and R_L are calculated with 10 different system sizes, $L = 100, 200, \ldots, 1000$, where L is measure in units of ΔL. The results are shown in Fig. 33. In Fig. 33a we plot ξ_L/L^2, and in Fig. 33b we plot R_L/L as a function of λ. The curves correspond to different system sizes $L = 100, 200, \ldots, 1000$. For a given value of λ, it is clear that the only point where $R_L \sim L$ and $\xi_L \sim L^2$ is $\lambda = 1$. Thus the one-dimensional system is critical only when the potential vanishes, and the particle is free. So $\lambda = 1$ is regarded as a trivial critical point. In Figs. 33c and 33d, we show ξ_L and R_L as a function of L^2 and L for fixed value of λ. The curve with circles corresponds to $\lambda = 1$, and the other five correspond to small deviations from the free particle case with $\lambda = 1.02, 1.04, 1.06, 1.08$, and 1.10. The only case that can be adjusted to a straight line is $\lambda = 1$. In the presence of a weak potential, the scaling of ξ_L and R_L deviates from the critical scaling represented by the straight lines.

In summary, this approach is based on the breakdown of the free-particle scaling properties as the strength of the attractive external potential is made strong enough. This general idea can certainly be applied to systems with more than one particle as long as the unbound solution can be well represented by noninteracting free particles. This approach is general and might be used with other simulation techniques, such as Monte Carlo methods [182], to obtain critical parameters for few-electron atoms and simple molecular systems.

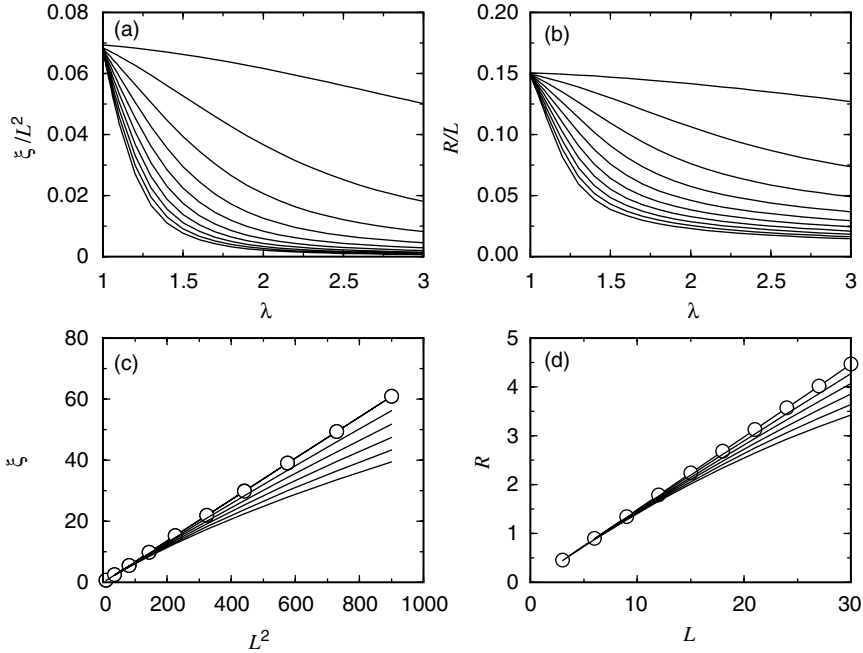

Figure 33. Pöschl–Teller potential: Panels (a) and (b) show the scaled correlation length ξ/L^2 and the scaled radial mean distance R/L as a function of the potential strength λ for different system sizes with $L = 3, 6, 9, \ldots, 30$. The grid spacing is kept fixed $\Delta L = 0.03$, so the smallest system has $N_L = 100$ and the largest has $N_L = 1000$ points. Panels (c) and (d) illustrate the scaling of $a\xi$ and R with the system size L for different values of $\lambda = 1(\bigcirc), 1.02, 1.04, 1.06, 1.08, 1.10$. All numerical values are in atomic units.

IX. FINITE-SIZE SCALING FOR QUANTUM DOTS

Quantum dots are a cluster (hundreds or few thousands) of atoms or molecules (Cds, CdSe, ... GaAs, InAs,...) and are small enough that their electronic states are discrete. They present the opportunity to synthesize atomlike building blocks so that we can measure electronic properties, and they have generated much current experimental and theoretical interest [183–193]. Quantum dots of nearly identical sizes self-assemble into a planar array. (The dots become passivated against collapse by coating them with organic ligands.) For Ag nanodots (for example) the packing is hexagonal. The lower-lying electronic states of an isolated dot are discrete, being determined by the confining potential (and therefore the size) of the dot. Because of their larger size, it takes only a relatively low energy to add another electron to a dot, as revealed by scanning tunneling microscopy [195,196]. This energy is much lower than the

corresponding energy for ordinary atoms and most molecules. It follows that when dots are close enough to be exchange coupled, which is the case in an array, the charging energy can be quite low. Here we review a computational method that allows the contributions of such ionic configurations even for extended arrays. The technical problem is that the Coulombic repulsion between two electrons (of opposite spins) that occupy the same dot cannot be described in a one-electron approximation. It requires allowing for correlation of electrons. Most methods that explicitly include correlation effects scale as some high power of the number of atoms (here, dots) and are computationally intractable. For example, a hexagonal array of only 19 dots, 3 dots per side, has already 2,891,056,160 low electronic configurations. Earlier exact computations including charging energy were limited to a hexagonal array of only 7 dots, 2 dots per side [197]. Yet current measurements of both static [198] and transport [199] properties use arrays of at least 100 dots per side. The simplest Hamiltonian that includes both the Coulombic (or charging energy) effects and the exchange coupling is the Hubbard model [200]. This model can be solved exactly for a one-dimensional chain, but for a two-dimensional array it is, so far, analytically intractable. In the absence of a closed solution, various methods have been developed [201]. Renormalization group (RG) methods are receiving increasing attention because of their nonperturbative nature, which allows application to the intermediate-to-strong coupling regime. In the following, we will show the applications of a real-space block renormalization group (BRG) method [202–204] on a two-dimensional triangular lattice with hexagonal blocks as shown in Fig. 34. Specifically, the size-dependence of the Mott metal–insulator transition (MIT) is studied.

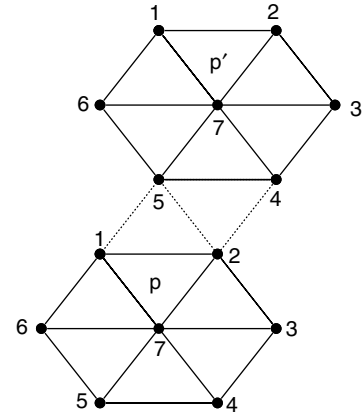

Figure 34. Schematic diagram of the triangular lattice with hexagonal blocks. Only two neighboring blocks p and p' are drawn here. The dotted lines represent the interblock interactions, and the solid lines represent the intrablock ones.

The used model is the Hubbard model [203], and the Hamiltonian is written as

$$\mathscr{H} = -t \sum_{\langle i,j\rangle,\sigma} [c^{+}_{i\sigma} c_{j\sigma} + \text{H.c.}] + U \sum_{i} n_{i\uparrow} n_{i\downarrow} - \mu \sum_{i} (n_{i\uparrow} + n_{i\downarrow}) \tag{149}$$

where t is the nearest-neighbor hopping term, U is the local repulsive interaction, and μ is the chemical potential. $c^{+}_{i\sigma}(c_{i\sigma})$ creates (annihilates) an electron with spin σ in a Wannier orbital located at site i; the corresponding number operator is $n_{i\sigma} = c^{+}_{i\sigma} c_{i\sigma}$ and $\langle\ \rangle$ denotes the nearest-neighbor pairs. H.c. denotes the Hermitian conjugate.

Only the half-filled system is considered since the corresponding electron interactions are most prominent in this case, which leads to $\mu = U/2$. Hence, Eq. (149) can be rewritten as

$$\mathscr{H} = -t \sum_{\langle i,j\rangle,\sigma} [c^{+}_{i\sigma} c_{j\sigma} + \text{H.c.}] + U \sum_{i} \left(\frac{1}{2} - n_{i\uparrow}\right)\left(\frac{1}{2} - n_{i\downarrow}\right) + K \sum_{i} I_i \tag{150}$$

where $K = -U/4$ and I_i is the unit operator. As to the lattice structure, we use the nonpartite triangular lattice, because MIT emerges at finite $U = U_c$. It is well known that MIT on a square lattice can only take place at $U = 0$ due to the perfect nesting of the Fermi surface. If we don't study the exotic case with $U < 0$, which is possible in a strongly polarizable medium, the square lattice is not an optimal option for our purpose. The physical quantity we are concerned will be the charge gap, $\triangle_g$, which is defined as

$$\triangle_g = E(N_e - 1) + E(N_e + 1) - 2E(N_e) \tag{151}$$

where $E(N_e)$ denotes the lowest energy for an N_e–electron system. In our case, N_e is equal to the site number N_s of the lattice. This quantity is the discretized second derivative of the ground-state energy with respect to the number of particles—that is, the inverse compressibility.

The essence of the BRG method is to map the above many-particle Hamiltonian on a lattice to a new one with fewer degrees of freedom and with the same low-lying energy levels [205]. Then the mapping is repeated, leading

to a final Hamiltonian for which an exact solution can be obtained. The procedure can be divided into three steps: First divide the N–site lattice into appropriate n_s–site blocks labeled by $p(p = 1, 2, \ldots, N/n_s)$ and separate the Hamiltonian $\mathscr{H}$ into intrablock part $\mathscr{H}_B$ and interblock $\mathscr{H}_{IB}$:

$$\mathscr{H} = \mathscr{H}_B + \mathscr{H}_{IB} = \sum_p H_p + \sum_{\langle p,p' \rangle} V_{p,p'} \tag{152}$$

where

$$\mathscr{H}_p = -t \sum_{\langle i^{(p)}, j^{(p)} \rangle} [c^+_{i^{(p)}\sigma} c_{j^{(p)}\sigma} + \text{H.c.}] + U \sum_{i^{(p)}} n_{i^{(p)}\uparrow} n_{i^{(p)}\downarrow} - \mu \sum_{i^{(p)}} (n_{i^{(p)}\uparrow} + n_{i^{(p)}\downarrow}) \tag{153}$$

and

$$V_{p,p'} = -t \sum_{\langle i^{(p,b)}, j^{(p',b)} \rangle} [c^+_{i^{(p,b)}\sigma} c_{j^{(p',b)}\sigma} + \text{H.c.}] \tag{154}$$

in which $i^{(p)}$ denotes the *ith* site on the *pth* block and $i^{(p,b)}$ denotes the border site of the block p.

The second step is to solve $\mathscr{H}_p$ exactly to get the eigenvalues E_{p_i} and eigenfunctions $\Phi_{p_i}(i = 1, 2, \ldots, 4^{n_s})$. Then we can build the eigenfunctions of $\mathscr{H}_B$ by direct multiplication of Φ_{p_i}, which can be written as $|\Psi_B(i_1, i_2, \ldots, i_{N/n_s})\rangle = |\Phi_{1i_1}\rangle|\Phi_{2i_2}\rangle \ldots |\Phi_{N/n_s i_{N/n_s}}\rangle (i_1, i_2, \ldots \in \{1, 2, \ldots, 4^{n_s}\})$.

The last step is to treat each block as one site on a new lattice and treat the correlations between blocks as hopping interactions. The original Hilbert space has four states per site. By following the above procedure, one obtains an equivalent Hamiltonian with $(4^{n_s})^{N/n_s} = 4^N$, degrees of freedom, which is the same as the original Hamiltonian. But in the realistic case, if we only care about the properties related to some special energy levels of the system, it is not necessary to keep all the states for a block to obtain the new Hamiltonian. For example, when studying the metal–insulator–transition [206], we may only need to consider the ground-state and the first excited-state energies.

The above scheme is a general procedure for applying the BRG method. In order to make the new Hamiltonian more tractable, it is desirable to make it have the same structure as the original one; that is, the reduction in size should not be accompanied by a proliferation of new couplings. Then we can use the iteration procedures to solve the model. To achieve this goal, it is necessary to keep only four states in step 2, which can be understood from the following

renormalized intrasite Hamiltonian. The four selected states are taken to be

$$|\Phi_{p1}\rangle \equiv |0\rangle'_p \tag{155}$$

$$|\Phi_{p2}\rangle \equiv c'^{+}_{p\uparrow\downarrow}|0\rangle'_p = |\uparrow\downarrow\rangle'_p \tag{156}$$

$$|\Phi_{p3}\rangle \equiv c'^{+}_{p\uparrow}|0\rangle'_p = |\uparrow\rangle'_p \tag{157}$$

$$|\Phi_{p4}\rangle \equiv c'^{+}_{p\downarrow}|0\rangle'_p = |\downarrow\rangle'_p \tag{158}$$

where $c'^{+}_{p\sigma}(c'_{p\sigma})$ is the creation (annihilation) operator of the block state $|\sigma\rangle'_p$ and their corresponding energies are E_i $(i = 1, 2, 3, 4)$.

Our next task is to rewrite the old Hamiltonian $\mathscr{H} = \mathscr{H}_B + \mathscr{H}_{IB}$ in the space spanned by the truncated basis

$$\mathscr{H}' = \sum_{\Psi_B^{\text{Truncated}}\bar{\Psi}_B^{\text{Truncated}}} |\Psi_B^{\text{Truncated}}\rangle\langle\Psi_B^{\text{Truncated}}|H|\bar{\Psi}_B^{\text{Truncated}}\rangle\langle\bar{\Psi}_B^{\text{Truncated}}| \tag{159}$$

where the truncated basis is given by

$$|\Psi_B^{\text{Truncated}}(i_1, i_2, \ldots, i_{N/n_s})\rangle = |\Phi_{1i_1}\rangle|\Phi_{2i_2}\rangle \ldots |\Phi_{N/n_s i_{N/n_s}}\rangle \times (i_1, i_2, \ldots \in \{1, 2, 3, 4\}) \tag{160}$$

In order to avoid proliferation of additional couplings in $\mathscr{H}'$, the four states kept from the block cannot be arbitrarily chosen. Some definite conditions must be satisfied in order to make $\mathscr{H}'$ have the same structure as $\mathscr{H}$. Substituting $\mathscr{H}$ into $\mathscr{H}'$ and using the product of different operators (see Table III), we can get the expression for $\mathscr{H}_p$:

$$\begin{aligned}\mathscr{H}_p &= |0\rangle'_p E_1 \langle 0|'_p + |\uparrow\downarrow\rangle'_p E_2 \langle\downarrow\uparrow|'_p + |\downarrow\rangle'_p E_4 \langle\downarrow|'_p + |\uparrow\rangle'_p E_3 \langle\uparrow|'_p \\ &= E_1 + (E_3 - E_1)n'_{p,\uparrow} + (E_4 - E_1)n'_{p,\downarrow} + (E_1 + E_2 - E_3 - E_4)n'_{p,\uparrow}n'_{p,\downarrow}\end{aligned} \tag{161}$$

TABLE III
The Internal Product of Different Operator Transformations[a]

	$\langle 0\|'$	$\langle\uparrow\|'$	$\langle\downarrow\|'$	$\langle\uparrow\downarrow\|'$
$\|0\rangle'$	$1 - n'_\uparrow - n'_\downarrow + n'_\uparrow n'_\downarrow$	$c'_\uparrow - n'_\downarrow c'_\uparrow$	$c'_\downarrow - n'_\uparrow c'_\downarrow$	$c'_\downarrow c'_\uparrow$
$\|\uparrow\rangle'$	$c'^{+}_\uparrow - c'^{+}_\uparrow n'_\downarrow$	$n'_\uparrow - n'_\uparrow n'_\downarrow$	$c'^{+}_\uparrow c'_\downarrow$	$-n'_\uparrow c'_\downarrow$
$\|\downarrow\rangle'$	$c'^{+}_\downarrow - c'^{+}_\downarrow n'_\uparrow$	$c'^{+}_\downarrow c'_\uparrow$	$n'_\downarrow - n'_\downarrow n'_\uparrow$	$n'_\downarrow c'_\uparrow$
$\|\uparrow\downarrow\rangle'$	$c'^{+}_\uparrow c'^{+}_\downarrow$	$-n'_\uparrow c'^{+}_\downarrow$	$c'^{+}_\uparrow n'_\downarrow$	$n'_\uparrow n'_\downarrow$

[a] In this table the product reads $|0\rangle'\langle 0|' = 1 - n'_\uparrow - n'_\downarrow + n'_\uparrow n'_\downarrow$, etc.

Note that by keeping only four states from the block states in the beginning gives no other extra couplings in the new Hamiltonian.

Comparing the above intrasite Hamiltonian with Eq. (149), we get the next conditions in order to copy the intrasite structure of the old Hamiltonian; that is, $E_3 = E_4$. Because of the additional vacuum energy E_1 in the new Hamiltonian, we rewrite the intrasite part of Eq. (149) as

$$\mathscr{H}_B = U \sum_i n_{i\uparrow} n_{i\downarrow} - \mu \sum_i (n_{i\uparrow} + n_{i\downarrow}) + K \sum_i I_i \tag{162}$$

where we introduce another parameter K to the original system and I_i is a unit operator. The new intrasite Hamiltonian is given by

$$\mathscr{H}'_B = (E_1 + E_2 - 2E_3) \sum_p n'_{p\uparrow} n'_{p\downarrow} - (E_1 - E_3) \sum_p (n'_{p\uparrow} + n'_{p\downarrow}) + E_1 \sum_p I_p \tag{163}$$

Then the renormalized parameters U, μ, and K can be obtained from the following relations:

$$U' = E_1 + E_2 - 2E_3 \tag{164}$$

$$\mu' = E_1 - E_3 \tag{165}$$

$$K' = E_1 \tag{166}$$

in which E_1, E_2, and E_3 are functions of the old parameters t, U, μ, K.

For the half-filled case, μ is fixed to be $U/2$. Moreover, by using the particle–hole symmetry, $E_1 = E_2$, the renormalization group equations for U and K take the form

$$U' = 2(E_1 - E_3) \tag{167}$$

$$K' = (E_1 + E_3)/2 \tag{168}$$

To illustrate this procedure, let us consider the triangular lattice with hexagonal blocks as shown in Fig. 34. For this nonbipartite lattice the interaction between blocks can be written as

$$\begin{aligned} V_{pp'} = (-t) \sum_{\sigma, i_1, i'_1 i_2, i'_2} \{ & [|\Phi_{pi_1}\rangle\langle\Phi_{pi_1}| c^+_{1^{(p)}\sigma} |\Phi_{pi'_1}\rangle\langle\Phi_{pi'_1}|] \\ & \times [|\Phi_{p'i_2}\rangle\langle\Phi_{p'i_2}| c_{5^{(p')}\sigma} |\Phi_{p'i'_2}\rangle\langle\Phi_{p'i'_2}|] \\ & + [|\Phi_{pi_1}\rangle\langle\Phi_{pi_1}| c^+_{2^{(p)}\sigma} |\Phi_{pi'_1}\rangle\langle\Phi_{pi'_1}|] \\ & \times [|\Phi_{p'i_2}\rangle\langle\Phi_{p'i_2}| c_{4^{(p')}\sigma} |\Phi_{p'i'_2}\rangle\langle\Phi_{p'i'_2}|] \\ & + [|\Phi_{pi_1}\rangle\langle\Phi_{pi_1}| c^+_{2^{(p)}\sigma} |\Phi_{pi'_1}\rangle\langle\Phi_{pi'_1}|] \\ & \times [|\Phi_{p'i_2}\rangle\langle\Phi_{p'i_2}| c_{5^{(p')}\sigma} |\Phi_{p'i'_2}\rangle\langle\Phi_{p'i'_2}|] + \text{H.c.}\} \end{aligned} \tag{169}$$

Since we would like to keep $V_{pp'}$ of the form

$$V_{pp'} = (-t') \sum_{\sigma} [c'^{+}_{p\sigma} c'_{p'\sigma} + \text{H.c.}] \tag{170}$$

we use the product transformation in Table III to simplify Eq. (169):

$$V_{pp'} = \sum_{\sigma,\langle i,j\rangle} \{\langle\sigma|'_p c^{+}_{i^{(p)}\sigma}|0\rangle'_p + [\langle -\sigma, \sigma|'_p c^{+}_{i^{(p)}\sigma}| - \sigma\rangle'_p - \langle\sigma|'_p c^{+}_{i^{(p)}\sigma}|0\rangle'_p] n'_{p-\sigma}\} c'^{+}_{p\sigma}$$
$$\times \{\langle 0|'_{p'} c_{j^{(p')}\sigma}|\sigma\rangle'_{p'} + [\langle -\sigma|'_{p'} c_{j^{(p')}\sigma}|\sigma, -\sigma \downarrow\uparrow\rangle'_{p'} - \langle\sigma|'_{p'} c_{j^{(p')}\sigma}|0\rangle'_{p'}] n'_{p'-\sigma}\} c'_{p'\sigma} + \text{H.c.}$$
$$(\langle ij\rangle = \langle 1,5\rangle, \langle 2,4\rangle, \langle 2,5\rangle) \tag{171}$$

It can be easily seen now that in order to make all the extra couplings vanish, it is necessary to make further restrictions upon the selected states,

$$\langle -\sigma, \sigma|'_p c^{+}_{i^{(p)}\sigma}|_p - \sigma\rangle'_p = \langle\sigma|'_p c^{+}_{i^{(p)}\sigma}|0\rangle'_p \tag{172}$$

$$\langle -\sigma|'_{p'} c_{j^{(p')}\sigma}|\sigma, -\sigma\rangle'_{p'} = \langle 0|'_{p'} c_{j^{(p')}\sigma}|\sigma\rangle'_{p'} \tag{173}$$

Using calculations similar to those of the other neighboring interactions of the block, we can finally obtain the following conditions:

$$\langle -\sigma, \sigma|'_p c^{+}_{i^{(p)}\sigma}|_p - \sigma\rangle'_p = \langle\sigma|'_p c^{+}_{i^{(p)}\sigma}|0\rangle'_p = \lambda \tag{174}$$

for all the border sites on the block. Then the new hopping term becomes

$$V_{pp'} = \nu\lambda^2 \sum_{\sigma} c'^{+}_{p\sigma} c'_{p'\sigma} \tag{175}$$

where ν represents the number of couplings between neighboring blocks. In Fig. 34, $\nu = 3$. The last renormalization group equation is readily obtained:

$$t' = \nu\lambda^2 t \tag{176}$$

Up to now, we have given a general discussion of the conditions under which no proliferation of couplings results from the application of the BRG method to nonpartite lattice. Because on the border of a nonpartite lattice block there is only one type of site, the above procedures can be extended to other lattices with different dimensions or blocks without much difficulty.

After deriving the conditions for the renormalization group equations, the next task is to select states that satisfy these conditions. At this stage the

symmetry properties of the lattice play an important role. From Eqs. (170) and (171), it can be easily seen that if we assume the particle number in the state $|0\rangle'$ to be $N_e - 1$, then in $|\uparrow\rangle', |\downarrow\rangle'$ and $|\uparrow\downarrow\rangle'$ there should be $N_e, N_e, N_e + 1$ particles, respectively. Moreover, if the spin in $|0\rangle'$ is S_z, the spins for $|\uparrow\rangle', |\downarrow\rangle'$, and $|\uparrow\downarrow\rangle'$ should be $S_z + 1/2, S_z - 1/2$, and S_z. The total electron number N_e and the spin S_z for each block are good quantum numbers since their corresponding operators commute with the Hubbard Hamiltonian. So when we diagonalize the Hubbard Hamiltonian of the selected block, we keep N_e and S_z fixed to be $(N_e - 1, S_z)$, $(N_e, S_z + 1/2)$, $(N_e, S_z - 1/2)$, and $(N_e + 1, S_z)$, respectively. Thus we obtain four groups of eigenenergies and eigenstates corresponding to the above quantum numbers. From each group, we select the lowest-energy state to form the final required four states. It should be mentioned that the lowest-energy state has to be selected according to definite special symmetry considerations, which shall be discussed in the next paragraph. In order to obtain the insulating to conducting gap, which is defined to be the energy difference between extracting one electron from the system and adding one electron to it, N_e is selected to be equal to N_s. For S_z, we choose it to be zero so as to make the block have the same spin property as the one-site. So now the renormalized lattice will be composed of N/n_s renormalized "sites" with N/n_s "particles."

Instead of forcing the above conserved quantities upon the selected states in analogy to the one site properties in a consistent way, here we get them directly from the no-coupling-proliferation conditions. λ does not depend on σ in Eq. (174); this can be guaranteed by the particle–hole symmetry, which means that only in half-filled lattice can the renormalized Hamiltonian have exactly the same form as the original one [207]. Moreover, the irrelevance of λ with respect to the border site $i^{(p,b)}$ can be shown by requiring the selected states to belong to the same irreducible representation of the spatial group of the lattice. For the triangular lattice with hexagonal blocks, the Hamiltonian is invariant under C_{6v} [208]. So if we choose the same one-dimensional irreducible representation of the group C_{6v} for $|0\rangle', |\uparrow\rangle', |\downarrow\rangle'$, and $|\uparrow\downarrow\rangle'$, the conditions can be satisfied.

Eqs. (167), (168), and Eq. (176) are the so-called RG flow equations. Usually, they are iterated until we get the fixed point. The charge gap for an infinite lattice can then be written as

$$\Delta_g = \lim_{n\to\infty} U^{(n)} \tag{177}$$

Because of the implicit functional in RG flow equations, it is very difficult to obtain any other useful information except the critical transition point U_c from the above procedures. In the following, we will handle these procedures in another way, namely, instead of letting RG flow to infinity for a fixed initial parameters (U, k, t), we can stop the RG flow at some stage. Thus the energy gap obtained from Eq. (151) will correspond to a system of fixed size. For

example, if we stop the RG flow at the first iteration, then obtained t' and U' will be for hexagonal block mapped from a system of 7^2 sites. Because we can solve a hexagonal block Hamiltonian exactly, the energy gap for a system of 49 sites can be obtained easily.

In this way, we can study the variations of Δ_g against the system size of $7^2, 7^3, 7^4, 7^5, 7^6 \ldots$. We call this procedure a multistage real-space RG method, which is well-adapted to start the finite-size scaling analysis.

In Fig. 35a, the size dependence of relationship between $\triangle_g$ and U in the unit of t is presented. But from this figure, it is somewhat difficult to decide the transition point for $\triangle_g$ to reach zero as U is decreased from big values. To explicitly display the critical phenomenon, we construct Fig. 35b by scaling $\triangle_g$ with respect to N at first. Here $N = N_e = N_s$. Now it is very easy to get the critical value of $(U/t)_c$ at the crossing point of all the curves corresponding to different system size, which is found to be 12.5. The same value is obtained by letting RG equations flow to infinity, which should be expected. But this kind of scaling gives us more. In Fig. 35c, all the data collapse to one curve once we carry out a second step of scaling with $U/t - (U/t)_c$ by N. It is an obvious evidence for the occurrence of a quantum phase transition with U to be the

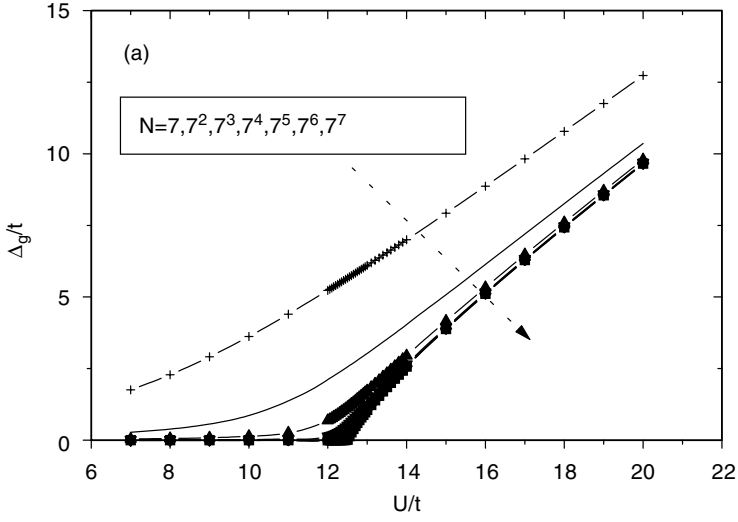

Figure 35. Variations of the charge gap Δ_g against the on-site electron interaction U for different system sizes, that is, the number of sites: $7(+)$, $7^2(\times)$, $7^3(\blacktriangle)$, $7^4(\blacktriangledown)$, $7^5(\blacklozenge)$, $7^6(\bullet)$, $7^7(\blacksquare)$. More points are calculated around the transition point. In (a), no scaling is utilized. In (b), the charge gap is scaled by $1/N^{0.405}$ to display clearly the phase transition. In (c), all the data are collapsed onto one curve by scaling both axis with respect to N.

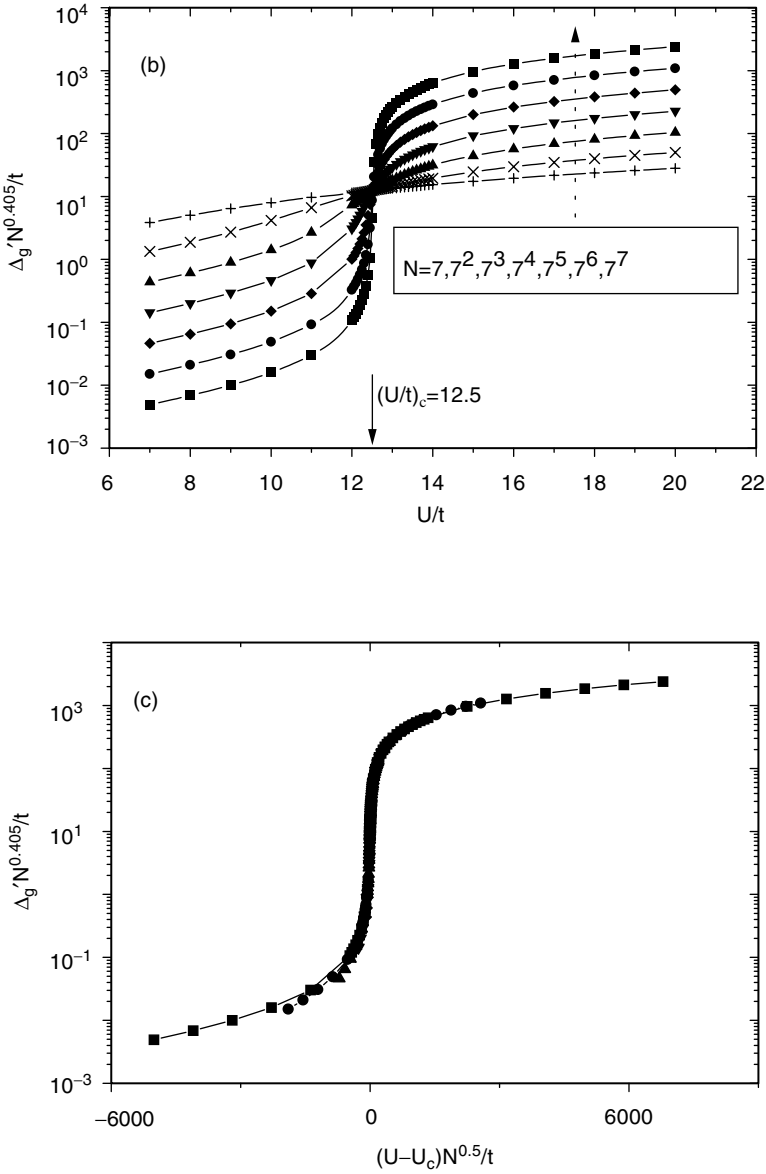

Figure 35 (*Continued*)

tuning parameter. Hence we can write down the following equation:

$$\triangle_g N^{0.405} = f\left[qN^{0.5}\right] \tag{178}$$

where $f(x)$ is a universal functions independent of the size and $q = U/t - (U/t)_c$ measures the distance of the electron correlations from its critical value for MIT. By using $N = L^2$ for 2D systems, the above equation can be rewritten as

$$\triangle_g = L^{-0.91} f[qL] \tag{179}$$

from which we can get two scaling relationship for the charge gap. One is the finite-size scaling at the transition point–that is, when $q = 0$, $\triangle_g \sim 1/L^{0.91}$. As shown in Ref. 209, in Anderson MIT, when the electron correlation energy dominate the Fermi energy, the average inverse compressibility $(= \Delta_g)$ exhibits a scaling as $1/L$ with respect to the system size. Here it shows a slower decay as L increases. The other one is the bulk scaling around the transition point for infinite systems, $\triangle_g \sim q^{0.91}$. According to the scaling analysis of the Gutzwiller solution for the Mott MIT in the Hubbard model [210], $\triangle_g \sim q^{0.5}$. Since the Gutzwiller solution is a mean field approximation and the upper critical dimension for it to give a correct description of this critical phenomenon is $d_c = 3$, it is understandable that our above 2D results cannot be merged into the mean-field theory.

By introducing a critical exponent $y_\triangle$ for $\triangle_g$, from the one-parameter scaling theory, we can have

$$\triangle_g = q^{y_\triangle} f\left(\frac{L}{\xi}\right) \tag{180}$$

in which $\xi = q^{-\upsilon}$ is the correlation length with υ to be the corresponding critical exponent and L denotes the system size. By using $N = L^2$ for 2D systems, the above equation can be rewritten as

$$\triangle_g = N^{-(y_\triangle/2\upsilon)} f\left(qN^{1/2\upsilon}\right) \tag{181}$$

Comparing Eq. (180) and Eq. (181), we can easily get

$$y_\triangle = 0.91, \qquad \upsilon = 1 \tag{182}$$

By relating $y_\triangle$ to the dynamic exponent z with $y_\triangle = z\nu$, we can have $z \approx 0.91$. It should be meaningful to compare the obtained results here with those from other kinds of MIT in 2D systems.

For filling-control or density-driven MIT, there are two types of universality classes. One is characterized by $z = 1/\nu = 2$, which is the case for all 1D systems as well as for several transitions at higher dimensions, such as transitions between insulator with diagonal order of components and metal with diagonal order components and small Fermi volume. Another one is characterized by $z = 1/\nu = 4$. Numerical calculations have shown that the Hubbard model on a square lattice is an example of this class. The large dynamic exponent is associated with suppression of coherence, which is associated with strong incoherent scattering of charge by a large degeneracy of component excitations.

For Anderson MIT, most of the analytical, numerical, and experimental research have produced $\upsilon > 1$, such as $\upsilon = 1.35$ [211], 1.54 [212], and 1.62 [213]. Our work leads to $z = 0.91$ and $\nu = 1$, which might imply that Mott MIT does belong to any universality class mentioned above. But because of the approximations involved in real-space RG method and the sensitivity of the critical exponents upon the used approaches, more work, especially analytical work, is much needed to reveal the implications and the underlying mechanism for $z = 0.91$ and $\upsilon = 1$. Since we lack in the results from other approaches for comparisons, z and ν are far from decided. Our work tends to show $z \approx \nu \approx 1$. The research aiming to check this guess is still in progress.

In summary, by using a multistage real-space renormalization group method, we show that the finite-size scaling can be applied in Mott MIT. And the dynamic and correlation length critical exponents are found to be $z = 0.91$ and $\upsilon = 1$, respectively. At the transition point, the charge gap scales with size as $\triangle_g \sim 1/L^{0.91}$.

X. CONCLUDING REMARKS

In this review chapter, we show how the finite-size scaling ansatz can be combined with the variational method to extract information about critical behavior of quantum Hamiltonians. This approach is based on taking the number of elements in a complete basis set as the size of the system. As in statistical mechanics, the finite-size scaling can then be applied directly to the Schrödinger equation. This approach is general and gives very accurate results for the critical parameters, for which the bound-state energy becomes absorbed or degenerate with a continuum. To illustrate the applications in quantum calculations, we present detailed calculations for both short- and long-range potentials, atomic and simple molecular systems, resonances, and quantum dots.

The field of quantum critical phenomena in atomic and molecular physics is still in its infancy; and there are many open questions about the interpretations of the results, including whether or not these quantum phase transitions really do exist. The possibility of exploring these phenomena experimentally in the

field of quantum dots offers an exciting challenge for future research. This finite-size scaling approach is general and might provide a powerful way in determining critical parameters for the stability of atomic and molecular systems in external fields, for selectively breaking chemical bonds, and for design and control electronic properties of materials using artificial atoms.

Acknowledgments

We would like to thank our collaborators Qicun Shi for his major contributions in applying FSS to molecular systems, Juan Pablo Neirotti for his contributions to the studies of few-electron atoms, Alexie Sergeev for his work on generalizing the calculations to N-electron atoms, Ricardo Sauerwein for developing the path integral for quantum criticality, and Jiaxiang Wang for his work on quantum dots.

We would like also to acknowledge the financial support of the Office of Naval Research (N00014-97-1-0192) and The National Science Foundation (NSF-501-1393-0650). One of us (PS.) thanks CONICET and SECYTUNC for partial financial support.

References

1. B. Benderson, *More Things in Heaven and Earth, A Celebration of Physics at the Millennium*, Springer, APS, New York, 1999, pp. 501–665.
2. J. J. Binney, N. J. Dowrick, A. J. Fisher, and M. E. J. Newman, *The Theory of Critical Phenomena: An Introduction to the Renormalization Group*, Oxford University Press, New York, 1992.
3. S. L. Sondhi, S. M. Girvin, J. P. Carini, and D. Shahar, *Rev. Mod. Phys.* **69**, 315 (1997).
4. S. Sachdev, *Quantum Phase Transitions*, Cambridge University Press, New York, 1999.
5. D. Voss, *Science* **282**, 221 (1998).
6. H. L. Lee, J. P. Carini, D. V. Baxter, W. Henderson, and G. Gruner, *Science* **287**, 633 (2000).
7. P. Serra and S. Kais, *Phys. Rev. Lett.* **77**, 466 (1996).
8. J. P. Neirotti, P. Serra, and S. Kais, *Phys. Rev. Lett.* **79**, 3142 (1997).
9. P. Serra, J. P. Neirotti, and S. Kais, *Phys. Rev. Lett.* **80**, 5293 (1998).
10. S. Kais and P. Serra, *Int. Rev. Phys. Chem.* **19**, 97 (2000).
11. Q. Shi and S. Kais, *Mol. Phys.* **98**, 1485 (2000).
12. M. K. Scheller, R. N. Compton, and L. S. Cederbaum, *Science* **270**, 1160 (1995).
13. X. Wang and L. Wang, *Phys. Rev. Lett.* **83**, 3402 (1999).
14. R. Rost, J. Nygard, A. Pasinski, and A. Delon, Phys. Rev. Lett. **78**, 3093 (1997).
15. Y. P. Kravchenko and M. A. Lieberman, *Phys. Rev. A* **56**, R2510 (1997).
16. F. Remacle and R. D. Levine, *Proc. Natl. Acad. Sci. USA* **97**, 553 (2000).
17. H. R. Sadeghpour, J. L. Bohn, M. J. Cavagnero, B. D. Esry, I. I. Fabrikant, J. H. Macek, and A. R. P. Rau, *J. Phys. B* **33**, R93 (2000).
18. H. E. Camblong, L. N. Epele, H. Fanchiotti, and C. A. García Canal, *Phys. Rev. Lett.* **87**, 220402 (2001).
19. J. Zs. Mezei, J. Mitroy, R. G. Lovas, and K. Varga, *Phys. Rev. A* **64**, 032501 (2001).
20. R. S. Berry, *Nature (London)* **393**, 212 (1998).
21. P. Nigra, M. Carignano, and S. Kais, *J. Chem. Phys.* **115**, 2621 (2001).

22. M. E. Fisher, in *Critical Phenomena*, Proceedings of the 51st Enrico Fermi Summer School, Varenna, Italy, M. S. Green, ed., Academic Press, New York, 1971.
23. M. N. Barber, Finite-Size Scaling, in *Phase Transitions and Critical Phenomena*, C. Domb and J. L. Lebowitz, eds., Academic Press, New York, 1983.
24. V. Privman, ed., *Finite Size Scaling and Numerical Simulations of Statistical Systems*, World Scientific, Singapore, 1990.
25. J. L. Cardy, *Finite-Size Scaling*, Elsevier Science Publishers, New York, 1988.
26. P. Serra, Preprint, 2002.
27. F. H. Stillinger and D. K. Stillinger, *Phys. Rev. A* **10**, 1109 (1974).
28. J. Katriel and E. Domany, *Int. J. Quantum Chem.* **8**, 559 (1974).
29. D. R. Hershbach, J. Avery, and O. Goscinsky, *Dimensional Scaling in Chemical Physics*, Kluwer, Dordrecht, 1993.
30. P. Serra and S. Kais, *Phys. Rev. A* **55**, 238 (1997).
31. P. Serra and S. Kais, *Chem. Phys. Lett.* **260**, 302 (1996).
32. P. Serra and S. Kais, *J. Phys. A* **30**, 1483 (1997).
33. For reviews see A. Chartterjee, *Phys. Rep.* **186**, 249 (1990).
34. E. Witten, *Phys. Today* **33** (7), 38 (1980).
35. C. A. Tsipis, V. S. Popov, D. R. Hershbach, and J. S. Avery, *New Methods in Quantum Theory*, Kluwer, Dordrecht, 1996.
36. S. Kais, S. M. Sung, and D. R. Hershbach, *Int. J. Quantum Chem.*, **49**, 657–674 (1994).
37. D. D. Frantz and D. R. Hershbach, *Chem. Phys.* **126**, 59 (1988); *J. Chem. Phys.* **92**, 6688 (1990).
38. J. G. Loeser, *J. Chem. Phys.* **86**, 5635 (1987).
39. M. Cabrera, A. L. Tan, and J. G. Loeser, *J. Phys. Chem.* **97**, 2467 (1993).
40. D. Z. Goodson and D. R. Hershbach, *J. Chem. Phys.* **86**, 4997 (1987); D. J. Doren and D. R. Hershbach, *J. Phys. Chem.* **92**, 1816 (1988).
41. H. E. Stanley, *Introduction to Phase Transitions and Critical Phenomena*, Oxford University Press, New York, 1971.
42. Q. Shi, S. Kais, F. Remacle, and R. D. Levine, *CHEMPHYSCHEM* **2**, 434–442 (2001).
43. Q. Shi and S. Kais, *Int. J. Quantum Chem.* **85**, 307 (2001).
44. J. Avery, *Hyperspherical Harmonics; Applications in Quantum Theory*, Kluwer Academic Publishers, Dordrecht, Netherlands, 1989.
45. B. Simon, *J. Funct. Analysis* **1977**, 25, 338.
46. N. G. Bruijn, *Asymptotic Methods in Analysis*, Dover, New York, 1981.
47. M. Klaus and B. Simon, *Ann. Phys. (NY)* **130**, 251 (1980).
48. M. Lassaut, I. Bulboaca, and R. J. Lombard, *J. Phys. A* **29**, 2175 (1996).
49. See, for example, A. Galindo and P. Pascual, *Quantum Mechanics*, Vol. I, Springer-Verlag, Berlin (1990).
50. S. Flügge, *Practical Quantum Mechanics*, Springer-Verlag, Berlin (1999).
51. F. Cooper, A. Khare, and U. Sukhatme, *Phys. Rep.* **251**, 267 (1995).
52. S. Kais, *Exact Models*, in *The Encyclopedia of Computational Chemistry*, P. v. R. Schleyer, N. L. Allinger, T. Clark, J. Gasteiger, P. A. Kollman, H. F Schaefer III, and P. R. Schreiner, eds., John Wiley & Sons, Chichester, 1998, pp. 959–963.
53. V. M. Eleonsky and V. G. Korolev, *Phys. Rev. A* **55**, 2580 (1997).
54. P. Serra, J. P. Neirotti, and S. Kais, *J. Phys. Chem. A* **102**, 9518 (1998).

55. M. Abramowitz and I. A. Stegun, eds., *Handbook of Mathematical Functions*, Dover, New York, 1972.
56. P. M. Morse and H. Feschbach, *Methods of Theoretical Physics*, Vol. II, McGraw-Hill, New York, 1953.
57. F. H. Stillinger, *J. Math. Phys.* **20**, 1891 (1979).
58. W. M. Frank and D. J. Land, *Rev. Mod. Phys.* **43**, 36 (1971).
59. M. J. Mortiz, C. Eltschka, and H. Friedrich, *Phys. Rev. A* **63**, 042102 (2001); *ibid.* **64**, 022101 (2001).
60. I. S. Gradshteyn and I. M. Ryzhik, *Table of Integrals, Series and Products*, 5th ed., Academic Press, San Diego, 1994.
61. M. K. Scheller, N. Compton, and L. S. Cederbaum, *Science* **270**, 1160 (1995).
62. A. V. Sergeev and S. Kais, *Int. J. Quantum Chem.* **75**, 533 (1999).
63. E. H. Lieb, *Phys. Rev. Lett.* **52**, 315 (1982).
64. M. Hoffmann-Ostenhof, T. Hoffmann-Ostenhof, and B. Simon, *J. Phys. A* **16**, 1125 (1983).
65. J.-M. Richard, *Few-Body Systems*, preprint: physics/0111111, in press.
66. S. Kais and Q. Shi, *Phys. Rev. A* **62**, 060502(R) (2000).
67. Walter Thirring, *A Course in Mathematical Physics*, Vol. III, Springer-Verlag, New York, 1986.
68. C. N. yang and T. D. Lee, *Phys. Rev.* **87**, 404 (1952).
69. T. D. Lee and C. N. Yang, *Phys. Rev.* **87**, 410 (1952).
70. M. P. Nightingale, *Physica* **83A**, 561 (1976).
71. See, for example, C. J. Thompson, *Classical Statistical Mechanics*, Clarendon Press, London, 1988.
72. F. R. Gantmacher, *The Theory of Matrices*, Chelsea, New York, 1959.
73. M. P. Nightingale, *Proceedings of the Koninklijke Nederlandse Akademie van Wetenschappen*, series B, Vol. 82, 1979.
74. P. D. Beale, P. M. Duxbury, and J. Yeomans, *Phys. Rev. B* **31**, 7166 (1985).
75. B. Derrida, *J. Phys. A* **14**, L5 (1981); B. Derrida and H. Saleur, *J. Phys. A* **18**, L1075 (1985).
76. P. Serra and J. F. Stilck, *Europhys Lett.* **17**, 423 (1992); *Phys. Rev. E* **49**, 1336 (1994).
77. B. Derrida and L. De Seze, *J. Phys.* **43**, 475 (1982).
78. P. J. Reynolds, H. E. Stanly, and W. Klein, *Phys. Rev. B* **21**, 1223 (1980).
79. H. Nakanishi and P. J. Reynolds, *Phys. Lett. A* **71**, 252 (1979).
80. H. Nakanishi and H. E. Stanley, *Phys. Rev. B* **22**, 2466 (1980).
81. S. B. Lee and H. Nakanishi, *J. Phys. A* **33**, 2943 (2000).
82. Z. Glumac and K. Uzelac, *J. Phys. A* **22**, 4439 (1989).
83. L. P. Kadanoff and G. Baym, *Quantum Statistical Mechanics*, Addison-Wesley, Reading, MA, 1989.
84. L. P. Kadanoff, *Statistical Physics: Statics, Dynamics and Renormalization*, World Scientific, Singapore, 2000.
85. B. Hatfield, *Quantum Field Theory of Point Particles and Strings*, Addison-Wesley, Reading, MA, 1992.
86. See, for example, in E. Merzbacher, *Quantum Mechanics*, 2nd ed., John Wiley & Sons, New York, 1998.
87. J. P. Neirotti, P. Serra, and S. Kais, *J. Chem. Phys.* **108**, 2765 (1998).

88. P. Serra, J. P. Neirotti, and S. Kais, *Phys. Rev. A* **57**, R1481 (1998).
89. R. Bulirsch and J. Stoer, *Numer. Math.* **6**, 413 (1964).
90. M. Henkel in Ref. 24, Chapter VIII.
91. V. M. Vainberg, V. L. Eletskii, and V. S. Popov, *Sov. Phys. JETP* **1981**, 54, 833.
92. F. J. Rogers, H. C. Graboske, and D. J. Harwood, *Phys. Rev. A* **1**, 1577 (1970).
93. P. Serra, and S. Kais, *Chem. Phys. Lett.* **319**, 273 (2000).
94. See, for example, N. Goldenfeld, *Lectures on Phase Transitions and the Renormalization Group*, Addison-Wesley, Reading, MA, 1992.
95. B. Nienhuis and M. Nauenberg, *Phys. Rev. Lett.* **35**, 477 (1975).
96. E. A. Hylleraas, *Z. Phys.* **65**, 209 (1930).
97. T. Kato, in *Perturbation Theory for Linear Operators*, 2nd ed., Springer, New York, 1976.
98. C. W. Scherr and R. E. Knight, *Rev. Mod. Phys.* **35**, 436 (1963).
99. F. M. Stillinger Jr., *J. Chem. Phys.* **45**, 3623 (1966).
100. J. Midtdal, *Phys. Rev. A* **138**, 1010 (1965).
101. W. P. Reinhardt, *Phys. Rev. A* **15**, 802 (1977).
102. J. D. Baker, D. E. Freund, R. N. Hill, and J. D. Morgan III, *Phys. Rev. A* **41**, 1247 (1990).
103. I. A. Ivanov, *Phys. Rev. A* **51**, 1080 (1995).
104. G. W. F. Drake and Zong-Chao Yan, *Chem. Phys. Lett.* **229**, 489 (1994).
105. E. A. Hylleraas, *Z. Physik* **48**, 469 (1928); *ibid.* **54**, 347 (1929).
106. A. K. Bhatia and A. Temkin, *Rev. Mod. Phys.* **36**, 1050 (1964).
107. H. Grosse and L. Pittner, *J. Math. Phys.* **24**, 1142 (1983).
108. R. N. Hill, *Phys. Rev. Lett.* **38**, 643 (1977).
109. T. Kato, *Trans. Am. Math. Soc.* **70**, 212 (1951).
110. G. W. F. Drake, *Phys. Rev. Lett.* **24**, 126 (1970).
111. E. Brändas and O. Goscinski, *Int. J. Quantum Chem.* **4**, 571 (1970).
112. E. Brändas and O. Goscinski, *Int. J. Quantum Chem. Symp.* **6**, 59 (1972).
113. G. A. Arteca, F. M. Fernández, and E. A. Castro, *J. Chem. Phys.* **84**, 1624 (1986).
114. Z. Yan and G. W. F. Drake, *Phys. Rev. A* **52**, 3711 (1995).
115. E. H. Lieb, *Phys. Rev. A* **29**, 3018 (1984).
116. L. A. Cole and J. P. Perdew, *Phys. Rev. A* **25**, 1265 (1982).
117. S. J. Chakravorty and E. R. Davidson, *J. Phys. Chem.* **100**, 6167 (1996).
118. S. Kais, J. P. Neirotti, and P. Serra, *Int. J. Mass Spectrom.* **182/183**, 23–29 (1999).
119. H. Hogreve, *J. Phys. B: At. Mol. Opt. Phys.* **31**, L439 (1998).
120. D. R. Bates, *Adv. At. Mol. Opt. Phys.* **27**, 1 (1991).
121. M.-J. Nadeau, M. A. Garwan, X.-L. Zhao, and A. E. Litherland, *Nucl. Instrum. Methods Phys. Res. B* **123**, 521 (1997).
122. H. Hotop and W. C. Lineberger, *J. Phys. Chem. Ref. Data* **14**, 731 (1985).
123. D. Berkovits and E. Boaretto et al., *Phys. Rev. Lett.* **75**, 414 (1995).
124. W. Hunziker, *Helv. Phys. Acta* **48**, 145 (1975).
125. G. M. Zhislin, *Theor. Math. Phys.* **7**, 571 (1971).
126. R. Benguria and E. H. Lieb, *Phys. Rev. Lett.* **50**, 1771 (1983).
127. Q. Shi and S. Kais, *Mol. Phys.* **100**, 475 (2002).

128. X. B. Wang, C. F. Ding, and L. S. Wang, *Phys. Rev. Lett.* **81**, 3351 (1998).
129. J. Ackermann and H. Hogreve, *J. Phys. B* **25**, 4069 (1992).
130. B. J. Laurenzi and M. F. Mall, *Int. J. Quant. Chem.* **xxx**, 51 (1986).
131. T. K. Rebane, *Sov. Phys. JETP* **71**, 1055 (1990).
132. Z. Chen and L. Spruch, *Phys. Rev. A* **42**, 133 (1990).
133. D. B. Kinghorn and L. Adamowicz, *J. Chem. Phys.* **110**, 7166 (1999).
134. B. J. Laurenzi, *J. Chem. Phys.* **65**, 217 (1976).
135. T. K. Rebane, *Sov. Phys. JETP* **71**, 1055 (1990).
136. H. Hogreve, *J. Chem. Phys.* **98**, 5579 (1993).
137. A. Martin, J. Richard, and T. T. Wu, *Phys. Rev. A* **52**, 2557 (1995).
138. B. Grémaud, D. Delande, and N. Billy, *J. Phys. B* **31**, 383 (1998).
139. C. L. Pekeris, *Phys. Rev.* **112**, 1649 (1958).
140. For example, A. R. Curtis and J. K. Reid, *J. Inst. Math. Appl.* **8**, 344 (1971).
141. P. R. Amestony, T. A. Davis, and I. S. Duff, *SIAM J. Matrix Anal. Appl.* **17**, 886 (1996).
142. C. Lanczos, *J. Res. Natl. Bur. Stand. B* **45**, 255 (1950).
143. Y. K. Ho, *Phys. Rev. A* **48**, 4780 (1993).
144. A. M. Frolov, *Phys. Rev. A* **60**, 2834 (1999).
145. R. Krivec, V. B. Mandelzweig, and K. Varga, *Phys. Rev. A* **61**, 062503 (2000).
146. C. D. Lin, *Phys. Rep.* **257**, 1 (1995).
147. E. A. G. Armour and W. B. Brown, *Acc. Chem. Res.* **26**, 168 (1993).
148. A. P. Mills, Jr. *Phys. Rev. Lett.* **46**, 717 (1981).
149. A. Martin, *Heavy Ion Phys.* **8**, 285 (1998).
150. J. M. Rost and D. Wintgen, *Phys. Rev. Lett.* **69**, 2499 (1992).
151. C. L. Pekeris, *Phys. Rev.* **112**, 1649 (1958).
152. J. R. Rice, *Matrix Computations and Mathematical Software*, McGraw-Hill, New York, 1981.
153. B. N. Parlett, *The Symmetric Eigenvalue Problem*, Prentice-Hall, Englewood Cliffs, NJ, 1980.
154. E. R. Cohen, and B. N. Taylor, *Phys. Today* **8**, BG 7 (1998).
155. R. S. Dyck, D. L. Farnham, Jr., and P. B. Schwinberg, *Phys. Rev. Lett.* **70**, 2888 (1993).
156. P. Serra, S. Kais, and N. Moiseyev, *Phys. Rev. A* **64**, 062502 (2001).
157. N. Moiseyev, *Phys. Rep.* **302**, 211 (1998).
158. H. Friedrich, *Theoretical Atomic Physics*, 2nd ed., Springer, Berlin, 1998.
159. R. G. Newton, *Scattering Theory of Waves and Particles*, McGraw-Hill, New York, 1966.
160. N. Moiseyev, P. R. Certain, and F. Weinhold, *Mol. Phys.* **36**, 1613 (1978).
161. N. Moiseyev, P. Froelich, and E. Watkins, *J. Chem. Phys.* **80**, 3623 (1984).
162. E. Narevicius, D. Neuhauser, H. J. Korsc, and N. Moiseyev, *Chem. Phys. Lett.* **276**, 250 (1997).
163. M. Rittby, N. Elander, and E. Brandas, *Phys. Rev. A* **24**, 1636 (1981).
164. B. Simon, *Ann. Phys.* **97**, 279 (1976).
165. G. Raggio, private communication.
166. C. Domb and J. L. Lebowitz, *Phase Transition and Critical Phenomena*, Vol. 9, Academic Press, London, 1992.
167. A. F. J. Siegert, *Phys. Rev.* **56**, 750 (1939)
168. H.-D. Meyer and O. Walter, *J. Phys. B* **15**, 3647 (1982).

169. H. S. Taylor and L. D. Thomas, *Phys. Rev. Lett.* **28**, 1091 (1972).
170. C. Laughlin, B. L. Burrows, and M. Cohen, *J. Phys. B* **35**, 701 (2002).
171. B. Szafran, J. Adamowsky and S. Bednarek, *Physica E* **4**, 1 (1999).
172. M. Čížek and H. Horáček, *J. Phys. A* **29**, 6325 (1996).
173. M. Suzuki, X. Hu, M. Katori, A. Lipowski, N. Hatano, K. Minami, and Y. Nomnomura, *Coherent Anomaly Method; Mean Field, Fluctuations and Systematics*, World Scientific, Singapore, 1995.
174. R. A. Sauerwein and S. Kais, *Chem. Phys. Lett.* **333**, 451 (2001).
175. H. Kleinert, *Path Integrals*, World Scientific, Singapore, 1995.
176. N. Makri, *Annu. Rev. Phys. Chem.* **50**, 167 (1999).
177. M. L. Bellac, *Quantum and Statistical Field Theory*, Oxford University Press, New York, 1998.
178. A. Lasota and M. C. Mackey, *Chaos, Fractals and Noise*, Springer, Berlin, 1991.
179. M. Doi and S. F. Edwards, *The Theory of Polymer Dynamics*, Oxford Press, New York, 1989.
180. G. Jongeward and P. G. Wolynes, *J. Chem. Phys.* **79**, 3517 (1983).
181. G. Pöschl and E. Teller, *Z. Phys.* **83**, 143 (1933).
182. D. Bressanini and P. J. Reynolds, *in advances in Chemical Physics*, Vol. 105, Wiley, New York, 1999, p. 37.
183. F. Remacle and R. D. Levine, *CHEMPHYSCHEM* **2**, 20 (2001).
184. L. Jacak, P. Hawrylak, and A. Wols, *Quantum Dots*, Springer, Berlin, 1998.
185. T. Chakraborty, *Quantum Dots: A Survey of the Properties of Artificial Atoms*, Elsevier, New York, 1999.
186. A. P. Alivisatos, *Science* **271**, 933 (1996).
187. C. B. Murray, C. R. Kagan, and M. G. Bawendi, *Science* **270**, 1335 (1995).
188. R. L. Whetten, J. T. Khoury, M. M. Alvarez, et al., *Adv. Mater.* **8**, 428 (1996).
189. G. Markovich, C. P. Collier, S. E. Henrichs, et al., *Acc. Chem. Res.* **32**, 415 (1999).
190. C. A. Stafford and S. DasSarma, *Phys. Rev. Lett.* **72**, 3590 (1994).
191. C. R. Kagan, C. B. Murray, M. Nirmal, et al., *Phys. Rev. Lett.* **76**, 1517 (1996).
192. G. C. Schatz, *J. Mol. Strut. (Theochem.)* **573**, 73 (2001).
193. K. C. Beverly, J. L. Sample, J. F. Sampaio, et al., *Proc. Natl. Acad. Sci. USA, in press (2002).*
194. M. A. Kastner, *Phys. Today* **46**, 24 (1993).
195. R. C. Ashoori, *Nature* **379**, 413 (1996).
196. U. Banin, Y. W. Cao, D. Katz, and O. Millo, *Nature* **400**, 542 (1999).
197. F. Remacle and R. D. Levine, *J. Phys. Chem. A* **104**, 10435 (2000).
198. J. L. Sample, K. C. Berverly, P. R. Chaudhari, et al., *Adv. Mater.* **14**, 124 (2002).
199. K. C. Beverly, J. F. Sampaio, and J. R. Heath, *J. Phys. Chem. B* **106**, 2131 (2002).
200. J. Hubbard, *Proc. R. Soc. London A* **276**, 238 (1963).
201. P. Fulden, *Electron Correlation in Molecules and Solids*, Springer-Verlag, Berlin, 1995.
202. J. E. Hirsch, *Phys. Rev. B* **22**, 5259 (1980).
203. J. Perez-Conde and P. Pfeuty, *Phys. Rev. B* **47**, 856 (1993).
204. B. Bhattacharyya and S. Sil, *J. Phys. Condens. Matter* **11**, 3513 (1999).
205. J. X. Wang, S. Kais, and R. D. Levine, *Int. J. Mol. Sci.* **3**, 4 (2002).
206. T. W. Burkhardt and J. M. J. van Leuven, in *Topics in Current Physics*, Springer-Verlag, Berlin, 1982.

207. F. Remacle, C. P. Collier, J. R. Heath, et al., *Chem. Phys. Lett.* **291**, 453 (1998).

208. N. F. Mott, *Metal–Insulator Transitions*, Taylor & Francis, London, 1990.

209. G. Benenti, X. Waintal, J.-L. Pichard and D. L. Shepelyansky, arXiv:cond/0003208.

210. M. A. Continentino, *Quantum Scaling in Many-Body Systems*, World Scientific Lecture Notes in Physics, Vol. 67, World Scientific, Singapore,

211. M. Schreiber, B. Kramer, and A. MacKinnon, *Physica Scripta* **T25**, 67 (1989); E. Hofstetter and M. Schreiber, *Europhys. Lett.* **21**, 933 (1993).

212. A. MacKinnon, *J. Phys. Condens. Matter* **6**, 2511 (1994).

213. F. Milde, R. A. Romer, M. Schreiber, and V. Uski, *J. Eur. Phys. B* **15**, 685 (2000).